

# **Marker-Independent Assessment of Molecular Activation Patterns in Macrophages**

## **Dissertation**

der Mathematisch-Naturwissenschaftlichen Fakultät  
der Eberhard Karls Universität Tübingen  
zur Erlangung des Grades eines  
Doktors der Naturwissenschaften  
(Dr. rer. nat.)

vorgelegt von  
Nora Feuerer  
aus Regensburg

Tübingen

2022

Gedruckt mit Genehmigung der Mathematisch-Naturwissenschaftlichen Fakultät der Eberhard Karls Universität Tübingen.

Tag der mündlichen Qualifikation:	25.01.2023
Dekan:	Prof. Dr. Thilo Stehle
1. Berichterstatter/-in:	Prof. Dr. Katja Schenke-Layland
2. Berichterstatter/-in:	Prof. Dr. Peter Loskill

„Leben ist mehr als Hetzen und Jagen,  
Leben ist mehr als nur Theorie.  
Leben ist mehr als Zweifeln und Fragen,  
Leben ist hier, jetzt oder nie.“

- *Rolf Zuckowski*



## Table of Contents

<b>Table of Contents</b> .....	<b>I</b>
<b>Abstract</b> .....	<b>IV</b>
<b>Zusammenfassung</b> .....	<b>VII</b>
<b>Abbreviations</b> .....	<b>IX</b>
<b>List of Figures</b> .....	<b>XII</b>
<b>List of Tables</b> .....	<b>XIV</b>
<b>List of Publications &amp; Contributions</b> .....	<b>XVI</b>
<b>1. Introduction</b> .....	<b>2</b>
1.1. Macrophage Function and Plasticity .....	2
1.1.1. Macrophage Origin and their Role in Innate Immunity .....	2
1.1.2. The Spectrum Wheel of Macrophage Activation .....	4
1.1.3. Mechanosensing of Macrophages .....	6
1.1.4. In Vitro Systems to Model Human Macrophage Biology .....	8
1.2. Raman Microscopy in Cell Biology .....	10
1.2.1. The Raman Effect and Raman Scattering .....	10
1.2.2. Raman Microspectroscopy and Raman Imaging on Biological Samples .....	12
1.2.3. Raman Microspectroscopy in the Context of Conventional Imaging Techniques in Molecular Cell Biology .....	14
<b>2. Objective of the Thesis</b> .....	<b>18</b>
<b>3. Results and Discussion</b> .....	<b>21</b>
3.1. Enzymatic Dissociation from Electrospun Substrates Selectively Impacts Macrophage Surface Antigens .....	21

## Table of Contents

3.2. Raman Microspectroscopy Discriminates Macrophage Activation in a Marker-Independent Manner .....	25
3.2.1. Macrophage Activation is Predominantly Characterized by a Change in Lipid Composition .....	28
3.2.2. Raman Microspectroscopy Identifies Macrophage Activation Induced by Surface Topography of Titanium Disks .....	29
3.3. Raman Microspectroscopy Identifies Biochemical Activation Fingerprints in THP-1 and Monocyte Derived Macrophages .....	32
3.3.1. THP-1 and Monocyte Derived Macrophages Differ in their Molecular Composition.....	34
3.3.2. THP-1 and MDMs Differ in their Molecular Remodeling Capacity upon LPS and IFN $\gamma$ Stimulation .....	35
<b>4. General Conclusion &amp; Outlook .....</b>	<b>40</b>
<b>References .....</b>	<b>43</b>
<b>Acknowledgments .....</b>	<b>52</b>
<b>Declaration .....</b>	<b>54</b>
<b>Curriculum Vitae .....</b>	<b>56</b>
<b>Appendices .....</b>	<b>60</b>



## Abstract

Tissue repair, regeneration, and fibrosis are processes regulated by inflammatory monocytes and monocyte-derived macrophages (MDMs) that circulate in peripheral blood or reside in tissue. After a traumatic injury, monocytes and macrophages undergo significant phenotypic and functional changes that allow them to play essential roles in the initiation, maintenance, and resolution stages of tissue repair. Macrophages are also highly sensitive to physical stimuli in their environment and sense, for example, the degree of stiffness of the surrounding extracellular matrix. This makes them promising targets in biomaterial research, as the macrophage response is a crucial factor for long-term implant survival and performance. In addition, designing implant materials in a way that reduces inflammation and facilitates tissue integration has the potential to significantly reduce surgical costs and increase the quality of life for many patients. The research on how the physical properties of implant materials influence macrophage biology is still in its infancy. This work investigates how alternative analysis methods to classical immunological techniques can help overcome the current challenges in macrophage biomaterial research. It was therefore investigated how standard methods like flow cytometry perform in identifying macrophage phenotype after detachment from extracellular matrix-mimicking biomaterials. Our findings show that the detachment of adherent macrophages from a substrate induces significant bias depending on the analyzed surface antigens. Raman microspectroscopy (RM) is a non-invasive spectroscopic method that does not require fixation or antibody staining of biological samples. RM was therefore implemented as an alternative for single cell analysis of adherent macrophages. It was shown that macrophage activation can be robustly identified based on distinct Raman fingerprint spectra and that this method can be employed on macrophages adherent to biomaterial substrates to identify activation and phenotype in a marker-independent manner. Lipid Raman spectra were found to be significantly altered between macrophage phenotypes, making lipids an ideal target for the identification of macrophage polarization using RM. Lastly, it was investigated, if the myeloid leukemia-derived monocytic cell line THP-1 shows similar molecular activation when compared to primary MDMs as identified by RM. THP-1 protein and phospholipid levels were significantly altered by proinflammatory activation in THP-1 macrophages while MDMs also showed altered nucleic acid and non-membrane intracellular lipid composition.



Altogether the findings of this thesis will contribute to a faster and more efficient development of regenerative biomaterials.



### Zusammenfassung

Monozyten und Makrophagen sind Zellen des angeborenen Immunsystems, welche sowohl Bakterien und andere Pathogene durch Phagozytose eliminieren als auch maßgeblich die Wundheilung und die Reparatur von Gewebeschäden steuern. Makrophagen reagieren besonders empfindlich auf inflammatorische oder physikalische Reize ihrer unmittelbaren Umgebung und können beispielsweise den Grad der Steifigkeit der umgebenden extrazellulären Matrix wahrnehmen. Eine zentrale Rolle spielen Makrophagen deshalb auch bei der Verträglichkeit und Lebensdauer von Implantaten. Die Entwicklung regenerativer Biomaterialien, welche den Heilungsprozess fördern und chronische Entzündungen verhindern, kann die Lebensqualität vieler Patienten erheblich verbessern und Kosten im Gesundheitswesen senken. Welche Eigenschaften eines Materials besonders heilungsfördernd sind, ist bisher jedoch kaum erforscht. Der Kern dieser Arbeit beschäftigt sich deshalb damit, wie die Makrophagen-Aktivierung durch Materialoberflächen zuverlässig identifiziert werden kann. Im ersten Teil wird gezeigt, dass Standardmethoden, wie die Durchflusszytometrie oder Zytokin-Assays, bei der Identifizierung des Makrophagen-Phänotyps zu Verzerrungen der Ergebnisse führen können, da die Makrophagen von ihrem Substrat abgelöst werden müssen. Der zweite Teil dieser Arbeit untersucht, wie die Raman Mikrospektroskopie (RM) dazu beitragen kann, die Wechselwirkung zwischen Zelle und Material auf molekularer Ebene zu verstehen ohne ungewollte Artefakte zu generieren. Da die RM in situ durchgeführt werden kann, ist keine weitere Vorbereitung der Zellen notwendig und Makrophagen können direkt auf ihrem Trägersubstrat analysiert werden. Die RM wurde deshalb als Alternative für die Einzelzellanalyse von adhärennten Makrophagen eingesetzt. Es konnte erfolgreich gezeigt werden, dass die Aktivierung von Makrophagen auf der Grundlage unterschiedlicher Raman-Fingerprint-Spektren zuverlässig identifiziert werden kann und, dass mittels RM sowohl Aktivierung als auch Phänotyp von Makrophagen auf Trägermaterialien mit unterschiedlicher Oberflächenstruktur identifiziert werden können. Des Weiteren wurde gezeigt, dass insbesondere die Lipidzusammensetzung zum molekularen Fingerabdruck verschiedener Makrophagen-Aktivierungsmuster beiträgt. Der letzte Teil der Arbeit untersucht, ob die von der myeloischen Leukämie abgeleitete Zelllinie THP-1 eine ähnliche molekulare Aktivierung aufweist wie primäre Makrophagen. Bei beiden Zelltypen handelt es sich um populäre in vitro Modelle für humane Makrophagen, dennoch gilt es bei der

Anwendung spezifische Vor- und Nachteile gegeneinander abzuwägen. Ggf. können sich beide Modelle stark in ihren Aktivierungsmustern unterscheiden. Hier zeigen wir mittels RM, dass sich Protein- und Phospholipidspiegel durch proinflammatorische Aktivierung in THP-1-Makrophagen signifikant verändert, während primäre humane Makrophagen eine veränderte Nukleinsäure- und intrazelluläre Lipidzusammensetzung aufweisen..

**Abbreviations**

CARS	Coherent anti-stokes Raman spectroscopy
CCD	Charged coupled device
CD	Cluster of differentiation
DNA	Desoxyribonucleic acid
ECM	Extracellular matrix
EDTA	Ethylenediaminetetraacetic acid
ELISA	Enzyme-linked immune sorbent assay
ERK	extracellular signal-regulated kinase
FC	Flow cytometry
HPA	Hypothalamic-pituitary-adrenal axis
IFN $\gamma$	Interferon $\gamma$
IL	Interleukin
IR	Infrared spectroscopy
LPS	Lipopolysaccharide
MAPK	Mitogen-activated protein kinase
MDMs	Monocyte-derived macrophage
MPS	Mononuclear phagocyte system
mRNA	Messenger ribonucleic acid
PALM	Photoactivated localization microscopy
PBMCs	Peripheral blood mononuclear cells
PCA	Principal component analysis
PLA	Poly(lactic acid)
PMA	Phorbol 12-myristate-13-acetate
PMDS	Promocell macrophage detachment solution

## Abbreviations

PMN	Polymorphonuclear leukocyte
PU	Polyurethane
RM	Raman microspectroscopy
SEM	Scanning electron microscopy
STORM	Stochastic optical reconstruction microscopy
TAM	Tumor-associated macrophage
TCA	True component analysis
Ti	Titanium
Ti A	Acid etched titanium
Ti M	Machine polished titanium
TLR	Toll-like receptor
TNF $\alpha$	Tumor necrose factor $\alpha$
TRAAK	Twik-related arachidonic acid-activated K <sup>+</sup> channel
TREK	TWIK1-related K <sup>+</sup> channel
TRPV	Transient receptor potential vallinoid channel
VEGF	Vascular endothelial growth factor



**List of Figures**

Figure 1 Overview of tissue-specific macrophages .....	3
Figure 2 Macrophage ontogeny and development .....	4
Figure 3 Schematic illustration of mechanosensing mechanisms in macrophages. ...	8
Figure 4 Principle of Raman scattering.....	11
Figure 5 Raman peaks of eukaryotic cells.....	13
Figure 6 Principles of Raman spectroscopy and Raman imaging .....	14
Figure 7 Enzymatic dissociation selectively impacts macrophage surface antigens	22
Figure 8 Multivariate Data Analysis of Raman Spectra of Macrophage Activation ...	27
Figure 9 Raman microspectroscopy identifies lipid fingerprints of macrophage activation .....	29
Figure 10 Lipidome changes of macrophages activated by biomaterials can be identified by raman microspectroscopy.....	31
Figure 11 Schematic overview of experimental setup to assess molecular remodelling in THP-1 and MDMs after pro-inflammatory activation. ....	33





**List of Tables**

Table 1 Contributions .....XVI  
Table 2 Overview of Raman peaks assigned to four major cellular components  
analyzed in this work ..... 34



## List of Publications & Contributions

1. **Feuerer N\*, Carvajal Berrio DA\*, Billing F, Segan S, Weiss M, Rothbauer U, Marzi J, Schenke Layland K** "Raman Microspectroscopy Identifies Biochemical Activation Fingerprints in THP-1-and PBMC-Derived Macrophages." *Biomedicines* 10.5 (2022): 989.
2. **Feuerer N, Marzi J, Brauchle E, Carvajal Berrio D, Weiss M, Billing F, Jakobi M, Schneiderhan-Marra N, Shipp C, Schenke Layland K.** "Lipidome profiling with Raman Spectroscopy identifies macrophage response to surface topography of biomaterials." *PNAS*, 2021, 118 (52) e21113694118.
3. **Feuerer N, Morschl J, Daum R, Weiss M, Hinderer S, Schenke Layland K, Shipp C.** "Macrophage retrieval from 3D biomaterials: A detailed comparison of common dissociation methods." *J Immunol Regen Med*, 2021, 1, 100035.

*\*These authors contributed equally*

Table 1 Contributions

No.	1.	2.	3.
Accepted for publication	Yes	Yes	Yes
Number of Authors	8	10	7
Position of the Candidate in the List of Authors	1 (s.f.a.)	1	1
Scientific Ideas by Candidate (%)	30	55	55
Data generation (%)	55	55	50
Interpretation and Analysis by Candidate (%)	10	50	50
Paper writing by Candidate (%)	10	55	65

*s.f.a. = shared first author*

# Chapter 1

## Introduction

## 1. Introduction

### 1.1. Macrophage Function and Plasticity

Macrophages are a type of innate immune cell that adopt multifaceted roles in modulating inflammatory processes, maintaining tissue homeostasis, and the initiation of wound healing. Naive macrophages can exhibit a range of context-dependent activation states and their phenotype and functions are substantially influenced by their surroundings [1]. Macrophages are commonly divided into two subsets of classically activated (M1) macrophages and alternatively activated (M2) macrophages. M1 macrophages are considered pro-inflammatory and induced by recognition of lipopolysaccharides (LPS) either alone or in combination with Th1 cytokines such as interferon  $\gamma$  (IFN $\gamma$ ) [2, 3]. In return, they produce pro-inflammatory cytokines such as interleukin-1 (IL-1), IL-6, IL-12, IL-23, and tumor necrosis factor  $\alpha$  (TNF $\alpha$ ). In contrast, M2 macrophages are responsible for wound closure and/ or fibrotic events [3]. Due to the diversity of these different tasks, transcriptional and proteomic profiles of macrophage subtypes are quite distinct and range from the destruction or encapsulation of pathogens up to the repair of inflammation-related damage [4, 5]. Abnormal or prolonged macrophage activation is commonly associated with tissue damage, fibrosis, or even cancer [6-8].

#### 1.1.1. Macrophage Origin and their Role in Innate Immunity

The term macrophage is quite broad and usually refers to monocyte-derived phagocytotic cells in both peripheral blood and tissue. A characteristic of macrophages is their enormous diversity and plasticity. Almost every organ accommodates a specific type of macrophage, for example, osteoclasts (bone), alveoli (lung), microglia (brain), histiocytes (connective tissue), Langerhans cells (epidermis) or Kupffer cells (liver) (Figure 1). Macrophages have their origin in the yolk sac during embryonic development. These yolk sac-derived macrophages give rise to two distinct macrophage populations. They constitute the origin of both hematopoietic stem cells (HSCs) in the bone marrow, which later give rise to circulating peripheral blood mononuclear cells (PBMCs) but also directly replenish tissue resident macrophage populations (Figure 2) [9, 10]. In reaction to danger-associated molecular patterns (DAMPs), pathogen-associated molecular patterns (PAMPs), cytokines, or chemokines, they are recruited into the tissue to eliminate danger and restore homeostasis.

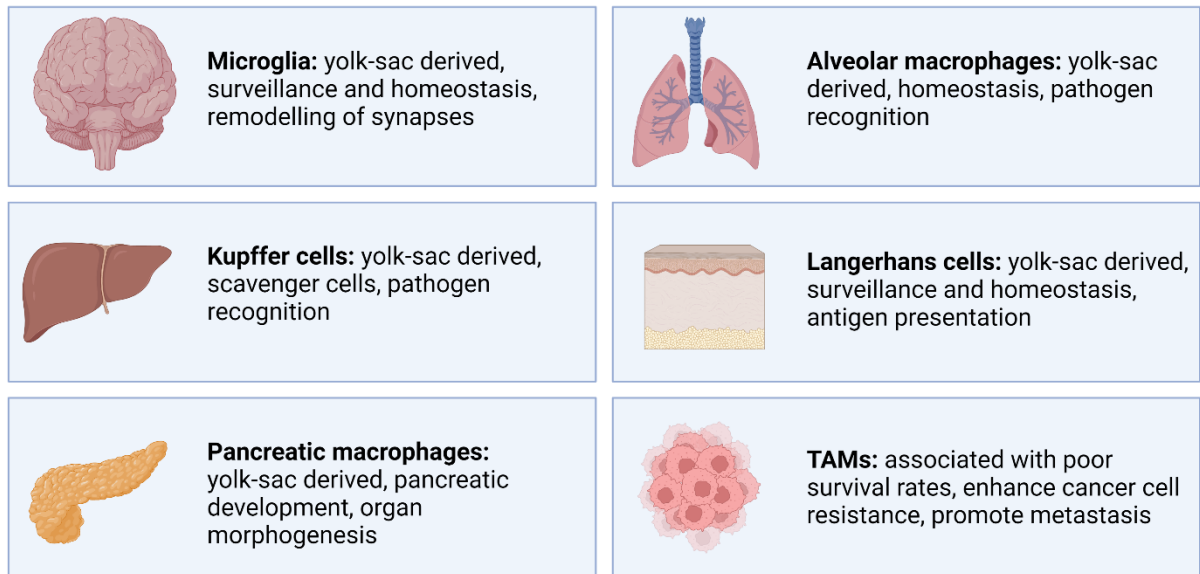


**Figure 1 Overview of tissue-specific macrophages**

*The majority of tissue-specific macrophages are yolk sac-derived and can self-renew. Macrophage function can vary greatly between tissues and malfunction of macrophage biology can lead to severe pathologies and even organ failure [11].*

The majority of tissue-specific macrophages exist independently from PBMC-derived macrophages. They are generated during embryonic development and it has been recently shown that tissue-specific macrophages inherently can self-renew [10, 12-14]. In 1972 van Furth and Cohn introduced the mononuclear phagocyte system (MPS) as a promising classification system for macrophages, blood monocytes, and their precursors and based it on morphology, function, origin, and kinetic characteristics. Initially, the MPS did not include the conventional dendritic cell (DC).

Early on, DCs have been characterized by their distinct morphology, a superior ability to present antigens, their migration to lymph nodes, and the lack of active endocytosis [15] and were thus thought to be distinct from macrophages. However, a terminology controversy over the meaning of DCs has emerged recently [16] as new macrophage types have emerged that share some of these functions and for example migrate to lymph nodes for antigen presentation and T cell activation [17, 18].

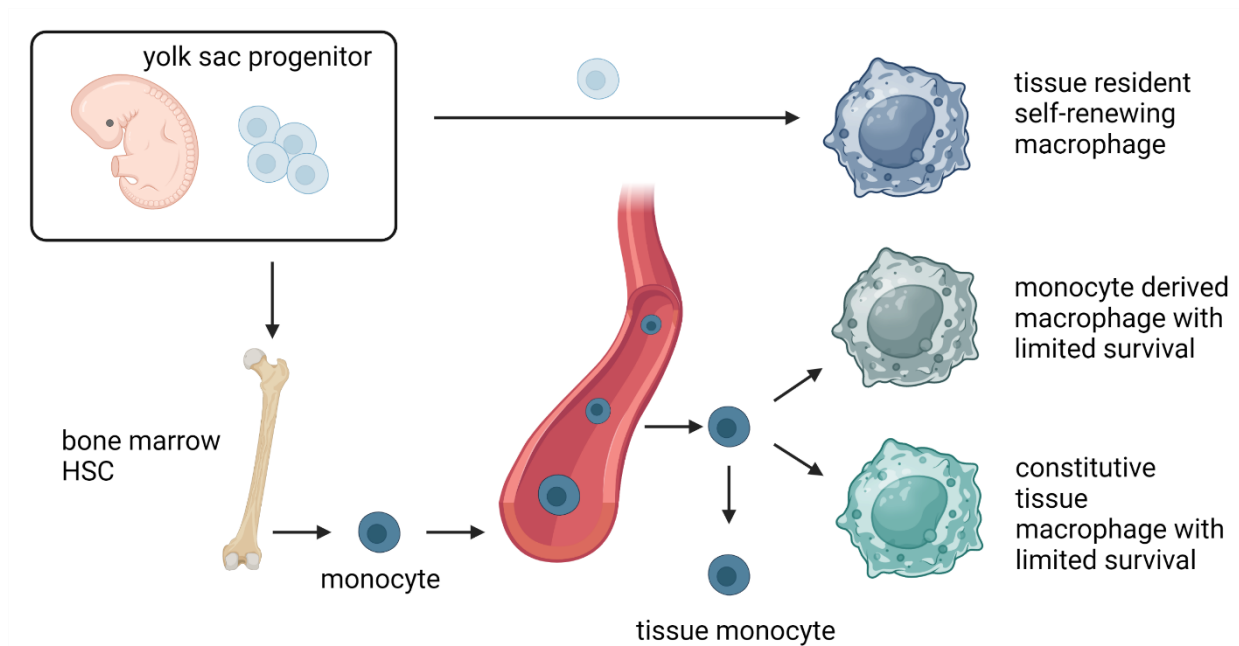


**Figure 2 Macrophage ontogeny and development**

*Macrophage development can take two paths: The majority of tissue-resident macrophages are directly derived from the yolk sac during embryonic development and can self-replenish during adulthood. However, macrophages can also mature from monocytes circulating in the blood. These monocytes are derived from a common myeloid progenitor in the bone marrow. Once they have matured into macrophages their lifespan is usually limited and, in contrast to most tissue-resident macrophages, they cannot self-renew. This figure was adapted from Williams et al. [9].*

### 1.1.2. The Spectrum Wheel of Macrophage Activation

Macrophages are one of the key sensors of danger in the host. Importantly, activation of macrophages by cellular debris can occur in experimental mice lacking lymphocytes, confirming that these mechanisms are not dependent on adaptive immune responses [19, 20]. Recognition of danger signals contained in necrotic cell debris is usually transmitted via Toll-like receptors (TLRs) and the interleukin-1 receptor (IL-1R) [21].

In an attempt to follow T cell nomenclature, macrophages have traditionally been classified into two categories, with M1 macrophages as pro-inflammatory (classically activated) and M2 macrophages (alternatively activated) as anti-inflammatory [22].

However, it soon became apparent that the M2 macrophage class was comprised of several very diverse subtypes. Despite a growing amount of information demonstrating



that the M2 label consists of cells with dramatically different biochemistry and physiology, this classification continues to persist in the literature [23, 24].

Today it is more common to describe macrophage activation as a continuum with many transitory activation profiles that range from killing pathogens and antigen presentation to the secretion of matrix metalloproteinases or even collagen to rapidly close wounds [25]. The focus of this work lies on three major groups of macrophage subtypes, which are described in more detail below.

**Pro-inflammatory macrophages (M1)** The phrase pro-inflammatory or classically activated macrophage usually refers to macrophages with enhanced microbicidal and tumoricidal properties [26]. Pro-inflammatory macrophages can be generated either through sterile inflammation (apoptosis, necrosis, or tumorigenesis) via interferons or TNF $\alpha$  or through inflammation involving intruding pathogens and the recognition of lipopolysaccharides (LPS) [1]. The release of pro-inflammatory cytokines by classically activated macrophages is a crucial immune defense mechanism, yet failure to return to homeostasis after elimination of the threat can in return also cause significant host harm. For example, the secretion of IL-1, IL-6, and IL-23 by pro-inflammatory macrophages has been linked to the formation and growth of TH17 cells [27-29]. These cells release IL-17, a cytokine linked to increased polymorphonuclear leukocyte (PMN) recruitment to tissues, which can lead to inflammatory autoimmune diseases [30].

**Wound-healing macrophages (M2a)** Wound-healing macrophages, like classically activated macrophages, can grow in response to innate or adaptive cues. IL-4 is known to be one of the earliest inherent signals generated upon tissue injury [31]. Although other granulocytes may potentially contribute, basophils and mast cells are crucial early sources of innate IL-4 production [32, 33]. This early IL-4 production rapidly increases arginase activity in macrophages, an enzyme that converts arginine to ornithine. Ornithine is a direct precursor of polyamines and collagen and a key element in ECM production [34, 35]. However, dysregulation of this ECM-enhancing activity of wound-healing macrophages can lead to fibrosis and eventually to organ failure, similar to classically activated macrophages in autoimmunity [6, 36, 37].

**Regulatory macrophages (M2c)** Regulatory macrophages, like the other two macrophage populations discussed above, can emerge as a result of innate or adaptive immune responses. Regulatory macrophages do not secrete extracellular

matrix, and instead express high levels of HLA-DR or CD86 for enhanced antigen presentation [38, 39]. However, in contrast to pro-inflammatory macrophages, regulatory macrophages dampen the immune response and are responsible for the prevention of chronic inflammation, which can cause severe harm to the surrounding tissue [39-41]. Numerous protocols are available on how to create regulatory macrophages, but no single molecular mechanism has been identified yet [40]. The hypothalamic–pituitary–adrenal (HPA) axis has been identified as an important regulator of M2c macrophage plasticity [42, 43]. In reaction to stress, adrenal cells release glucocorticoids, which dampen the transcription of pro-inflammatory cytokines, decrease mRNA stability and subsequently reduce macrophage-mediated host defense [44, 45].

### 1.1.3. Mechanosensing of Macrophages

Cells scan their physical environment using mechanosensors, which interact with the ECM or neighboring cells and provide signals to the cytoskeleton [46]. Actin and microtubule polymerization and depolymerization exert traction pressures on the environment of a cell. Integrins transmit tensional forces between the ECM and the cytoskeleton via focal adhesion complexes (FACs) and convert them into biochemical signals [47, 48]. High tensional forces lead to the unfolding of the cytoskeletal protein talin and the exposure of otherwise cryptic binding sites. In turn, another FAC protein, vinculin, can bind to talin and form a signaling complex that initiates phosphorylated signaling cascades. This initiates several downstream processes such as cytoskeletal alterations or the induction of transcriptional regulatory networks [49].

Thus, mechanosensing of macrophages is an essential part of the induction of the foreign body immune response, which leads to prolonged inflammation and fibrosis around implants and increases tissue stiffness [50, 51]. It has been shown that macrophage activation is influenced by physicochemical properties and surface structures of implant materials. For example, Hotchkiss et al. found that higher degrees of surface roughness on titanium implant materials enhanced the anti-inflammatory properties of primary murine macrophages [52].

Implant materials exhibiting a stiff, non-physiological e-modulus are associated with a more severe foreign body response, increased fibrosis, and thicker fibrous capsule development when compared to softer implants, implying that stiffness-enhanced inflammation has major pathogenic consequences [53-55]. Furthermore, an increase

in tissue stiffness is observed in several illnesses driven by macrophages [56]. While stiffness has a significant impact on macrophage activity, the molecular processes underlying macrophage activation are currently under investigation.

Stretch-activated ion channels allow ions to pass through the cell membrane and convert external physical stimuli into electrochemical activity which in turn initiates signaling cascades and modulates cell behavior. Known representatives of this group are for example transient receptor potential vanilloid channels (TRPV), the Twik-related arachidonic-acid activated K<sup>+</sup> channel (TRAAK), and the TWIK1-related K<sup>+</sup> channel (TREK1) [57], and the PIEZO channels 1 and 2, whose discovery by Coste and Patapoutian was honored with the Nobel Prize in 2021 [58]. Several recent studies found that the mechanically activated, non-specific cation channel Piezo1 is involved in several developmental processes and malfunction has been linked to various pathologies [59-61], as it transduces a variety of mechanical cues [53]. Piezo1 has been discovered as a mechanosensor of pressure and shear stress in myeloid cells attracted to the lung, heart, and bladder, and channel activity has been observed to induce inflammation [62]. However, under normal physiological conditions, macrophages are usually not exposed to such high mechanical forces. Thus, macrophages are more likely to sense physiological alterations in stiffness and composition of their surrounding ECM [63, 64]. While Piezo1 has been shown to sense stiffness in neural stem cells and glial cells [60, 65], its involvement in macrophage stiffness sensing is still in its infancy [53]. In 2021 Atcha et al. were able to demonstrate for the first time that IFN $\gamma$  and lipopolysaccharide LPS-induced inflammation is highly dependent on Piezo1 expression and depletion of Piezo1 increases IL4 and IL13-induced healing responses in murine macrophages [53]. An overview of mechanosensing mechanisms in macrophages is given in Figure 3.

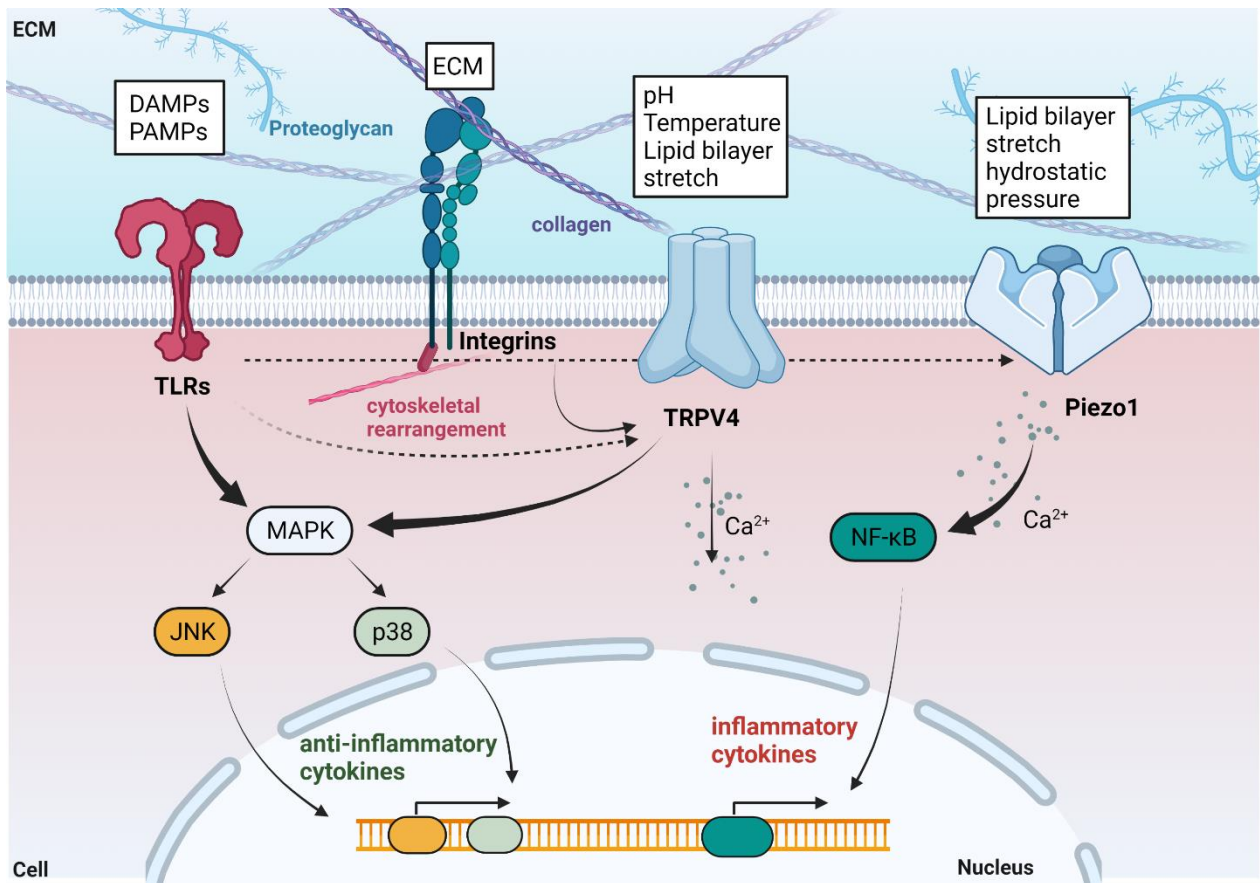


**Figure 3 Schematic illustration of mechanosensing mechanisms in macrophages.**

Macrophages can sense strain and pressure via several mechanisms and receptors. Integrins sense variations in ECM stiffness and are directly linked to the cytoskeleton. TRPV4 is activated by mechanical and chemical stimuli, which leads to calcium ion influx and the activation of several transcription factors, including MAPK, JNK, and p38. The translocation of these transcription factors to the nucleus induces the expression of anti-inflammatory cytokines. Piezo1 is activated by mechanical stimuli only and, like TRPV4, allows the influx of calcium ions. However, activation of Piezo1 leads to translocation of the transcription factor NF-κB and the induction of proinflammatory cytokines. In addition, all receptors can also be activated indirectly via interaction with toll-like receptors (TLRs). This figure was adapted from Orsini et al. [66].

#### 1.1.4. In Vitro Systems to Model Human Macrophage Biology

Human macrophage in vitro models differ in several phenotypic and functional aspects. It is therefore mandatory to holistically describe the macrophage model used for a study. Biological origin, activating stimulants, and surface antigens chosen for characterization are important factors to consider [24]. Several comprehensive

validations of human macrophage phenotypic indicators, as well as maturation and activation strategies, have been described [67, 68]. Surface markers can be useful indicators of macrophage function. For example, the expression of scavenger receptors allows for the analysis of phagocytic activity in macrophages [69]. Furthermore, cell-cell interaction is critical for macrophage function in disease progression and tissue homeostasis. For example, macrophage-derived factors are known to influence, among other things, infection response, inflammation resolution, adipose tissue biology, and cancer progression [2, 41].

The THP-1 acute monocytic leukemia cell line is a common macrophage in vitro model system. Since it is an immortalized cell line, THP-1 cells can be maintained in culture and passaged for extended periods of time. The variability of the individual passages is significantly lower than that of primary cells derived from different donor individuals [70]. THP-1 cells acquire a macrophage-like phenotype after differentiation with phorbol 12-myristate 13-acetate (PMA) or other stimuli, which mimics primary human macrophages in various ways [71, 72]. THP-1 cells' malignant background may elicit different responses than primary somatic cells in their normal context and the biological significance of the THP-1 cell model has recently been questioned [73]. The two model systems differ in key functions, including response to pro-inflammatory stimuli, cell-cell interaction, and polarization potential, among others [73, 74].

THP-1 cells can respond to the polarization techniques utilized for primary macrophages, but to a degree that can considerably differ from what is seen in human peripheral blood monocyte-derived macrophages (MDMs) [74]. It is thus important to assess the physiological behavior of THP-1-derived macrophages as an alternate model system to primary macrophages in a new experimental setting. [73].

## 1.2. Raman Microscopy in Cell Biology

Raman spectroscopy has evolved into a valuable tool for chemists, physicists, biologists, and materials scientists alike as it allows the study of chemical structure, crystallinity, and other molecular interactions within a sample. It is a type of vibrational spectroscopy, i.e., it measures the molecular vibrations caused by chemical bonds that interact with a monochromatic light source.

### 1.2.1. The Raman Effect and Raman Scattering

Raman spectroscopy is named after the Raman effect, also known as the inelastic scattering of light, which was discovered by C. V. Raman in 1928. They discovered that a small fraction of the scattered light lost or gained energy and did not maintain its original energetic level; this scattering is now known as Raman scattering [75]. Typically, a monochromatic light source is interacting with a specimen and the energy difference between the incident and scattered photons is analyzed. The amount of lost (Stokes) or acquired (anti-Stokes) energy corresponds to a specific molecular vibration and detection of these scattered photons results in a Raman spectrum comprised of several vibrational frequencies (Figure 4) [76]. Based on the chemical bonds within it, each molecule has its fingerprint or spectrum [77, 78].

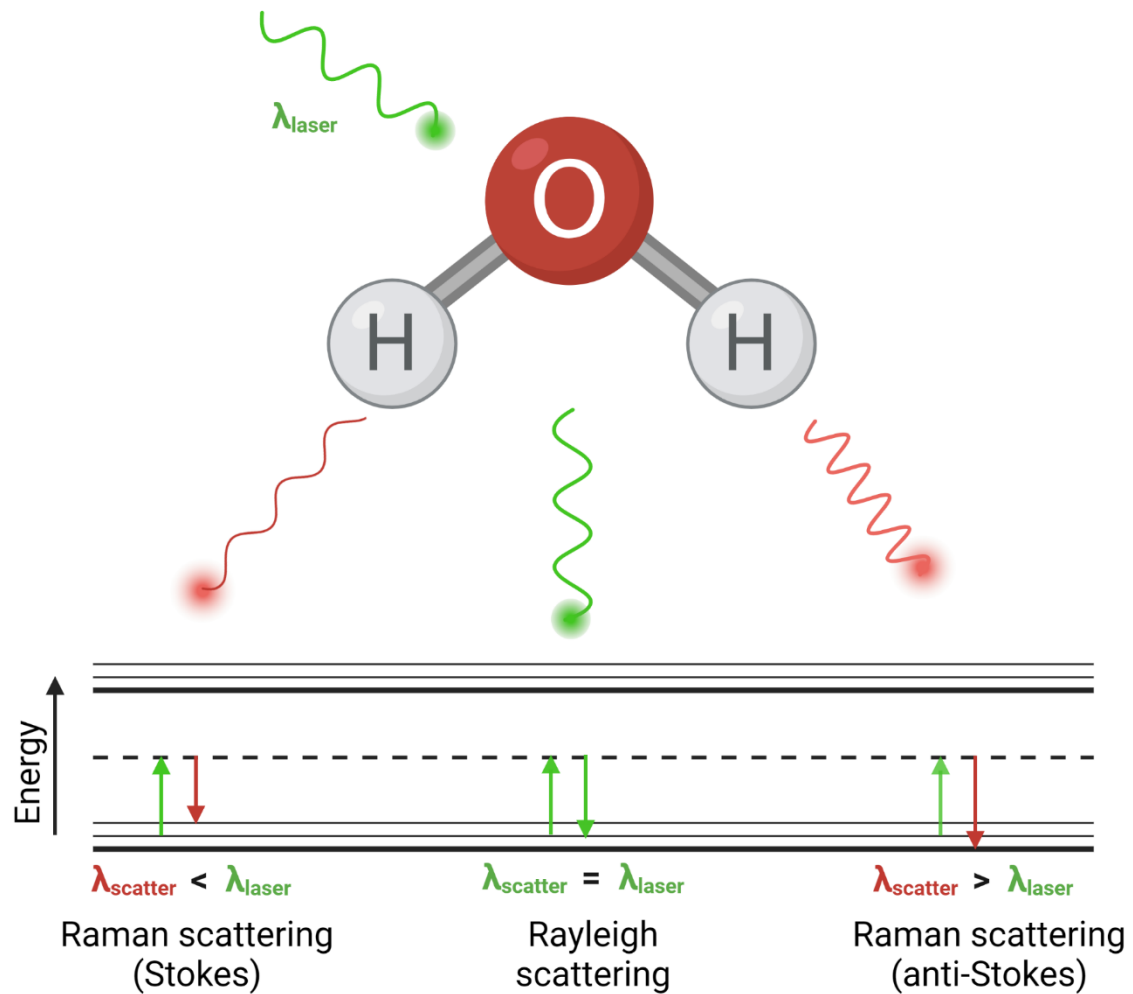


#### Figure 4 Principle of Raman scattering

When light interacts with a molecule, energy can be maintained (Rayleigh scattering) or shifted (Raman scattering). If energy is lost, this shift is defined as Stokes, while a gain of energy is defined as anti-Stokes. In most cases, the Stokes shift is more frequently observed at room temperature.  $\lambda$  = wavelength. Figure adapted after Lin et al. [79].

### 1.2.2. Raman Microspectroscopy and Raman Imaging on Biological Samples

Biological samples are usually comprised of many distinct molecules and functional groups and thus require elaborate data interpretation. One of the primary benefits of Raman spectroscopy is the ability to resolve major classes of biomolecules: proteins, lipids, and nucleic acids may be visualized based on their vibrational spectra, eliminating the requirement for cells to be labeled or stained before imaging (Figure 5) [80-82]. Because water has a weak Raman signal, unfixed cells can be observed in situ under normal physiological conditions, allowing for live-cell imaging [83]. However, extended acquisition periods and high laser intensities still prevent RM from being used for clinical or diagnostic purposes on a regular basis [77, 78]. This is primarily because spontaneous Raman scattering is a rare event: Only around 1 out of  $10^8$  photons that interact with a substance are inelastically scattered [84]. A variety of innovative techniques is beginning to overcome these limitations, allowing Raman spectroscopy to become an alternative to established methods of cell imaging. The combination of a Raman spectrometer with a standard confocal microscope was one of the most significant milestones in single cell Raman spectroscopy [85]. Confocal Raman spectroscopy can visualize or map samples in addition to collecting Raman spectra by connecting the Raman spectrometer to a camera, often a charged-coupled device (CCD), allowing for the visualization of intracellular components (Figure 6) [77, 78].

A typical Raman analysis can rapidly acquire a large, comprehensive set of data. The extraction of biological information, however, becomes more difficult with increasing data set size, and analysis of Raman data sets usually requires dimensionality reduction. To distinguish and visualize the spectral contribution of different biological structures, supervised or unsupervised learning algorithms are employed. This way, false color heat maps are created visualizing the distribution of DNA, lipids or ECM proteins in a biological sample. This makes RM a promising tool for the in vivo diagnosis of pathological tissue alterations and cancer diagnosis [86, 87]. For example, it was shown that Raman spectroscopy can reliably identify invasive glioma in situ during surgery with a sensitivity and specificity of 90% and above [88].



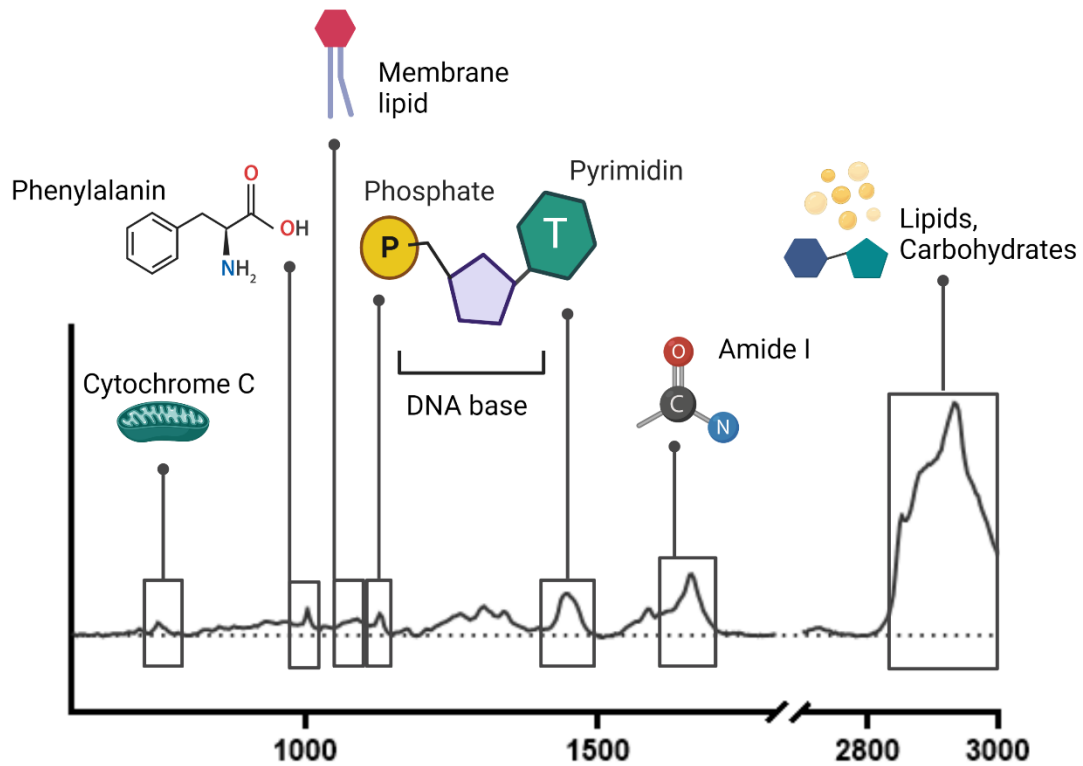


**Figure 5 Raman peaks of eukaryotic cells**

*Biological samples are comprised of many different chemical constituents, requiring careful interpretation of Raman spectra. However, some Raman peaks can be assigned to certain organic structures, such as cytochrome c (mitochondria), phosphate and pyrimidine (nucleic acids), Amide I and phenylalanine (proteins), phospholipids (membrane) or fatty acids (intracellular lipids, vesicles).*

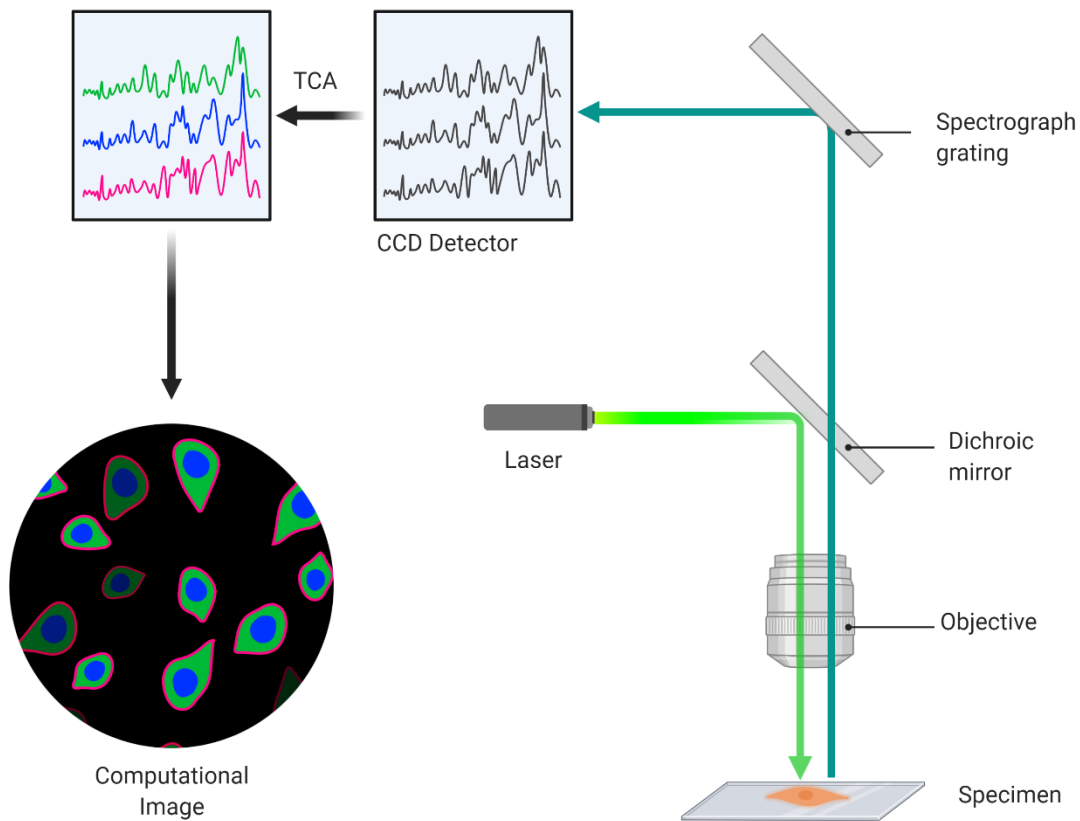


### Figure 6 Principles of Raman spectroscopy and Raman imaging

*A biological sample, e.g. cells or tissue, is scanned pixel by pixel using Raman spectroscopy. The obtained spectral information can further be used to identify cell components sharing certain spectral characteristics. False-color heat maps are then generated to visualize the sample and its components.*

#### 1.2.3. Raman Microspectroscopy in the Context of Conventional Imaging Techniques in Molecular Cell Biology

Today cells can be visualized by a variety of different imaging techniques. Traditionally, cell imaging is performed on fixed cells, primarily using brightfield, fluorescence, and electron microscopy [89]. While these approaches contribute essential structural and biochemical information, they only provide an endpoint analysis of the cell's condition at the time of the fixation [83]. Furthermore, cells are frequently labeled before imaging, which has the potential to create artifacts and distort the true intracellular state [77, 90]. Phase contrast and differential interference contrast microscopy allow for live cell imaging without prior staining [78, 91]. Images obtained using these techniques are often collected faster than those obtained using Raman spectroscopy. However, there

is a lack of chemical specificity and the possibility of artifacts introduced due to labeling. [90]

Fluorescence microscopy, which allows the detection of single molecules within a cell, is widely used in live cell imaging. It allows researchers to identify specific cellular structures by either using fluorophore-conjugated antibodies or intracellular expression of fluorescent proteins [92]. However, fluorescence microscopy relies on the fluorescent labeling of the cells, which can directly impact cell physiology. As a result, fluorescence imaging may not reflect the actual cellular environment when compared to Raman-related techniques. Fluorescence microscopy techniques can be enhanced to provide cellular resolution below 20 nm (e.g. STORM (stochastic optical reconstruction microscopy) or PALM (photo-activated localization microscopy)) [93-96]. While Raman spectroscopy achieves resolution down to 200 nm [97], it does not require fluorescent markers and offers the advantage of increased chemical specificity.

Another vibrational spectroscopy approach that is commonly used for live cell imaging is infrared spectroscopy (IR). Both IR and Raman spectroscopy are considered non-invasive and non-destructive, can identify the underlying chemical structure of a specimen, and do not require sample preparation.

While IR spectroscopy detects heteronuclear functional group vibrations and polar bonds (particularly OH stretching in water), Raman spectroscopy is sensitive to homonuclear molecular connections. It may, for example, discriminate between C-C, C=C and C-H bonds [98]. In conclusion, water is a significant absorber of infrared radiation, and measurements of aqueous solutions can be challenging. Raman spectroscopy is therefore frequently favored over IR spectroscopy for live cell imaging because cells can be maintained under physiological settings [78].

While all the listed techniques here offer certain advantages in biomedical research, there is a great deal of interest in further developing Raman spectroscopy and imaging due to its potential for non-invasive in vivo illness diagnostics [99-102]



# Chapter 2

## Objective of the Thesis

### **2. Objective of the Thesis**

The focus of this work is to identify macrophage responses to environmental stimuli at the molecular level. For this purpose, alternative methods to conventional immunological assays, such as flow cytometry, were established. The first step of this work was to evaluate how well the activation of adherent macrophages can be analyzed using common surface antigens. Different dissociation methods and how they affect cell harvesting, viability as well as preservation of surface antigens were compared. Since most detachment methods either come at the expense of cell viability or result in degradation of surface antigens by enzymatic treatments, the second part of the thesis addresses non-invasive RM as an alternative analysis method. RM is a common method in materials science to analyze the purity of materials but is now increasingly applied in biology. However, data on how well RM can detect macrophage activation is still limited. In this work, we hypothesized that the molecular composition of macrophages changes by the different activation stimuli to such an extent that different Raman fingerprints are generated, which can be used to identify cells with unknown activation status. RM can also be used on adherent macrophages, for example, to investigate their activation by implant materials without the need for further processing of the cells.

Primary human macrophages can be isolated directly from the peripheral blood of patients or volunteers with relatively little effort and used for further in vitro cell culture. However, working with primary immune cells also has some inherent drawbacks. The human immune system is extremely heterogeneous between individuals in order to be able to protect a population from various infections. However, with a small number of subjects, this variability makes it difficult to make general statistical statements about large populations. The third part of this thesis, therefore, deals with the THP-1 cell line and its comparability with primary human macrophages and how both cell types differ in their molecular composition before and after activation. Although THP-1 cells are also derived from humans, they are of myeloid leukemia origin and differ substantially in some properties from macrophages derived directly from peripheral blood monocytes.



# Chapter 3

## Results & Discussion

The content is based on:

Feuerer N, Morschl J, Daum R, Weiss M, Hinderer S, Schenke Layland K, Shipp C. "Macrophage retrieval from 3D biomaterials: A detailed comparison of common dissociation methods." J Immunol Regen Med, 2021, 1, 100035.

Feuerer N, Marzi J, Brauchle E, Carvajal Berrio D, Weiss M, Billing F, Jakobi M, Schneiderhan-Marra N, Shipp C, Schenke Layland K. "Lipidome profiling with Raman Spectroscopy identifies macrophage response to surface topography of biomaterials". PNAS, 2021, 118 (52) e2113694118.

Feuerer N\*, Carvajal Berrio DA\*, Billing F, Segan S, Weiss M, Rothbauer U, Marzi J, Schenke Layland K "Raman Microspectroscopy Identifies Biochemical Activation Fingerprints in THP-1-and PBMC-Derived Macrophages." Biomedicines 10.5 (2022): 989.

*\*These authors contributed equally*



### **3. Results and Discussion**

#### **3.1. Enzymatic Dissociation from Electrospun Substrates Selectively Impacts Macrophage Surface Antigens**

Macrophages can serve as promising models to assess and screen the immunocompatibility of potential implant materials *in vitro*. As macrophages are typically highly adherent and tend to infiltrate into porous substrates, their subsequent analysis by conventional analytical methods poses several challenges. In many cases, cell scraping is the method of choice to detach adherent macrophages from cell culture polystyrene and to avoid enzymatic alterations of surface antigens. In contrast to common ceramics or metals, many modern biosimilar materials have porous, ECM-mimicking structures that encourage cell infiltration to enhance the formation of new tissue. These materials do not allow the scraping of cells and several laborious steps are required to separate cells from their substrate. In addition, the scraping process imposes considerable stress on the cells, which manifests itself in increased apoptosis. Enzymatic digestion is a non-mechanical alternative that detaches cells from their substrate by proteolytic cleaving. However, this process is unspecific and prone to induce alterations in cell surface antigens. This is especially problematic for flow cytometry analysis, as it relies on surface antigens for phenotyping and assessment of activation status (Figure 7).

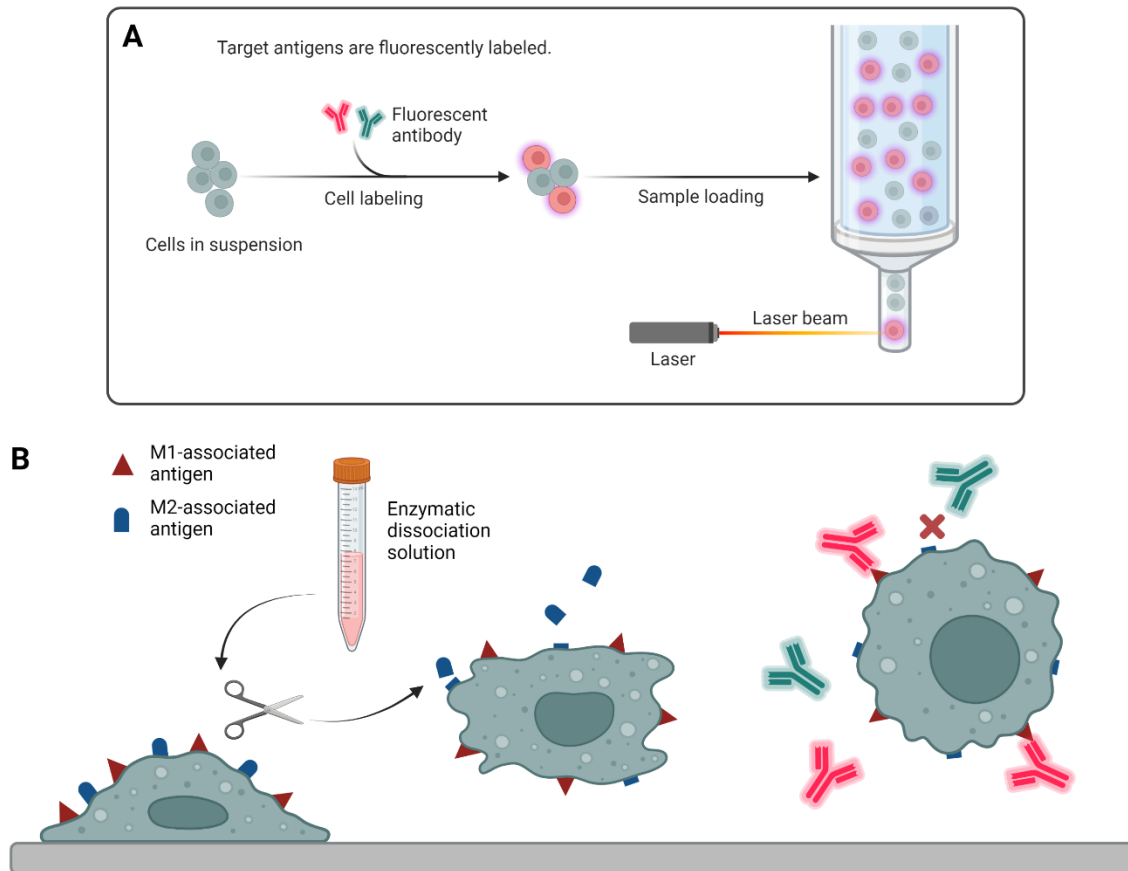


**Figure 7 Enzymatic dissociation selectively impacts macrophage surface antigens**

(A) To perform flow cytometry analysis, cells need to be in suspension. Fluorescently labeled antibodies are added to bind to selected antigens. The mean fluorescence intensity is then analyzed, providing insight into the presence and/or quantity of the labeled antigen. (B) Macrophages become strongly adherent during their time of culture. To be analyzed by flow cytometry, enzymatic detachment is usually necessary. However, common detachment protocols using Accutase or Trypsin selectively cleave some antigens necessary for macrophage phenotyping.

To evaluate the influence of dissociation solutions on common macrophage surface antigens, we treated in vitro cultured primary human macrophages with Trypsin, Accutase, ethylenediaminetetraacetic acid (EDTA), and a ready-to-use macrophage detachment solution by Promocell (PMDS). Yield, viability, phagocytic activity, and antigen conservancy were analyzed to compare efficiency and robustness. All

solutions were compared to a control of scraped cells that had not experienced further treatment.

The results showed that non-enzymatic EDTA solutions fail to effectively detach MDMs from well plates, while both trypsin and Accutase surpassed cell yields obtained by scraping (Feuerer et al., **Appendix I**, Fig. 1A). We hypothesize that this effect can be contributed to low proliferative activity in mature macrophages since this method relies on the chelation of bivalent cations by EDTA that are required for continuous cell adhesion. However, some degree of proliferative activity is necessary for this approach to take effect. It is noteworthy that the commercially available macrophage detachment solution did not have superior performance compared to the in-house made EDTA solution. Interestingly, while most protocols recommend detachment of MDMs with EDTA on ice, our results showed that temperature seems to play only a minor role in detachment success: cold shock did not significantly increase the cell yield compared to incubation with EDTA at 37 °C. In addition, we investigated how these methods influence cell viability, hypothesizing that scraping will result in the highest cell death rates compared to non-mechanical treatments. Scraping tended to result in the harvesting of less viable cells when compared to enzymatic detachment, but scraping still tended to perform better than the non-enzymatic solutions (Feuerer et al., **Appendix I**, Fig. 1B). A possible explanation for these findings is the low number of harvested cells by non-enzymatic solutions, indicating that mostly dead or apoptotic cells were harvested while viable cells remained stuck to the bottom of wells.

We additionally investigated the effect of Accutase treatment over time on the detection of surface markers. The results showed that, as previously observed, CD86 was the most stable of all tested markers, with only minor changes in the levels of detected protein over time for all donors. In contrast, both CD206 and CD163 showed greater variability across donors when compared to CD86, with some donors showing greater sensitivity to loss of surface antigen than others. HLA-DR was also highly variable, with some donors showing a different trend across time in the levels of protein detected (Feuerer et al., **Appendix I**, Fig. 4). Overall, we observed more variation in the detection of the M2 markers CD206 and CD163 compared to the M1 marker CD86, while HLA-DR also showed donor-dependent differences. Though it has been argued

before that these changes in MFI are negligible [74], we show here that in some cases MFIs are reduced up to almost 50%, significantly changing the interpretation of results and potentially altering macrophage phenotype classification.

MDMs are known for their phagocytic ability, especially the M2 phenotype which expresses CD206 (mannose receptor) and CD163 (hemoglobin scavenger receptor). As such, these cells typically possess increased phagocytic capacity compared to M1 macrophages, since one of their main functions is the clearance of cellular debris from damaged or infected tissue. Thus, we investigated how macrophage dissociation using Accutase impacts the uptake of dextran. In these experiments, MDMs were either treated with Accutase for 3 min or 10 min and subsequently harvested and reseeded with FITC-conjugated dextran beads. As controls, macrophages were either left untreated or harvested via scraping. Uptake of FITC-dextran was examined at 30 min and 3 h in all groups and subsequently measured using flow cytometry (FC). We observed the biggest difference in the uptake of dextran particles between the untreated control cells and treated cells. This effect was independent of the detachment procedure. There was a trend for MDMs treated with Accutase for 10 min to take up less dextran at the 30 min time point when compared with treatment for 3 min or scraping, but apart from this no major differences across experimental conditions were detected (Feuerer et al., **Appendix I**, Figure 5). This indicates that the dissociation process per se is far more disruptive to the phagocytosis of macrophages than the cleavage of CD206 or CD163.

To test if Accutase treatment can effectively detach MDMs from a biomaterial, we investigated MDM removal from electrospun polymers. Electrospinning is a popular technique to create non-woven scaffolds with randomly oriented fibers that mimic natural ECM. Electrospun materials serve as popular scaffolds for enhanced wound healing and tissue regeneration [103-105]. Since these materials are fibrous by nature, adherent cells are difficult to remove from the substrate as they typically infiltrate into the pores of the scaffold. Here, two polymers widely used in regenerative medicine were chosen. Poly(lactic acid) (PLA), a biodegradable polymer, and a non-degradable polyurethane (PU) [106, 107]. Both were electrospun and prepared for cell culture according to protocols that have been established previously in our laboratory [108,

109]. Monocytes from three donors, each with three technical replicates, were seeded on each electrospun scaffold and standard tissue culture polystyrene plates. The cells were then cultured and matured to MDMs before being treated for removal. The results showed that after a 10 min incubation with Accutase, the highest number of cells was detached from the polystyrene control (Feuerer et al., **Appendix I**, Fig. 6A, D). Results from the PLA scaffold (Feuerer et al., **Appendix I**, Fig. 6B, E) show that a similar percentage of cells were detached from this material as the control well plate. Detachment from electrospun PU, however, was less efficient since up to 90% of the cells remained on the scaffold after Accutase treatment (Feuerer et al., **Appendix I**, Fig. 6C, F). The cellular adhesion process is multifactorial and to a great extent determined by the substrate. Wettability, pore size, fiber size, and surface energy all influence cell adhesion [110]. While the analyzed scaffolds in this work did not significantly differ in wettability, the fiber size of PU was several-fold higher ( $775 \pm 163$  nm) compared to PLA ( $156 \pm 6$  nm). Large pores facilitate cell infiltration and provide more surface area for cells to adhere making pore size a possible factor in the success of cell detachment.

Ultimately, we were able to show that the choice of detachment method has a significant effect on viability and surface antigen stability. Typical macrophage classification antigens such as CD163 and CD206 are particularly affected by enzymatic treatment, so that cautious data interpretation is required when classifying macrophages by flow cytometry. Furthermore, our results suggest that the choice of detachment protocol should be made in dependence of the substrate and that further protocol optimization is likely to be required.

### 3.2. Raman Microspectroscopy Discriminates Macrophage Activation in a Marker-Independent Manner

As discussed in chapter 3.1, macrophages are strongly adherent cells. They recognize altered mechanical stimuli and substrates in their immediate environment and activate corresponding molecular programs. Since macrophages are extremely plastic cells, changes occur at both the cell's biological and metabolic levels. Both wound healing

and the tolerance of prostheses and implants often depend on the long-term response of macrophages, with chronic inflammation and severe scarring often being undesirable outcomes. It is, therefore, feasible to design biomaterials to support accelerated wound healing and prevent chronic inflammation. The main challenge is to identify material properties that favorably influence macrophages. However, this depends largely on how the macrophage response is characterized at the molecular level. Conventional methods either involve endpoint analyses with predefined antigen markers (flow cytometry) (Feuerer et al., **Appendix II**, Figure 1E-H) or sacrifice single cell resolution (e.g. enzyme-linked immune sorbent assay (ELISA) or multiplex assays) (Feuerer et al., **Appendix II**, Figure 1J-Q). In this part of the dissertation, an exploratory analysis method using Raman microspectroscopy is presented, which allows the analysis of single adherent macrophages without further cell preparation procedures (Figure 8). We also show that this method can be used to identify macrophage activation on various substrates.

Monocytes were seeded on cell culture polystyrene, matured to MDMs, and polarized using IFN $\gamma$  + LPS (M1), IL-4 + IL-13 (M2a), or IL-10 (M2c); In addition, monocytes were also seeded on different material substrates including glass, machine polished titanium (Ti M) and acid etched titanium (Ti A). Hyperspectral images were acquired of the adherent cells and based on their Raman spectra, major cell components were identified including proteins, nucleic acids, and lipids (Feuerer et al., **Appendix II**, Figure 2). Raman spectra were then extracted and further processed for principal component analysis (PCA). An overview of the workflow is given in Figure 6 A – D.

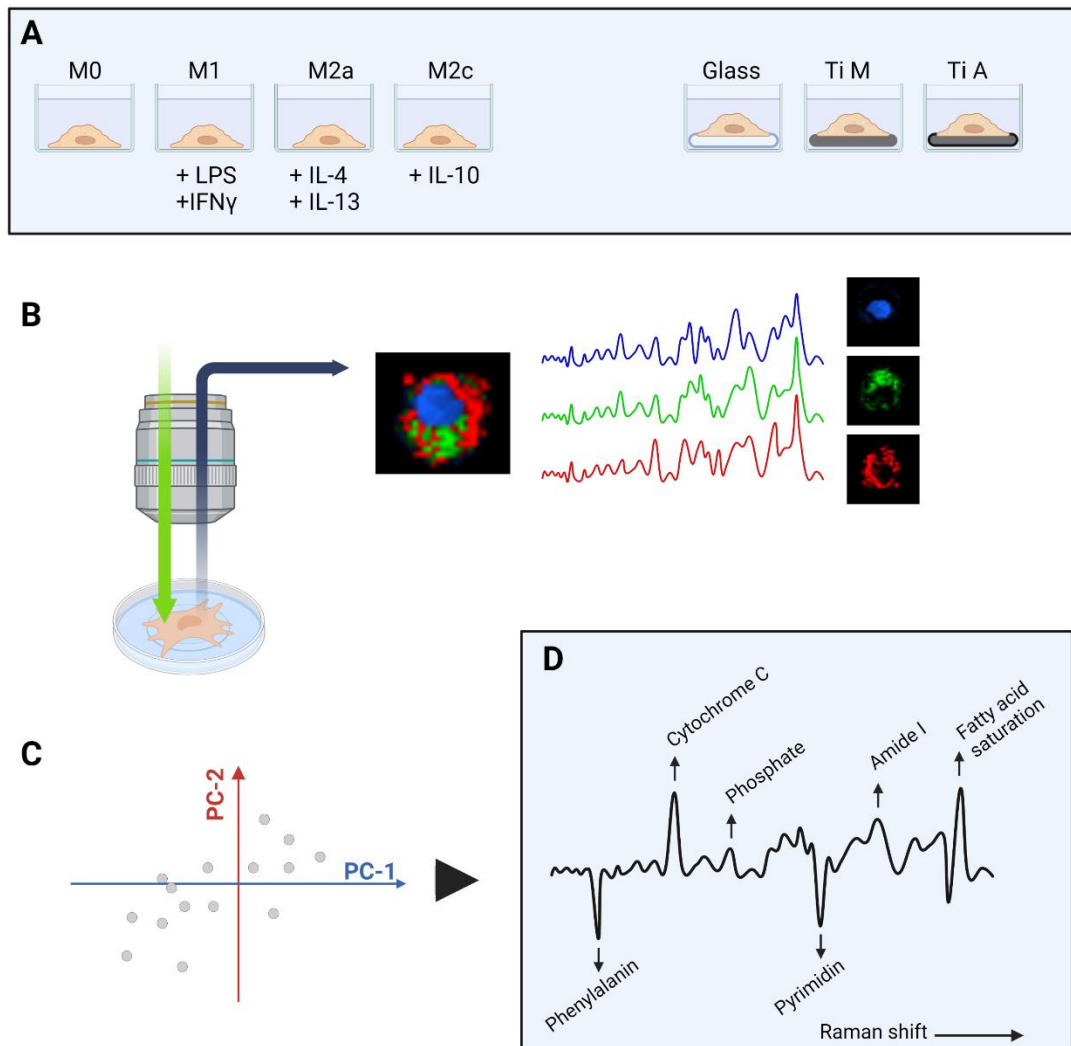


### Figure 8 Multivariate Data Analysis of Raman Spectra of Macrophage Activation

The macrophage response toward several exogenous stimulants was assessed using RM. (A) MDMs were either treated with pro- or anti-inflammatory cytokines or cultured on glass, machine polished titanium (Ti M) or acid etched titanium (Ti A). (B) Hyperspectral Raman images were acquired and cell components were visualized using false color intensity heat maps. (C) Spectra from cell components were extracted and analyzed using PCA. (D) PCA Loading plots were employed to identify specific biochemical changes in the cell.

### 3.2.1. Macrophage Activation is Predominantly Characterized by a Change in Lipid Composition

We found a significant separation of all four MDM subtypes when comparing lipid Raman spectra (Figure 9 A & B), indicating that lipid composition undergoes substantial changes during the polarization process (Feuerer et al., **Appendix II**, Figure 3 A-C) [111]. Raman peaks at  $1440\text{ cm}^{-1}$ ,  $1655\text{ cm}^{-1}$ ,  $2885\text{ cm}^{-1}$ , and  $3010\text{ cm}^{-1}$  attributed to the C=C double bond of unsaturated fatty acids, were shown to contribute to the separation of the polarized groups (Figure 9 C & D; Feuerer et al. **Appendix II**, Figure 3 D & E). It has been reported that the relative intensities of the C=C stretch at  $1655\text{ cm}^{-1}$  and the  $\text{CH}_2$  bending at  $1440\text{ cm}^{-1}$  provide insight into the ratio of saturated vs. unsaturated fatty acids within the cell [112]. In this work, we identified the presence of linoleic [113] and palmitoleic [114] acid in macrophage lipids detected by RM by comparing them to spectra reported in the literature [115]. TAGs were identified by their ester molecule, which is indicated by the  $1744\text{ cm}^{-1}$  peak [116]. All Raman peaks and their assignments are listed in Feuerer et al. **Appendix II**, SI Table 1.

Lipids regulate many cellular and immunological activities, such as energy storage and cell signaling. Linoleic acid and other polyunsaturated fatty acids have a substantial effect on the inflammatory process by controlling the expression of pro-inflammatory cytokines like IL-1 and IL-6 [113]. The degree of saturation in fatty acids, as shown by the loading plots in this work, significantly contributes to the PCA-based differentiation of macrophage subtypes. Macrophage lipid composition and RM's ability to track lipids were both demonstrated in prior studies [82, 117] with lipids playing a crucial role in both inflammation and MDM polarization [111, 118, 119]. A study by Montenegro-Burke et al. using supercritical fluid chromatography and mass spectrometry, confirms that M1, M2a and M2c polarized MDMs significantly differ in their membrane and intracellular lipid composition [118]. Fatty acid composition and turnover are closely linked to macrophage metabolic shifts during polarization, which makes lipid composition an ideal target for tracking macrophage polarization [111, 120, 121].



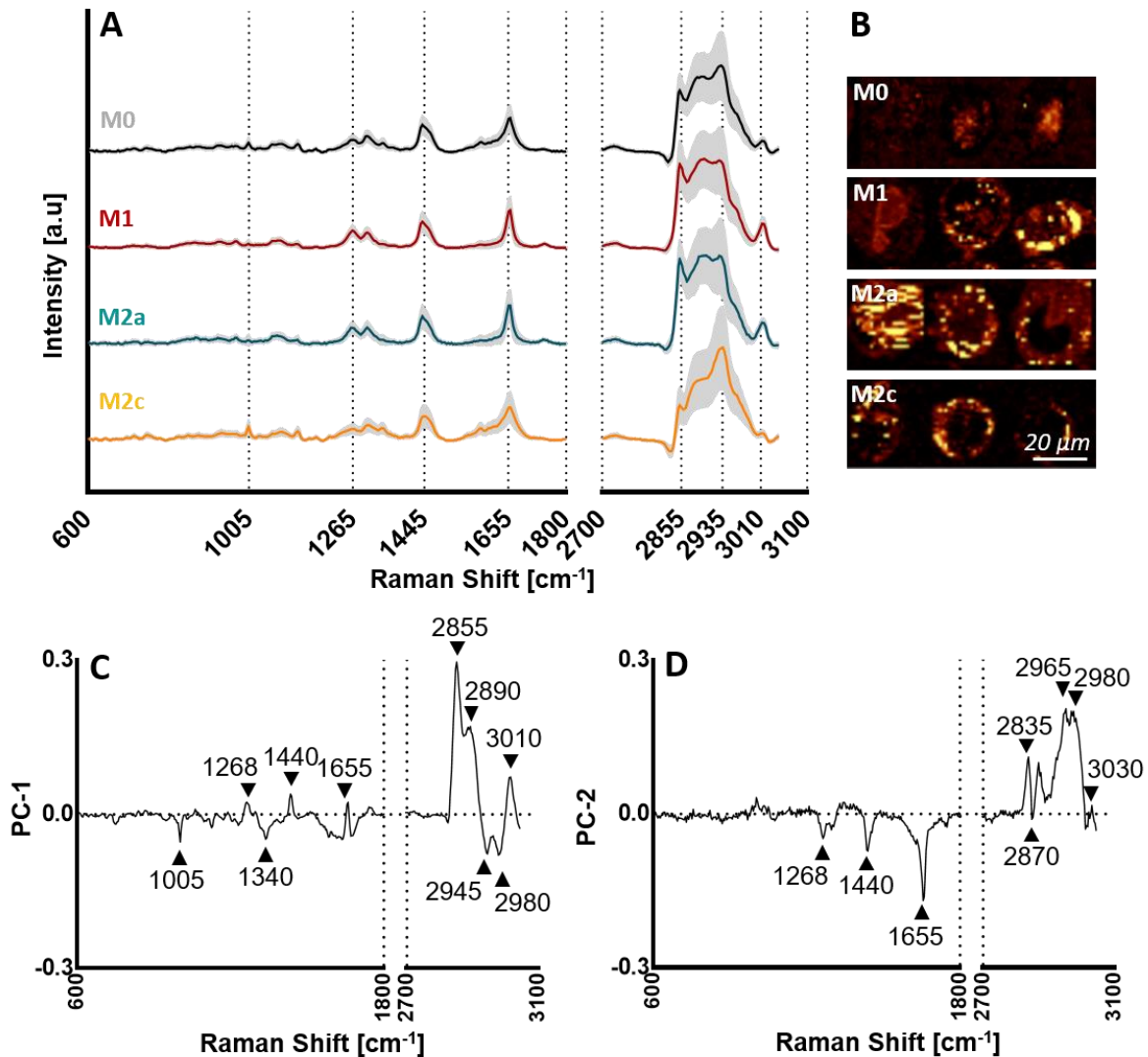


**Figure 9 Raman microspectroscopy identifies lipid fingerprints of macrophage activation**

(A) Fingerprint spectra of the lipid components were extracted from each macrophage subtype. (B) Heat maps show the distribution of lipid spectra within the cell. (C) PCA loading plot of PC-1. Marked peaks indicate Raman shifts with the highest contribution to the separation of all four subtypes. Peak assignment is listed in Feuerer et al. **Appendix II SI Table 1**. Figure adapted from Feuerer et al. [122].

### 3.2.2. Raman Microspectroscopy Identifies Macrophage Activation Induced by Surface Topography of Titanium Disks

We examined whether RM analysis might be utilized to track lipidome changes in MDMs and use the information to identify macrophage polarization. For this purpose,

glass and two titanium specimens with different surface topographies were used as culture substrates for human monocytes without the addition of any other stimulants like LPS or cytokines. Both brightfield and Raman images were acquired of the substrate-adherent MDMs after maturation (Figure 10 A). To put the MDM response into context, cytokine secretion and surface antigen expression were analyzed (Figure 10 B & C; Feuerer et al., **Appendix II**, Figure 4 G – N and SI Figure 3) showing a trend toward the M2 phenotype. When projected into the model of previously polarized MDMs, the means of M2c and macrophages adherent to Ti A clustered in close proximity to each other confirming the results obtained by FC (Figure 10 D). This finding is in accordance with other studies, demonstrating that rough, unorganized surfaces induce an anti-inflammatory M2c phenotype [52, 123, 124]. Poor survival and performance of common implants is linked to roughness-induced inflammation or fibrosis [125, 126]. However, changes in macrophage physiology are only poorly reflected when looking at established indicators of the cell response, such as cytokines and surface antigens [127]. In this setting, only the surface antigen CD206 was significantly increased (Figure 10 B) in MDMs cultured on titanium. CD206 is an M2a-associated surface receptor responsible for the scavenging of bacterial sugars and cellular debris and an indicator of increased phagocytosis [36]. Intriguingly, MCP-1, a chemoattractant cytokine responsible for the recruitment of monocytes, neutrophils, and lymphocytes, was significantly increased in M2a macrophages and macrophages adherent to Ti A but not in M1 macrophages.

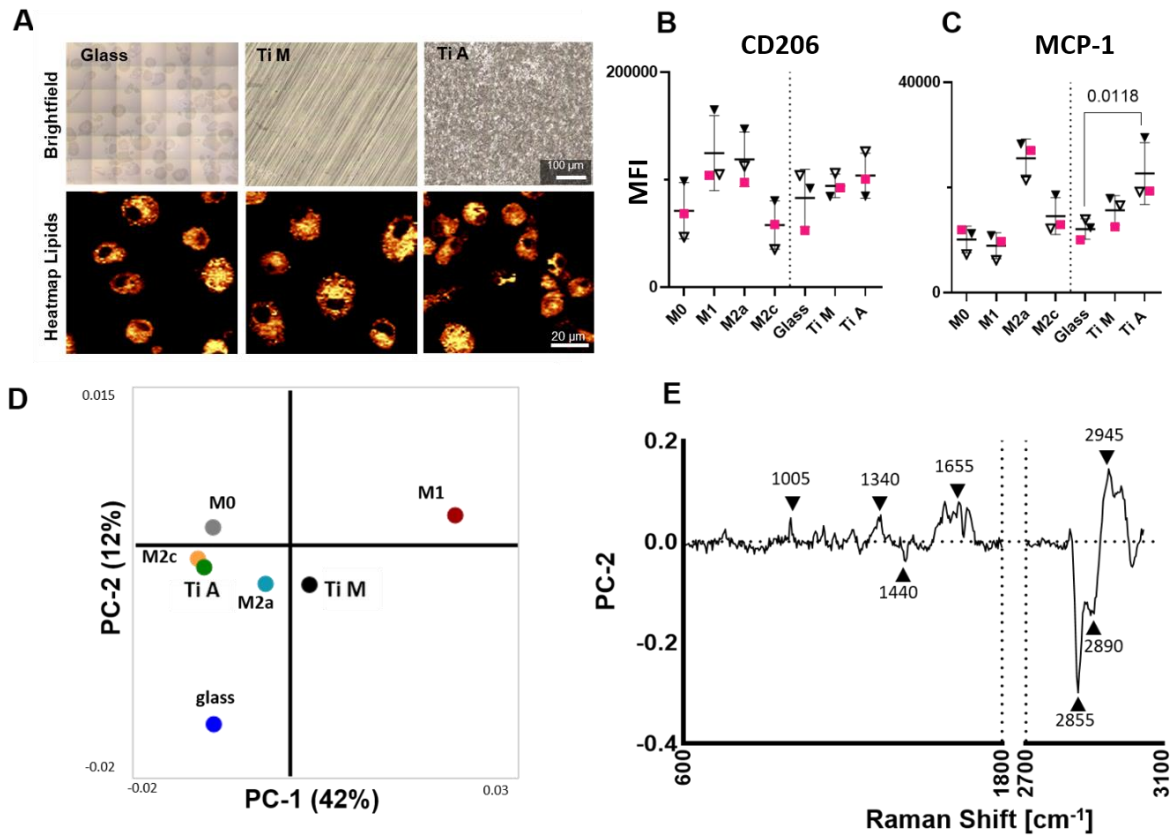


**Figure 10 Lipidome changes of macrophages activated by biomaterials can be identified by raman microspectroscopy**

(A) Brightfield images and Raman spectra heat maps of MDMs adherent to glass and titanium. (B) Cytokines expression of polarized MDMs and substrate-adherent MDMs. (D) PCA projection plot of polarized MDMs and substrate-adherent MDMs. (E) Loadings plot of PC-2 showing Raman shifts contributing to the separation of substrate-adherent MDMs on glass, Ti M, and Ti A. Peak assignment is listed in Feuerer et al. **Appendix II SI Table 1**. This figure is adapted from Feuerer et al. [122].

### 3.3. Raman Microspectroscopy Identifies Biochemical Activation Fingerprints in THP-1 and Monocyte Derived Macrophages

Monocyte-derived macrophages obtained from human peripheral blood and PMA-differentiated THP-1-derived macrophages were analyzed by RM, both before (resting) and after (activated) stimulation with LPS and IFN $\gamma$ . The spectral information obtained by RM was employed to detect molecular differences between both model systems induced by LPS and IFN $\gamma$ .

The THP-1 monocytic cell line and primary human MDMs circulating in the peripheral blood are both popular models for human macrophage biology. THP-1 immortalized cells are derived from the blood of an acute monocytic leukemia patient and differ from healthy, PBMC-derived macrophages in various aspects. [71-74]. For example, THP-1 monocytes are known to express significantly less CD14 than primary monocytes and are less susceptible to LPS treatment [128]. Furthermore, it was recently found that THP-1-derived macrophages have only limited ability to polarize into the M2 phenotype [74, 129].

To further elucidate molecular differences between both model systems during activation, RM was employed to holistically analyze THP-1-derived macrophages and MDMs before and after treatment with LPS and IFN $\gamma$ . While the response towards LPS and IFN $\gamma$  treatment has been analyzed by other groups using Raman spectroscopy [130, 131], to the best of our knowledge, no studies exist that compare occurring spectral changes between THP-1 and primary MDMs. We demonstrate that RM identifies chemical changes in nucleic acids, proteins, phospholipids, and fatty acids that occur during the inflammatory response of THP-1-derived macrophages and MDMs. In addition, we show that THP-1 derived macrophages and MDMs differ in their capacity to remodel during pro-inflammatory activation: While significant molecular changes were observed in MDMs in all four analyzed components, THP-1 derived macrophages only showed changes in phospholipids and protein content (Figure 11).

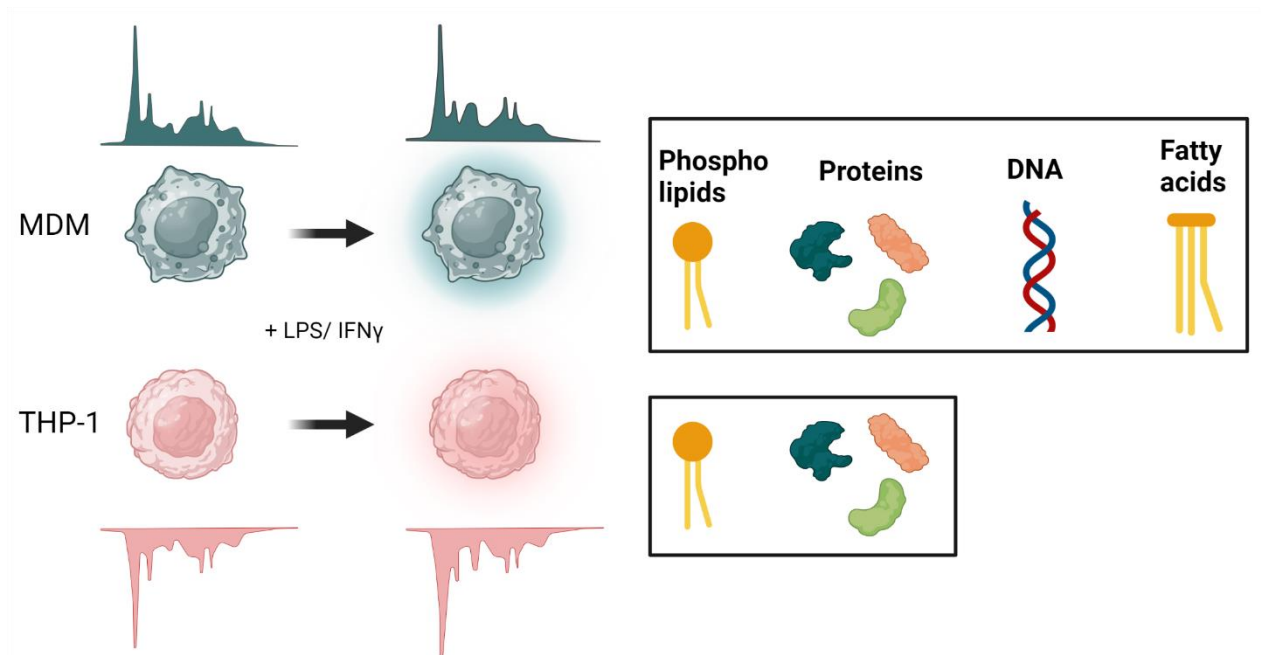


**Figure 11 Schematic overview of experimental setup to assess molecular remodelling in THP-1 and MDMs after pro-inflammatory activation.**

*THP-1-derived macrophages and MDMs were analyzed using RM before and after stimulation with LPS and IFN $\gamma$ . RM revealed that MDMs experience significant molecular changes in phospholipids, proteins, nucleic acids, and intracellular fatty acids. In contrast, THP-1-derived macrophages only showed changes in phospholipids and proteins.*

### 3.3.1. THP-1 and Monocyte Derived Macrophages Differ in their Molecular Composition

RM was employed to record hyperspectral images of THP-1-derived macrophages and MDMs. False color-coded intensity distribution heat maps were created using true component analysis (TCA) from Raman images (Feuerer & Carvajal et al., **Appendix III**, Figure 2 A & B). To define macrophage activation, routine FC analysis was performed in addition to RM measurements (Feuerer & Carvajal et al., **Appendix III**, Figure 1).

A total of four primary spectral components were found, ranging from nucleic acids (blue) through proteins (green) and two lipid-related components, intracellular fatty acids (red, also referred to as lipids A) and phospholipids (pink, also referred to as lipids B) (Feuerer & Carvajal et al., **Appendix III**, Figure 2 C).

**Table 2 Overview of Raman peaks assigned to four major cellular components analyzed in this work**

Component	Attributed Raman Peaks [ $\text{cm}^{-1}$ ]
<b>Cytoplasm</b>	749 , 1005 , 1585 and 1660
<b>Nucleic Acids</b>	785 , 1093 , 1340 and 1576
<b>Lipids A (intracellular fatty acids)</b>	1130 , 1265 , 1301 and 1445
<b>Lipids B (Phospholipids)</b>	1130 , 1265 , 1301 , 1445 , 719 and 876

Resting THP-1-derived macrophages and MDMs yielded comparable spectral signatures (Feuerer & Carvajal et al., **Appendix III**, Figure 3 B). All four components could be identified by PCA in both cell models (Feuerer & Carvajal et al., **Appendix III**, Figure 2). All analyzed peaks and their molecular assignments can be found in Feuerer & Carvajal et al., **Appendix III**, Table 1.

Component spectra of resting THP-1-derived macrophages and MDMs were compared using principal component analysis. PCA identified that most differences between THP-1 and MDMs can be found in the cytoplasmic component of

hyperspectral Raman images. PCA scores calculated from the cytoplasm revealed a very diverse scattering pattern with elevated cytochrome C bands at  $750\text{ cm}^{-1}$ ,  $1130\text{ cm}^{-1}$ , and  $1585\text{ cm}^{-1}$ , which are associated with mitochondrial activity and are known to have a major role in the immunological response [132].

In addition, increased bands at  $935\text{ cm}^{-1}$ ,  $1449\text{ cm}^{-1}$ , and  $1665\text{ cm}^{-1}$  (proline, valine, and amide I) were observed, which are typically associated with structural vibrations related to the 3D configuration of proteins. It can be hypothesized that inflammasome formation, a multiprotein complex involved in the initiation of the immune response, contributes to the signal [133-136]. These findings correlate with the observation that THP-1-derived macrophages showed increased cytokine expression in their resting state.

### 3.3.2. THP-1 and MDMs Differ in their Molecular Remodeling Capacity upon LPS and IFN $\gamma$ Stimulation

THP-1 and MDMs were activated by adding 100 ng/ mL LPS and 100 ng/ mL IFN $\gamma$  to the culture medium. Spectral Raman maps of 30 x 30 pixels were acquired before and after activation. In addition, FC analysis was performed to measure surface antigen and intracellular cytokine expression.

While FC analysis of surface antigens and intracellular cytokines provides the first evaluation of cell activation, it does not capture the long-term impacts of cellular remodeling. Previous research has indicated that THP-1-derived macrophages have a less significant polarization profile following pro-inflammatory activation than MDMs [74]. We were able to demonstrate that THP-1 macrophages and MDMs reacted to treatment with LPS/ IFN $\gamma$ ; however, Raman spectral analysis revealed unique remodeling patterns in specific cell components.

FC analysis identified differences in the expression of the chemokine MCP-1 and the surface antigen CD86, also known as B7.2., and the hemoglobin scavenger receptor CD163. While MCP-1 was increased in THP-1 macrophages after stimulation, a decrease was observed in MDMs. The opposite was observed for CD86, which increased significantly in MDMs after stimulation but not in THP-1 macrophages (Feuerer & Carvajal et al., **Appendix III**, Figure 1).

Since THP-1 is a cell line derived from monocytic leukemia, the failure to upregulate CD86 is likely based on an immune evasion mechanism typical for many cancers [137-139]. CD163 is a scavenger receptor and its upregulation indicates enhanced clearance of cellular debris and the onset of the healing process after tissue trauma. A significant loss of CD163 was observed in MDMs after activation but not in THP-1 macrophages. Most explanations that can account for these differences are hypothetical. For example, differences in genetic variability or alterations in molecular kinetics can contribute to the reported results.

Multivariate analysis of the Raman spectral data revealed that proinflammatory alterations in THP-1 were shown to be predominantly linked with changes in cytoplasmic content and phospholipids, in contrast to MDMs, which demonstrated significant differences before and after activation in all examined cellular components. The most significant Raman bands are depicted in the assigned loadings plots for each analysis (Feuerer & Carvajal et al., **Appendix III**, Figure 4 E).

Individual spectra from the cytoplasm of MDMs or THP-1 were analyzed using PCA before and after LPS-IFN activation (Feuerer & Carvajal et al., **Appendix III**, Figure 5). PC 4 explained 2% of the variance in THP-1 clustering, whereas PC 2 explained 4% of the variance in MDM separation. Analysis of the selected PC scores revealed that the score graph separations were statistically significant (Feuerer & Carvajal et al., **Appendix III**, Figure 5 C & D). Differences in cytoplasmic molecular composition were observed in the loading plots for both PCAs (Feuerer & Carvajal et al., **Appendix III**, Figure 5 E) following LPS-IFN $\gamma$  stimulation of THP-1 and MDM cells (Feuerer & Carvajal et al., **Appendix III**, Figure 5 E). The two groups' distinct spectrum patterns aided in the separation and assignment of molecular changes.

In conclusion, we found that proteins and phospholipids are the most sensitive and robust indicators of macrophage activation, based on PCA results. Changes in lipid composition, notably in the composition of phospholipids, have been linked to amide I substructure alterations before [118, 140, 141]. Chaudary et al. found similar results, reporting differing spectral patterns and alterations in THP-1 and primary blood-derived cells after monocyte-to-macrophage development [142]. However, it should be noted that their activation protocol for THP-1 and MDMs used PMA instead of LPS and IFN $\gamma$ .



Several studies demonstrate that a decreased expression of the LPS co-receptor CD14 on THP-1 cells leads to lower responsiveness to LPS when compared to MDMs [143]. This finding is also reflected in the Raman data, which demonstrate higher overall responsiveness in MDMs when compared to THP-1-derived macrophages.

Ultimately, we were able to demonstrate that RM and Raman imaging can robustly identify diverging molecular changes between THP-1 macrophages and MDMs driven by LPS and IFN $\gamma$  stimulation. PCA confirmed that THP-1 macrophages were less reactive towards LPS and IFN $\gamma$  than primary MDMs which showed molecular alterations in all identified subcellular structures, indicating a more systemic response to LPS and IFN $\gamma$ .



# Chapter 4

## General Conclusion & Outlook

### **4. General Conclusion & Outlook**

Biomaterial-mediated modulation of macrophages is an emerging therapeutic strategy to orchestrate downstream events of inflammation after tissue injury. The ability of the tissue to function and regenerate is dependent on managing the biophysical and biochemical milieu in a manner that remains largely unexplained. By using biomaterials as artificial microenvironments to study and control macrophage destiny, researchers can display and convey macrophage regulatory signals in a precise and near-physiological manner. Because macrophages are strongly adherent phagocytic cells that also carry the ability to present antigens to T cells, they are ideal targets for the development of immune-competent materials that promote endogenous regeneration and actively control macrophage polarization. Macrophage plasticity is an important nexus of the innate and adaptive immune response, and therefore pivotal for subsequent stages of regeneration and inflammation after encountering a non-physiological material. Understanding how different material designs activate macrophage phenotypes is essential for this new design paradigm.

Ultimately all three parts of this work aim at contributing to the goal of developing intelligent biomaterials that specifically and actively influence their environment and exert beneficial effects on immune cells and wound healing.

For this purpose, it was investigated how macrophage physiology is altered by different material surface topographies and how this change can be reliably and reproducibly analyzed.

We provide evidence that phenotyping of macrophages by flow cytometry is compromised through the process of dissociation necessary for suspension analysis. While multiplexed cytokine assays provide insight into the overall cytokine milieu, they usually lack single cell resolution and as macrophage populations are inherently heterogeneous, certain subpopulations might not be resolved. Furthermore, cytokines can accumulate over time depending on their degradation rates, obscuring subtle trend changes in the inflammatory process.

RM is becoming an increasingly popular tool in the biological sciences because it does not require pre-processing of cells like paraformaldehyde fixation or antibody staining.

The technology has developed over time to generate Raman fingerprints that can reliably distinguish different cell types. By resolving cellular components like proteins, lipids, and nucleic acids, we provide evidence that macrophage polarization induces significant changes in the lipidome and that these changes can be tracked and identified by RM. Based on this finding, we further demonstrate that distinguished Raman lipid fingerprints can be utilized to de novo identify polarization in macrophages induced by different material surface topographies.

Lastly, it was demonstrated that the choice of human macrophage in vitro model determines which molecular changes are induced by pro-inflammatory stimuli and therefore strongly affects the interpretation of results. This was also reflected in the observed Raman spectra which significantly differed between THP-1 macrophages and primary MDMs.

The development of immunocompetent materials carries enormous potential in the biomedical sector. If a material can orchestrate immune cells towards regeneration and wound healing, implants can be developed that fully integrate into the human body without scarring or inflammation, resulting in improved durability and performance. Furthermore, implant scaffolds can be engineered that first induce the formation of new tissue and then biodegrade, leaving a fully functional new organ behind. Other possible applications are the engineering of skin substitutes that significantly accelerate the healing process and prevent excessive scarring. Here we show that RM and Raman imaging are useful tools to efficiently identify material characteristics that support immune-mediated healing and regeneration.



## References

1. Murray, P.J. and T.A. Wynn, *Protective and pathogenic functions of macrophage subsets*. Nature reviews. Immunology, 2011. **11**(11): p. 723-737.
2. Wynn, T.A. and K.M. Vannella, *Macrophages in Tissue Repair, Regeneration, and Fibrosis*. Immunity, 2016. **44**(3): p. 450-462.
3. Murray, P.J. and T.A. Wynn, *Obstacles and opportunities for understanding macrophage polarization*. Journal of leukocyte biology, 2011. **89**(4): p. 557-563.
4. Jaguin, M., et al., *Polarization profiles of human M-CSF-generated macrophages and comparison of M1-markers in classically activated macrophages from GM-CSF and M-CSF origin*. Cellular Immunology, 2013. **281**(1): p. 51-61.
5. Gerrick, K.Y., et al., *Transcriptional profiling identifies novel regulators of macrophage polarization*. PLOS ONE, 2018. **13**(12).
6. Knipper, Johanna A., et al., *Interleukin-4 Receptor  $\alpha$  Signaling in Myeloid Cells Controls Collagen Fibril Assembly in Skin Repair*. Immunity, 2015. **43**(4): p. 803-816.
7. Minutti, C.M., et al., *Local amplifiers of IL-4R $\alpha$ -mediated macrophage activation promote repair in lung and liver*. Science, 2017. **356**(6342): p. 1076-1080.
8. Suarez-Lopez, L., et al., *MK2 contributes to tumor progression by promoting M2 macrophage polarization and tumor angiogenesis*. Proceedings of the National Academy of Sciences, 2018. **115**(18): p. E4236-E4244.
9. Williams Jesse, W., et al., *Macrophage Biology, Classification, and Phenotype in Cardiovascular Disease*. Journal of the American College of Cardiology, 2018. **72**(18): p. 2166-2180.
10. Ginhoux, F., et al., *Fate mapping analysis reveals that adult microglia derive from primitive macrophages*. Science, 2010. **330**(6005): p. 841-5.
11. Lahmar, Q., et al., *Tissue-resident versus monocyte-derived macrophages in the tumor microenvironment*. Biochimica et Biophysica Acta (BBA) - Reviews on Cancer, 2016. **1865**(1): p. 23-34.
12. Jakubzick, C., et al., *Minimal differentiation of classical monocytes as they survey steady-state tissues and transport antigen to lymph nodes*. Immunity, 2013. **39**(3): p. 599-610.
13. Yona, S., et al., *Fate mapping reveals origins and dynamics of monocytes and tissue macrophages under homeostasis*. Immunity, 2013. **38**(1): p. 79-91.
14. Hashimoto, D., et al., *Tissue-resident macrophages self-maintain locally throughout adult life with minimal contribution from circulating monocytes*. Immunity, 2013. **38**(4): p. 792-804.
15. Steinman, R.M. and Z.A. Cohn, *Identification of a novel cell type in peripheral lymphoid organs of mice. I. Morphology, quantitation, tissue distribution*. The Journal of experimental medicine, 1973. **137**(5): p. 1142-1162.
16. Geissmann, F., et al., *Unravelling mononuclear phagocyte heterogeneity*. Nature Reviews Immunology, 2010. **10**(6): p. 453-460.
17. Randolph, G.J., et al., *Differentiation of phagocytic monocytes into lymph node dendritic cells in vivo*. Immunity, 1999. **11**(6): p. 753-61.
18. Carpentier, S., et al., *Comparative genomics analysis of mononuclear phagocyte subsets confirms homology between lymphoid tissue-resident and*

- dermal XCR1+ DCs in mouse and human and distinguishes them from Langerhans cells.* Journal of Immunological Methods, 2016. **432**: p. 35-49.
19. Barbul, A., et al., *Wound healing in nude mice: a study on the regulatory role of lymphocytes in fibroplasia.* Surgery, 1989. **105**(6): p. 764-9.
  20. Daley, J.M., et al., *The phenotype of murine wound macrophages.* J Leukoc Biol, 2010. **87**(1): p. 59-67.
  21. Zhang, X. and D.M. Mosser, *Macrophage activation by endogenous danger signals.* The Journal of pathology, 2008. **214**(2): p. 161-178.
  22. Orecchioni, M., et al., *Macrophage Polarization: Different Gene Signatures in M1(LPS+) vs. Classically and M2(LPS-) vs. Alternatively Activated Macrophages.* Frontiers in Immunology, 2019. **10**.
  23. Martinez, F.O. and S. Gordon, *The M1 and M2 paradigm of macrophage activation: time for reassessment.* F1000prime reports, 2014. **6**: p. 13-13.
  24. Murray, P.J., et al., *Macrophage activation and polarization: nomenclature and experimental guidelines.* Immunity, 2014. **41**(1): p. 14-20.
  25. Xue, J., et al., *Transcriptome-based network analysis reveals a spectrum model of human macrophage activation.* Immunity, 2014. **40**(2): p. 274-288.
  26. Verreck, F.A.W., et al., *Phenotypic and functional profiling of human proinflammatory type-1 and anti-inflammatory type-2 macrophages in response to microbial antigens and IFN- $\gamma$ - and CD40L-mediated costimulation.* Journal of Leukocyte Biology, 2006. **79**(2): p. 285-293.
  27. Arnold, C.E., et al., *The activation status of human macrophages presenting antigen determines the efficiency of Th17 responses.* Immunobiology, 2015. **220**(1): p. 10-19.
  28. Barron, L. and T.A. Wynn, *Fibrosis is regulated by Th2 and Th17 responses and by dynamic interactions between fibroblasts and macrophages.* American Journal of Physiology-Gastrointestinal and Liver Physiology, 2011. **300**(5): p. G723-G728.
  29. Zhou, J., et al., *Exosomes Released from Tumor-Associated Macrophages Transfer miRNAs That Induce a Treg/Th17 Cell Imbalance in Epithelial Ovarian Cancer.* Cancer Immunology Research, 2018. **6**(12): p. 1578.
  30. Harrington, L.E., et al., *Interleukin 17-producing CD4+ effector T cells develop via a lineage distinct from the T helper type 1 and 2 lineages.* Nature Immunology, 2005. **6**(11): p. 1123-1132.
  31. R  szer, T., *Understanding the Mysterious M2 Macrophage through Activation Markers and Effector Mechanisms.* Mediators of Inflammation, 2015. **2015**: p. 816460.
  32. Seder, R.A., et al., *Production of interleukin-4 and other cytokines following stimulation of mast cell lines and in vivo mast cells/basophils.* International Archives of Allergy and Immunology, 1991. **94**(1-4): p. 137-140.
  33. Gessner, A., K. Mohrs, and M. Mohrs, *Mast cells, basophils, and eosinophils acquire constitutive IL-4 and IL-13 transcripts during lineage differentiation that are sufficient for rapid cytokine production.* The Journal of Immunology, 2005. **174**(2): p. 1063-1072.
  34. Gratchev, A., et al., *Alternatively activated macrophages differentially express fibronectin and its splice variants and the extracellular matrix protein  $\beta$ IG-H3.* Scandinavian journal of immunology, 2001. **53**(4): p. 386-392.



35. Weitkamp, B., et al., *Human macrophages synthesize type VIII collagen in vitro and in the atherosclerotic plaque*. The FASEB journal, 1999. **13**(11): p. 1445-1457.
36. Wang, J., et al., *Microcystin-LR ameliorates pulmonary fibrosis via modulating CD206+ M2-like macrophage polarization*. Cell Death & Disease, 2020. **11**(2): p. 136.
37. Nikolic-Paterson, D.J., S. Wang, and H.Y. Lan, *Macrophages promote renal fibrosis through direct and indirect mechanisms*. Kidney International Supplements, 2014. **4**(1): p. 34-38.
38. Mosser, D.M. and J.P. Edwards, *Exploring the full spectrum of macrophage activation*. Nature reviews immunology, 2008. **8**(12): p. 958 - 969.
39. Edwards, J.P., et al., *Biochemical and functional characterization of three activated macrophage populations*. J Leukoc Biol, 2006. **80**(6): p. 1298-307.
40. Lucas, M., et al., *ERK activation following macrophage FcγR ligation leads to chromatin modifications at the IL-10 locus*. The Journal of Immunology, 2005. **175**(1): p. 469-477.
41. Mantovani, A., et al., *The chemokine system in diverse forms of macrophage activation and polarization*. Trends in Immunology, 2004. **25**(12): p. 677-686.
42. Haj-Mirzaian, A., et al., *Role of hypothalamic-pituitary-adrenal-axis, toll-like receptors, and macrophage polarization in pre-atherosclerotic changes induced by social isolation stress in mice*. Scientific Reports, 2021. **11**(1): p. 1-15.
43. Brown, D.H. and B.S. Zwilling, *Activation of the hypothalamic-pituitary-adrenal axis differentially affects the anti-mycobacterial activity of macrophages from BCG-resistant and susceptible mice*. Journal of neuroimmunology, 1994. **53**(2): p. 181-187.
44. Lim, H.-Y., et al., *Glucocorticoids exert opposing effects on macrophage function dependent on their concentration*. Immunology, 2007. **122**(1): p. 47-53.
45. Long, F., et al., *Rapid nongenomic inhibitory effects of glucocorticoids on phagocytosis and superoxide anion production by macrophages*. Steroids, 2005. **70**(1): p. 55-61.
46. Chen, Y., et al., *Receptor-mediated cell mechanosensing*. Molecular biology of the cell, 2017. **28**(23): p. 3134-3155.
47. Puleo, J.I., et al., *Mechanosensing during directed cell migration requires dynamic actin polymerization at focal adhesions*. Journal of Cell Biology, 2019. **218**(12): p. 4215-4235.
48. van den Dries, K., et al., *Modular actin nano-architecture enables podosome protrusion and mechanosensing*. Nature communications, 2019. **10**(1): p. 1-16.
49. Luo, T., et al., *Molecular mechanisms of cellular mechanosensing*. Nature Materials, 2013. **12**(11): p. 1064-1071.
50. Goswami, R., et al., *Mechanosensing by TRPV4 mediates stiffness-induced foreign body response and giant cell formation*. Science Signaling, 2021. **14**(707): p. eabd4077.
51. Gruber, E.J. and C.A. Leifer, *Molecular regulation of TLR signaling in health and disease: mechano-regulation of macrophages and TLR signaling*. Innate immunity, 2020. **26**(1): p. 15-25.
52. Hotchkiss, K.M., et al., *Titanium surface characteristics, including topography and wettability, alter macrophage activation*. Acta biomaterialia, 2016. **31**: p. 425-434.

53. Atcha, H., et al., *Mechanically activated ion channel Piezo1 modulates macrophage polarization and stiffness sensing*. Nature Communications, 2021. **12**(1): p. 3256.
54. Previtiera, M.L. and A. Sengupta, *Substrate Stiffness Regulates Proinflammatory Mediator Production through TLR4 Activity in Macrophages*. PLoS One, 2015. **10**(12): p. e0145813.
55. Blakney, A.K., M.D. Swartzlander, and S.J. Bryant, *The effects of substrate stiffness on the in vitro activation of macrophages and in vivo host response to poly(ethylene glycol)-based hydrogels*. J Biomed Mater Res A, 2012. **100**(6): p. 1375-86.
56. Pakshir, P. and B. Hinz, *The big five in fibrosis: Macrophages, myofibroblasts, matrix, mechanics, and miscommunication*. Matrix Biology, 2018. **68-69**: p. 81-93.
57. Brohawn, S.G., Z. Su, and R. MacKinnon, *Mechanosensitivity is mediated directly by the lipid membrane in TRAAK and TREK1 K<sup>+</sup> channels*. Proc Natl Acad Sci U S A, 2014. **111**(9): p. 3614-9.
58. Coste, B., et al., *Piezo1 and Piezo2 Are Essential Components of Distinct Mechanically Activated Cation Channels*. Science, 2010. **330**(6000): p. 55-60.
59. Pethő, Z., et al., *Mechanosensitive ion channels push cancer progression*. Cell Calcium, 2019. **80**: p. 79-90.
60. Chen, X., et al., *A Feedforward Mechanism Mediated by Mechanosensitive Ion Channel PIEZO1 and Tissue Mechanics Promotes Glioma Aggression*. Neuron, 2018. **100**(4): p. 799-815.e7.
61. Ranade, S.S., et al., *Piezo1, a mechanically activated ion channel, is required for vascular development in mice*. Proc Natl Acad Sci U S A, 2014. **111**(28): p. 10347-52.
62. Solis, A.G., et al., *Mechanosensation of cyclical force by PIEZO1 is essential for innate immunity*. Nature, 2019. **573**(7772): p. 69-74.
63. Roedig, H., et al., *Biglycan is a new high-affinity ligand for CD14 in macrophages*. Matrix Biol, 2018.
64. Luu, T.U. and W.F. Liu, *Regulation of Macrophages by Extracellular Matrix Composition and Adhesion Geometry*. Regenerative Engineering and Translational Medicine, 2018. **4**(4): p. 238-246.
65. Pathak, M.M., et al., *Stretch-activated ion channel Piezo1 directs lineage choice in human neural stem cells*. Proc Natl Acad Sci U S A, 2014. **111**(45): p. 16148-53.
66. Orsini, E.M., et al., *Stretching the Function of Innate Immune Cells*. Front Immunol, 2021. **12**: p. 767319.
67. Ambarus, C.A., et al., *Systematic validation of specific phenotypic markers for in vitro polarized human macrophages*. Journal of immunological methods, 2012. **375**(1-2): p. 196-206.
68. Vogel, D.Y.S., et al., *Human macrophage polarization in vitro: Maturation and activation methods compared*. Immunobiology, 2014. **219**(9): p. 695-703.
69. N, A.G., et al., *Phagocytosis imprints heterogeneity in tissue-resident macrophages*. J Exp Med, 2017. **214**(5): p. 1281-1296.
70. Chanput, W., J.J. Mes, and H.J. Wichers, *THP-1 cell line: an in vitro cell model for immune modulation approach*. International immunopharmacology, 2014. **23**(1): p. 37-45.

71. Maeß, M.B., et al., *Reduced PMA enhances the responsiveness of transfected THP-1 macrophages to polarizing stimuli*. Journal of immunological methods, 2014. **402**(1-2): p. 76-81.
72. Lund, M.E., et al., *The choice of phorbol 12-myristate 13-acetate differentiation protocol influences the response of THP-1 macrophages to a pro-inflammatory stimulus*. Journal of immunological methods, 2016. **430**: p. 64-70.
73. Tedesco, S., et al., *Convenience versus biological significance: are PMA-differentiated THP-1 cells a reliable substitute for blood-derived macrophages when studying in vitro polarization?* Frontiers in pharmacology, 2018. **9**: p. 71.
74. Shiratori, H., et al., *THP-1 and human peripheral blood mononuclear cell-derived macrophages differ in their capacity to polarize in vitro*. Molecular Immunology, 2017. **88**: p. 58-68.
75. Raman, C.V., *A Change of Wave-length in Light Scattering*. Nature, 1928. **121**(3051): p. 619-619.
76. Ferraro, J.R., *Introductory raman spectroscopy*. 2003: Elsevier.
77. Pezzotti, G., *Raman spectroscopy in cell biology and microbiology*. Journal of Raman Spectroscopy, 2021. **52**(12): p. 2348-2443.
78. Smith, R., K.L. Wright, and L. Ashton, *Raman spectroscopy: an evolving technique for live cell studies*. Analyst, 2016. **141**(12): p. 3590-3600.
79. Lin, L., et al., *Surface-enhanced Raman scattering nanotags for bioimaging*. Journal of Applied Physics, 2021. **129**(19): p. 191101.
80. Daum, R., et al., *Non-invasive detection of DNA methylation states in carcinoma and pluripotent stem cells using Raman microspectroscopy and imaging*. Scientific reports, 2019. **9**(1): p. 1-13.
81. Kallepitis, C., et al., *Quantitative volumetric Raman imaging of three dimensional cell cultures*. Nat Commun, 2017. **8**: p. 14843.
82. Stiebing, C., et al., *Raman imaging of macrophages incubated with triglyceride-enriched oxLDL visualizes translocation of lipids between endocytic vesicles and lipid droplets*. Journal of Lipid Research, 2017. **58**(5): p. 876-883.
83. Matthäus, C., et al., *Infrared and Raman microscopy in cell biology*. Methods in cell biology, 2008. **89**: p. 275-308.
84. Chase, B., *Fourier transform Raman spectroscopy*. Analytical Chemistry, 1987. **59**(14): p. 881A-890A.
85. Puppels, G., et al., *Studying single living cells and chromosomes by confocal Raman microspectroscopy*. Nature, 1990. **347**(6290): p. 301-303.
86. Lombardini, A., et al., *High-resolution multimodal flexible coherent Raman endoscope*. Light: Science & Applications, 2018. **7**(1): p. 1-8.
87. Harmsen, S., et al., *Detection of premalignant gastrointestinal lesions using surface-enhanced resonance Raman scattering–nanoparticle endoscopy*. ACS nano, 2019. **13**(2): p. 1354-1364.
88. Jermyn, M., et al., *Intraoperative brain cancer detection with Raman spectroscopy in humans*. Sci Transl Med, 2015. **7**(274): p. 274ra19.
89. Allen, T.D., *Microscopy: A Very Short Introduction*. 2015: Oxford University Press.
90. Schnell, U., et al., *Immunolabeling artifacts and the need for live-cell imaging*. Nature methods, 2012. **9**(2): p. 152-158.
91. Stephens, D.J. and V.J. Allan, *Light microscopy techniques for live cell imaging*. Science, 2003. **300**(5616): p. 82-6.

92. Montero Llopis, P., et al., *Best practices and tools for reporting reproducible fluorescence microscopy methods*. Nature Methods, 2021. **18**(12): p. 1463-1476.
93. Zhao, W., et al., *Sparse deconvolution improves the resolution of live-cell super-resolution fluorescence microscopy*. Nature Biotechnology, 2021.
94. Leung, B.O. and K.C. Chou, *Review of Super-Resolution Fluorescence Microscopy for Biology*. Applied Spectroscopy, 2011. **65**(9): p. 967-980.
95. Rust, M.J., M. Bates, and X. Zhuang, *Sub-diffraction-limit imaging by stochastic optical reconstruction microscopy (STORM)*. Nature methods, 2006. **3**(10): p. 793-796.
96. Shtengel, G., et al., *Interferometric fluorescent super-resolution microscopy resolves 3D cellular ultrastructure*. Proceedings of the National Academy of Sciences, 2009. **106**(9): p. 3125-3130.
97. Gong, L., et al., *Higher-order coherent anti-Stokes Raman scattering microscopy realizes label-free super-resolution vibrational imaging*. Nature Photonics, 2020. **14**(2): p. 115-122.
98. Wilson, E.B., J.C. Decius, and P.C. Cross, *Molecular Vibrations: The Theory of Infrared and Raman Vibrational Spectra*. 2012: Dover Publications.
99. Guerrini, L. and R.A. Alvarez-Puebla, *Surface-enhanced Raman spectroscopy in cancer diagnosis, prognosis and monitoring*. Cancers, 2019. **11**(6): p. 748.
100. Abramczyk, H., et al., *A look into the use of Raman spectroscopy for brain and breast cancer diagnostics: linear and non-linear optics in cancer research as a gateway to tumor cell identity*. Expert review of molecular diagnostics, 2020. **20**(1): p. 99-115.
101. Weiss, M., et al., *Cold atmospheric plasma for potential in vivo applications: Raman microspectrometry determined effects on cervical cancer cells*. European Journal of Obstetrics and Gynecology and Reproductive Biology, 2019. **234**: p. e162-e163.
102. Becker, L., et al., *Raman Imaging and Fluorescence Lifetime Imaging Microscopy for Diagnosis of Cancer State and Metabolic Monitoring*. Cancers, 2021. **13**(22): p. 5682.
103. Underwood, R.A., et al., *Quantifying the effect of pore size and surface treatment on epidermal incorporation into percutaneously implanted sphere-templated porous biomaterials in mice*. Journal of Biomedical Materials Research Part A, 2011. **98A**(4): p. 499-508.
104. Madden, L.R., et al., *Proangiogenic scaffolds as functional templates for cardiac tissue engineering*. Proceedings of the National Academy of Sciences, 2010. **107**(34): p. 15211-15216.
105. Dawson, E.R., et al., *Increased Internal Porosity and Surface Area of Hydroxyapatite Accelerates Healing and Compensates for Low Bone Marrow Mesenchymal Stem Cell Concentrations in Critically-Sized Bone Defects*. Applied Sciences, 2018. **8**(8): p. 1366.
106. Noga, S., et al., *Polyurethane composites as a potential 3D scaffold for Mesenchymal Stem Cells in cartilage regeneration*. Engineering of Biomaterials, 2019. **22**.
107. Santoro, M., et al., *Poly (lactic acid) nanofibrous scaffolds for tissue engineering*. Advanced drug delivery reviews, 2016. **107**: p. 206-212.

108. Daum, R., et al., *Fibronectin Adsorption on Electrospun Synthetic Vascular Grafts Attracts Endothelial Progenitor Cells and Promotes Endothelialization in Dynamic In Vitro Culture*. *Cells*, 2020. **9**(3).
109. Hinderer, S., et al., *Engineering of a bio-functionalized hybrid off-the-shelf heart valve*. *Biomaterials*, 2014. **35**(7): p. 2130-9.
110. Di Cio, S. and J.E. Gautrot, *Cell sensing of physical properties at the nanoscale: Mechanisms and control of cell adhesion and phenotype*. *Acta Biomaterialia*, 2016. **30**: p. 26-48.
111. Batista-Gonzalez, A., et al., *New Insights on the Role of Lipid Metabolism in the Metabolic Reprogramming of Macrophages*. *Frontiers in Immunology*, 2020. **10**(2993).
112. Wu, H., et al., *In vivo lipidomics using single-cell Raman spectroscopy*. *Proceedings of the National Academy of Sciences of the United States of America*, 2011. **108**(9): p. 3809-3814.
113. Pauls, S.D., et al., *Anti-inflammatory effects of  $\alpha$ -linolenic acid in M1-like macrophages are associated with enhanced production of oxylipins from  $\alpha$ -linolenic and linoleic acid*. *J Nutr Biochem*, 2018. **57**: p. 121-129.
114. Wang, S., et al., *In vitro fatty acid enrichment of macrophages alters inflammatory response and net cholesterol accumulation*. *The British journal of nutrition*, 2009. **102**(4): p. 497-501.
115. Czamara, K., et al., *Raman spectroscopy of lipids: a review*. *Journal of Raman Spectroscopy*, 2015. **46**(1): p. 4-20.
116. Takahashi, H., et al., *Observation of the changes in the chemical composition of lipid droplets using Raman microscopy*. *Physical Chemistry Chemical Physics*, 2020. **22**(38): p. 21646-21650.
117. Matthäus, C., et al. *Monitoring intra-cellular lipid metabolism in macrophages by Raman-and CARS-microscopy*. in *Biophotonics: Photonic Solutions for Better Health Care II*. 2010. International Society for Optics and Photonics.
118. Montenegro-Burke, J.R., et al., *Lipid profiling of polarized human monocyte-derived macrophages*. *Prostaglandins & other lipid mediators*, 2016. **127**: p. 1-8.
119. Bhaskar, V., et al., *Monoclonal antibodies targeting IL-1 beta reduce biomarkers of atherosclerosis in vitro and inhibit atherosclerotic plaque formation in Apolipoprotein E-deficient mice*. *Atherosclerosis*, 2011. **216**(2): p. 313-20.
120. Korbecki, J. and K. Bajdak-Rusinek, *The effect of palmitic acid on inflammatory response in macrophages: an overview of molecular mechanisms*. *Inflammation Research*, 2019. **68**(11): p. 915-932.
121. Im, S.-S., et al., *Linking lipid metabolism to the innate immune response in macrophages through sterol regulatory element binding protein-1a*. *Cell metabolism*, 2011. **13**(5): p. 540-549.
122. Feuerer, N., et al., *Lipidome profiling with Raman microspectroscopy identifies macrophage response to surface topographies of implant materials*. *Proceedings of the National Academy of Sciences*, 2021. **118**(52).
123. Barth, K.A., J.D. Waterfield, and D.M. Brunette, *The effect of surface roughness on RAW 264.7 macrophage phenotype*. *Journal of Biomedical Materials Research Part A*, 2013. **101A**(9): p. 2679-2688.
124. Zhang, Y., et al., *Titanium surfaces characteristics modulate macrophage polarization*. *Materials Science and Engineering: C*, 2019. **95**: p. 143-151.

125. Jordana, F., L. Susbielles, and J. Colat-Parros, *Periimplantitis and Implant Body Roughness: A Systematic Review of Literature*. *Implant Dentistry*, 2018. **27**(6): p. 672-681.
126. Atlan, M., et al., *Breast implant surface texture impacts host tissue response*. *Journal of the Mechanical Behavior of Biomedical Materials*, 2018. **88**: p. 377-385.
127. Bloise, N., et al., *Engineering Immunomodulatory Biomaterials for Regenerating the Infarcted Myocardium*. *Frontiers in Bioengineering and Biotechnology*, 2020. **8**(292).
128. Bosshart, H. and M. Heinzemann, *THP-1 cells as a model for human monocytes*. *Ann Transl Med*, 2016. **4**(21): p. 438.
129. Tedesco, S., et al., *Convenience versus Biological Significance: Are PMA-Differentiated THP-1 Cells a Reliable Substitute for Blood-Derived Macrophages When Studying in Vitro Polarization?* *Frontiers in Pharmacology*, 2018. **9**.
130. Töpfer, N., et al., *Raman spectroscopy reveals LPS-induced changes of biomolecular composition in monocytic THP-1 cells in a label-free manner*. *Integr Biol (Camb)*, 2019.
131. Pavillon, N., et al., *Noninvasive detection of macrophage activation with single-cell resolution through machine learning*. *Proceedings of the National Academy of Sciences of the United States of America*, 2018. **115**(12): p. E2676-E2685.
132. Tur, J., et al., *Macrophages and mitochondria: a critical interplay between metabolism, signaling, and the functional activity*. *Advances in immunology*, 2017. **133**: p. 1-36.
133. Stone, N., et al., *Near-infrared Raman spectroscopy for the classification of epithelial pre-cancers and cancers*. *Journal of Raman spectroscopy*, 2002. **33**(7): p. 564-573.
134. Huang, Z., et al., *Near-infrared Raman spectroscopy for optical diagnosis of lung cancer*. *International journal of cancer*, 2003. **107**(6): p. 1047-1052.
135. Liu, Z., et al., *Circulation and long-term fate of functionalized, biocompatible single-walled carbon nanotubes in mice probed by Raman spectroscopy*. *Proceedings of the National Academy of Sciences*, 2008. **105**(5): p. 1410-1415.
136. Pétrilli, V., et al., *The inflammasome: a danger sensing complex triggering innate immunity*. *Current opinion in immunology*, 2007. **19**(6): p. 615-622.
137. Ugurel, S., et al., *Down-regulation of HLA class II and costimulatory CD86/B7-2 on circulating monocytes from melanoma patients*. *Cancer Immunology, Immunotherapy*, 2004. **53**(6): p. 551-559.
138. Chen, L., et al., *Tumor immunogenicity determines the effect of B7 costimulation on T cell-mediated tumor immunity*. *The Journal of experimental medicine*, 1994. **179**(2): p. 523-532.
139. Li, J., et al., *The expression of costimulatory molecules CD80 and CD86 in human carcinoma cell lines: its regulation by interferon  $\gamma$  and interleukin-10*. *Cancer Immunology, Immunotherapy*, 1996. **43**(4): p. 213-219.
140. Shirota, K., et al., *Detection of Sphingomyelin Clusters by Raman Spectroscopy*. *Biophysical journal*, 2016. **111**(5): p. 999-1007.
141. Zhang, C., et al., *Quantitative profiling of glycerophospholipids during mouse and human macrophage differentiation using targeted mass spectrometry*. *Scientific reports*, 2017. **7**(1): p. 412-412.

142. Chaudhary, N., et al., *Discrimination of immune cell activation using Raman micro-spectroscopy in an in-vitro & ex-vivo model*. Spectrochimica Acta Part A: Molecular and Biomolecular Spectroscopy, 2021. **248**: p. 119118.
143. Bosshart, H. and M. Heinzelmann, *Lipopolysaccharide-mediated cell activation without rapid mobilization of cytosolic free calcium*. Molecular immunology, 2004. **41**(10): p. 1023-1028.

### Acknowledgments

My sincere gratitude goes to the following people, without whom I would not have been able to complete this research:

First, I would like to thank my supervisor Katja Schenke-Layland for her dedicated support and guidance. Katja continuously provided scientific advice, mentorship, and encouragement and was always willing and enthusiastic to assist in any way she could throughout the research project. I owe the success of this work mostly to her.

My special thanks also go to Julia Marzi, Christopher Shipp, and Svenja Hinderer, for their great mentoring, patience, and motivation but also for their outstanding scientific input. Especially Julia I would like to pay tribute to her support during the last months.

Simone Liebscher, Simone Pöschel, and Daniel Carvajal Berrio have not only been the best friends and colleagues but also never failed to support this work with their many years of technical and scientific expertise in Flow Cytometry, Fluorescence Microscopy, and Raman Microspectroscopy.

A big shout out to all the Schenke-Layland lab members who always provided a friendly and welcoming atmosphere, emotional support when needed, and stimulating discussions (scientific or other).

I also would like to thank my friends and colleagues from the NMI, especially Kathrin, Ruben, Dmitri, Flo, Bernadette, Pauline, and Elena for making lab life worthwhile and incredibly fun.

Finally, I would like to express my heartfelt thanks to my family and husband who have supported and encouraged me during the past years.

*Figures and graphics were created using BioRender.com.*





## Declaration

Ich erkläre hiermit, dass ich die zur Promotion eingereichte Arbeit mit dem Titel „Marker-independent Assessment of Molecular Activation Patterns in Macrophages“ selbständig verfasst, nur die angegebenen Quellen und Hilfsmittel benutzt und wörtlich oder inhaltlich übernommene Zitate als solche gekennzeichnet habe. Ich erkläre, dass die Richtlinien zur Sicherung guter wissenschaftlicher Praxis der Universität Tübingen beachtet wurden. Ich versichere an Eides statt, dass diese Angaben wahr sind und dass ich nichts verschwiegen habe. Mir ist bekannt, dass die falsche Angabe einer Versicherung an Eides statt mit Freiheitsstrafe bis zu drei Jahren oder mit Geldstrafe bestraft wird.

Tübingen, 11. April 2023

Nora Feuerer



## **Curriculum Vitae**

The curriculum vitae has been removed due to data protection concerns.

The curriculum vitae has been removed due to data protection concerns.

The curriculum vitae has been removed due to data protection concerns.



## **Appendices**

Appendix I Feuerer N, Morschl J, Daum R, Weiss M, Hinderer S, Schenke Layland K, Shipp C. Macrophage retrieval from 3D biomaterials: A detailed comparison of common dissociation methods. J Immunol Regen Med, 2021, 1, 100035.





Contents lists available at ScienceDirect

Journal of Immunology and Regenerative Medicine

journal homepage: [www.elsevier.com/locate/regen](http://www.elsevier.com/locate/regen)

## Macrophage retrieval from 3D biomaterials: A detailed comparison of common dissociation methods

Nora Feuerer<sup>a,b,\*</sup>, Johannes Morschl<sup>a,b</sup>, Ruben Daum<sup>a,b</sup>, Martin Weiss<sup>a,b</sup>, Svenja Hinderer<sup>a,b</sup>, Katja Schenke-Layland<sup>a,b,c,d</sup>, Christopher Shipp<sup>a</sup>

<sup>a</sup> NMI Natural and Medical Sciences Institute at the University of Tübingen, Reutlingen, Germany

<sup>b</sup> Department of Women's Health, Research Institute for Women's Health, Eberhard Karls University, Tübingen, Germany

<sup>c</sup> Cluster of Excellence IFIT (EXC 2180) "Image-Guided and Functionally Instructed Tumor Therapies", Eberhard Karls University, Tübingen, Germany

<sup>d</sup> Dept. of Medicine/Cardiology, University of California Los Angeles (UCLA), Los Angeles, CA, USA

### ARTICLE INFO

#### Keywords:

Macrophage polarization  
Macrophage dissociation  
Flow cytometry  
Biomaterials  
Electrospinning

### ABSTRACT

**Introduction:** The immune system is widely recognized as a crucial determinant in implant biocompatibility and tissue integration. In order to assess macrophage response to biomaterials, commonly used analysis techniques require the removal of cells from the material. This process inherently has a negative impact on the cells, but few studies have comprehensively compared different dissociation methods in terms of impact on cell yield, viability, phenotype and function.

**Methods:** Cell scraping, EDTA at 4 °C, EDTA at 37 °C, trypsin, Accutase and the PromoCell macrophage detachment solution were compared in terms of cell yield and viability. The effect of Accutase on cell surface antigen conservancy and cell functionality was investigated. Lastly, effect of Accutase detachment of macrophages from electrospun biomaterials was analyzed.

**Results:** The efficiency of common cell detachment protocols for human monocyte-derived macrophages (MDMs) varies significantly between enzymatic and non-enzymatic approaches. In terms of surface marker detection, we showed that enzymatic detachment not only selectively cleaves the M2 markers CD206 and CD163, but we also identified that this effect is variable across donors. Furthermore, we observed that the process of cell detachment impairs macrophage endocytic ability. Lastly, we tested the efficiency of enzymatic cell detachment on electrospun 3D matrices designed for tissue engineering.

**Conclusion:** Our results provide a thorough understanding of the advantages and disadvantages of commonly used cell dissociation methods and have important implications for studies investigating the macrophage response to biomaterials.

### 1. Introduction

Due to the increased age of populations in most developed countries, the substitution of diseased or dysfunctional tissue by synthetic implants is becoming increasingly common.<sup>1,2</sup> In many cases, the immune system has been identified as a major factor that influences whether an implant fails following implantation, or if it becomes successfully bio-integrated.<sup>3,4</sup> For bone grafts, artificial joints and soft tissue implants, neutrophils, T-cells and macrophages have been identified as main

contributors of chronic inflammation, aseptic loosening or calcification.<sup>5-7</sup> Monocytes and monocyte-derived macrophages (MDMs) in particular have emerged as key players in orchestrating implant inflammation, extracellular matrix (ECM) deposition, fibrosis and tissue regeneration.<sup>6,8,9</sup> It has now become a promising goal to design biomaterials that utilize the immune system in a targeted manner to improve biocompatibility and durability of implant materials, subsequently leading to decreased medical costs, less revision surgeries and better life quality for patients.<sup>6,10-12</sup>

**Abbreviations:** MDM, monocyte-derived macrophage; FC, flow cytometry; LPS, lipopolysaccharide; IFN $\gamma$ , interferon gamma; PBMC, peripheral blood mononuclear cell; M-CSF, macrophage colony-stimulating factor; 7-AAD, 7-amino-actinomycin D; EDTA, ethylenediaminetetraacetic acid; MFI, mean fluorescence intensity; ECM, extracellular matrix; PLA, poly (L-lactide); PU, polyurethane.

\* Corresponding author. Department of Women's Health, Research Institute for Women's Health, Eberhard Karls University, Tübingen, Germany.

E-mail address: [nora.feuerer@uni-tuebingen.de](mailto:nora.feuerer@uni-tuebingen.de) (N. Feuerer).

<https://doi.org/10.1016/j.regen.2020.100035>

Received 25 June 2020; Received in revised form 1 October 2020; Accepted 16 November 2020

Available online 5 December 2020

2468-4988/© 2020 The Authors.

Published by Elsevier Inc.

This is an open access article under the CC BY-NC-ND license

(<http://creativecommons.org/licenses/by-nc-nd/4.0/>).

MDMs are highly plastic cells that can either reinforce inflammation, or initiate tissue remodeling and healing. The presence of macrophages as well as the interplay in time and space of their polarization states is known to be crucial for normal wound healing and prevention of fibrosis.<sup>13,14</sup> Following biomaterial implantation, the resolution of inflammation is dependent on an effective transition from the pro-inflammatory M1 macrophage phenotype towards a resolving pro-regenerative M2 phenotype.<sup>15–17</sup> There is a general consensus that M1 and M2 macrophage phenotypes represent two extremes of a continuum and that many other states exist in between, adding further levels of complexity.<sup>18,19</sup> While it is well established that exogenous factors such as lipopolysaccharides (LPS), interferons (IFNs) or other cytokines can induce macrophage polarization, an understanding of how biomaterial properties affect macrophage behavior is in its infancy.<sup>20–24</sup> In the field of biomaterial research, cell culture is typically performed using polystyrene cell culture plates as controls, and in many cases, cells are also cultured on the biomaterial itself. Popular biomaterial and tissue engineering substrates include hydrogels, sponges, porous ceramics or other three dimensional (3D) matrices. In these cases, cell scraping cannot be used for cell dissociation as these surfaces are not planar and cells infiltrate into the pores. This highlights an urgent need for the in-depth analysis of alternative cell detachment methods that ensure harvest efficiency, cell viability and prevent alteration of cell surface proteins or cell functionality.

Today, three methods are widely employed as routine techniques used to assess the polarization state of macrophages: enzyme-linked immunosorbent assays (ELISA) (including multiplex assays) to measure cytokine secretion, reverse transcriptase polymerase chain reaction (RT-PCR) to assess gene expression, and flow cytometry (FC) to measure the expression of cell surface and intracellular proteins. In contrast to ELISA and PCR, FC is the only method that allows the analysis of protein expression on a single cell basis. This is of particular advantage when studying macrophage-biomaterial interactions, as it allows the identification of subgroups in non-uniform cell populations. To distinguish between M1 and M2 phenotypes, CD86 (M1), HLA-DR (M1), CD206 (M2) and CD163 are common surface markers for FC analysis. However, macrophages become strongly adherent during their time in culture. As cells need to be in suspension for FC analysis, this poses a special challenge to scientists because many common dissociation methods involve enzymatic cleavage, which can also negatively affect the cell surface markers being analyzed.<sup>25</sup>

As of now, a large number of diverse protocols are used to detach human PBMC-derived MDMs from their substrates.<sup>26,27</sup> Trypsin is often avoided, as it is assumed to be the most aggressive of enzymatic treatments and most prone to degrade cell surface antigens. Accutase is a popular alternative to trypsin, as it is held to be much gentler on surface proteins while at the same time not compromising detachment efficiency. However, Accutase is still enzymatically active and may also result in loss of cell surface proteins. Furthermore, despite these widely held beliefs little is known concerning the performance of Accutase in comparison to trypsin. Alternatives to enzymatic dissociation are detachment with ethylenediaminetetraacetic acid (EDTA). EDTA complexes bivalent cations that are needed for effective cell adhesion. EDTA may also be used in combination with cold shock at 4 °C to enhance the dissociation effect. An additional non-enzymatic method is the use of commercial detachment media that are designed specifically for the dissociation of macrophages from cell culture plates. Many of these come with relatively high costs and little reference data regarding their composition or efficiency.

To our knowledge, no data are available regarding how different biomaterials influence adhesion behavior of macrophages, nor is it known if routinely used dissociation protocols can be directly transferred to biomaterial substrates without suffering reduced dissociation efficiency. This comes with the danger of losing macrophage subpopulations that adhere more strongly to a certain substrate, and thus will result in biased results obtained by FC. To address this, we

compared the efficiency of human PBMC-derived MDMs dissociation with the following methods: 1) EDTA with and without cold shock, 2) trypsin, 3) Accutase, 4) a commercially available macrophage detachment solution and 5) cell scraping. Detachment methods were compared in terms of cell yield, viability, surface marker conservation and effect on cell function. In addition, we paid particular attention to how Accutase treatment may affect surface marker conservation of different donors, and if our findings can be transferred to 3D biomaterial matrices where cell scraping is not an option.

## 2. Material and methods

The ethics committee of the University Hospital of Tübingen approved the use of human donor blood cells in this study (495/2018BO2).

### 2.1. Fabrication of scaffolds

Poly (L-lactide) (PLA) was purchased from Sigma-Aldrich ( $M_n = 400,000$ ) and used at a concentration of 15% (w/v) in 1,1,1,3,3,3-Hexafluoro-2-propanol (HFP, Iris Biotech, Marktredwitz, Germany) and electrospun with an IME electrospinning device (Eindhoven, Netherlands) as described in Piccirillo et al.<sup>28</sup> Briefly, the solution was electrospun at 20 kV with an 18G needle, a collector distance set at 18 cm and a flowrate of 4 mL/h. In addition, a newly developed thermo-plastic polycarbonate-urethane (PU) was utilized.<sup>29</sup> The PU was dissolved in HFP at a concentration of 10% (w/v) and electrospun at 18 kV with a 24.5G needle, a collector distance of 25 cm and a flowrate of 4 mL/h. The scaffolds were sterilized for 20 min with 70% ethanol and washed with PBS prior to cell seeding.

### 2.2. Cell culture

Monocytes and macrophages were cultured at 37 °C and under a 5% CO<sub>2</sub> atmosphere. Cells were cultured in polystyrene, 12- or 24-well cell culture plates in culture medium (RPMI 1640 medium containing GlutaMax™ supplemented with 100 µg/mL streptomycin, 100 U/mL penicillin and 10% heat inactivated fetal bovine serum (FBS) (all from Thermo Fisher, Waltham, MA, USA).

### 2.3. Monocyte isolation

Whole blood was collected from healthy volunteers and isolation procedures were performed immediately after collection. To separate peripheral mononuclear cells (PBMCs) from erythrocytes and granulocytes, density gradient centrifugation using SepMate™ tubes and Lymphoprep™ (both from Stemcell, Cologne, Germany) was performed according to the manufacturer's instructions. In brief, fresh whole blood containing heparin as an anticoagulant was diluted 1:1 with PBS, layered over Lymphoprep™ in SepMate tubes and centrifuged at 1200 G for 10 min. Supernatants containing PBMCs were decanted into fresh, 50 mL falcon tubes and washed twice with PBS. PBMCs were then resuspended in cryopreservation medium (10% DMSO, 20% FBS, 70% RPMI). For long-term storage, PBMCs were frozen at a concentration of  $1 \times 10^7$  cells/mL at -150 °C. Monocytes were isolated by plastic adherence from frozen PBMCs as described by Delirezh et al.<sup>30</sup> Briefly, PBMCs were seeded at a concentration of  $5 \times 10^6$  cells/cm<sup>2</sup> and let adhere for 2 h at 37 °C and 5% CO<sub>2</sub> in culture medium. Non-adherent cells were then aspirated and removed. The remaining adherent monocytes were washed with PBS and continually cultured to mature into macrophages.

### 2.4. Macrophage maturation

Adherent monocytes were matured to macrophages over a period of 8 days in culture medium supplemented with 50 ng/mL macrophage

colony-stimulating factor (M-CSF, Biolegend, Amsterdam, Netherlands) at 37 °C and 5% CO<sub>2</sub>. Medium was changed at day 3 and 6.

### 2.5. Macrophage dissociation

Before dissociation, cells were washed 3x with FACS buffer (PBS + 2% FBS + 0.05 Mm NaN<sub>3</sub> + 0.1 Mm EDTA) to deplete cells of bivalent cations. Adherent macrophages were then detached using either Trypsin (10 min, Gibco), Accutase (10 min, Biolegend, Amsterdam, Netherlands), 10 mM EDTA (40 min),<sup>31</sup> a commercially available macrophage detachment solution (40 min, 4 °C) (PromoCell Macrophage Detachment Solution (PMDS) (Catalogue No: C-41330; PromoCell, Heidelberg, Germany) or scraping. Cells were detached at 37 °C and 5% CO<sub>2</sub> if not otherwise indicated. For Trypsin and Accutase treatments, essentially all cells fully detached after 10 min of incubation as shown in [Supplementary Figure 2](#).

### 2.6. Cell counting and viability

Cells were counted using a hemocytometer. Cell viability was assessed using either trypan blue (manual counting) or 7-AAD staining (flow cytometry) (Biolegend, CA, USA).

### 2.7. Flow cytometry

For FC analysis, harvested cells were blocked with 10% sterile-filtered, human, male AB serum (H2B, Limoges, France) in FACS buffer (PBS + 2% FBS + 0.05 Mm NaN<sub>3</sub> + 0.1 Mm EDTA) for 30 min at room temperature (RT) to prevent non-specific binding of antibodies. For cell surface marker staining, the following antibodies were used: CD86-Pacific Blue™ (clone IT2.2), HLADR-Brilliant Violet (clone L243), CD206-FITC (clone 15-2) and CD163-PE/Cy7 (clone RM3/1) (all Biolegend, CA, USA). For staining, all antibodies were diluted 1:50 with FACS buffer and cells were stained for 30 min at 4 °C in the dark and washed with FACS buffer subsequently. Data were acquired using a BD Biosciences LSRFortessa Cytometer (NJ, USA) and analyzed using FlowJo™ 10.4.2 (Tree Star, OR, USA). Cells were gated using forward scatter vs. sideward scatter properties to exclude debris, doublets and dead cells (7-AAD staining). Mean fluorescence intensities of the whole macrophage population were analyzed ([Supplementary Figure 1A + B](#)). Compensation controls were run for each experiment using software-based automatic compensation to consider potential fluorescence spill-over. In addition, fluorescence minus one (FMO) controls were run to determine performance of the antibody panel and the fluorescence staining pattern of each individual antibody.

### 2.8. Image acquisition and analysis

Mature MDMs were treated with Accutase for either 3 or 10 min followed by washing by gentle pipetting with PBS. For each substrate one specimen was left untreated as a control. To count adherent cells on cell culture plates or scaffolds, cells were fixed with 4% paraformaldehyde (PFA) for 15 min at RT, washed and stained with 4',6-diamidino-2-phenylindole (DAPI; Roche Diagnostics, Mannheim, Germany) for 10 min in the dark. Images were acquired using a Cell Observer fluorescence microscope (Zeiss, Oberkochen, Germany). The cell count was quantified by counting the DAPI-stained cell nuclei per area. Counting of nuclei was performed using the cell counter plugin of ImageJ.<sup>32</sup>

### 2.9. Dextran uptake

Macrophages were detached and re-seeded in culture medium containing 0.5 mg/mL fluorescein isothiocyanate (FITC)-dextran (MW 40.000 kDa, Sigma-Aldrich, MO, USA) for either 30 min or 3 h and compared to untreated, adherent cells. As a control for non-specific

binding of FITC-dextran to the cell surface, MDMs were incubated with FITC-dextran at 4 °C. This temperature permits binding to the cell surface but reduces cellular metabolism and therefore particle uptake. After incubation, the medium was aspirated, and cells were washed 2x with FACS buffer. Cells that had re-adhered during the incubation period with dextran were detached with Accutase for 10 min at 37 °C and 5% CO<sub>2</sub>.

### 2.10. Statistical analysis

All experiments were performed in technical triplicates and biological replicates (donors, indicated by "n"). Unless otherwise indicated, data were analyzed for significance using the Kruskal-Wallis Test with Dunn's post-hoc test with Graph Pad Prism 8.0.0 (Graph Pad Software Inc. San Diego, CA, USA). A p value < 0.05 was considered significant.

## 3. Results

### 3.1. Comparing the efficiency of dissociation methods for macrophage detachment

Our initial goal was to determine how effective common macrophage dissociation solutions are in detaching mature macrophages from polystyrene compared to the mechanically-based method of scraping. For optimal cell yields, trypsin, Accutase and the commercial detachment solution PMDS were applied according to the manufacturer's instructions. The results showed that non-enzymatic EDTA solutions fail to effectively detach MDMs from well plates, while both trypsin and Accutase surpassed cell yields obtained by scraping ([Fig. 1A](#)). It is noteworthy that the commercially available macrophage detachment solution did not have superior performance compared to the in-house made EDTA solution. Interestingly, while most protocols recommend detachment of MDMs with EDTA on ice, our results showed that temperature seems to play only a minor role in detachment success: cold shock did not significantly increase the cell yield compared to incubation with EDTA at 37 °C. In addition, we investigated how these methods influence cell viability, hypothesizing that scraping will result in highest cell death rates compared to non-mechanical treatments. In fact, scraping tended to result in the harvesting of less viable cells when compared to enzymatic detachment, but scraping still tended to perform better than the non-enzymatic solutions ([Fig. 1B](#)).

### 3.2. Impact of dissociation methods on surface marker detection

Having compared common detachment methods on cell yield and viability, we next investigated how different dissociation treatments impaired surface marker detection of the classical MDM polarization markers CD86, HLA-DR, CD206 and CD163.<sup>31,33,34</sup> Comparing the different methods, we observed that while HLA-DR and CD86 (M1 phenotype) did not significantly differ between the treatments, CD206 and CD163 (M2 phenotype) showed a significant decrease of mean fluorescence intensities (MFI) in the enzymatically-treated groups. Interestingly, cell scraping did not result in the highest conservation of MFIs, especially in M2 markers, when compared to EDTA solutions where MFIs were up to 50% increased. Besides the reduction in M2 marker intensity, it is notable that while temperature does appear to influence the mean MFI between the two EDTA treatments, a higher spread between donors was observed in groups incubated at 4 °C when compared to those incubated at 37 °C ([Fig. 2A–D](#)).

### 3.3. Time-dependent effects of accutase treatment on cell yield and surface marker detection

Accutase, in contrast to trypsin, is commonly used for the detachment of adherent cells for FC as it is widely believed to be gentler and less problematic for the detection of surface markers. Contrary to this

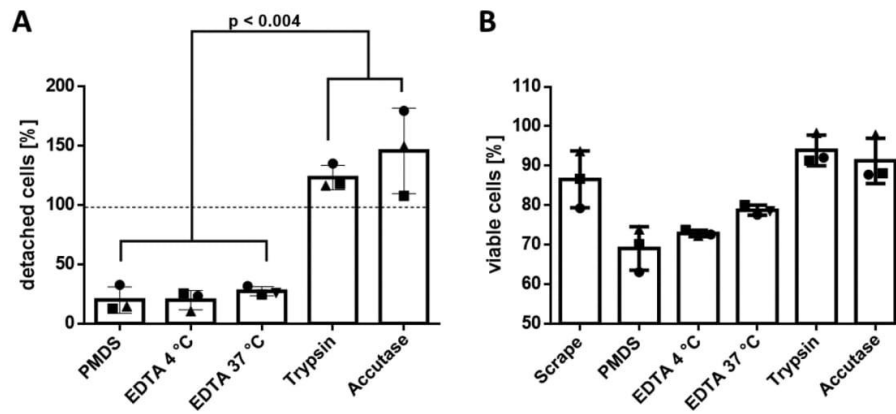


**Fig. 1.** Effectiveness of macrophage dissociation methods from tissue culture polystyrene. Adherent monocytes were matured over a period of 8 days to MDMs. For detachment, mature MDMs were incubated with the respective solution for the following time intervals: PMDS (40 min), EDTA (40 min), Trypsin (10 min) and Accutase (10 min). Unless otherwise indicated, cells were detached at 37 °C (A) Cell yields of dissociation solutions were normalized to scraping (dotted line). (B) Cell viability was assessed using staining with 7-AAD. Data are represented as mean ± SD (n = 3 unique donors). PMDS = PromoCell Macrophage Detachment Solution.

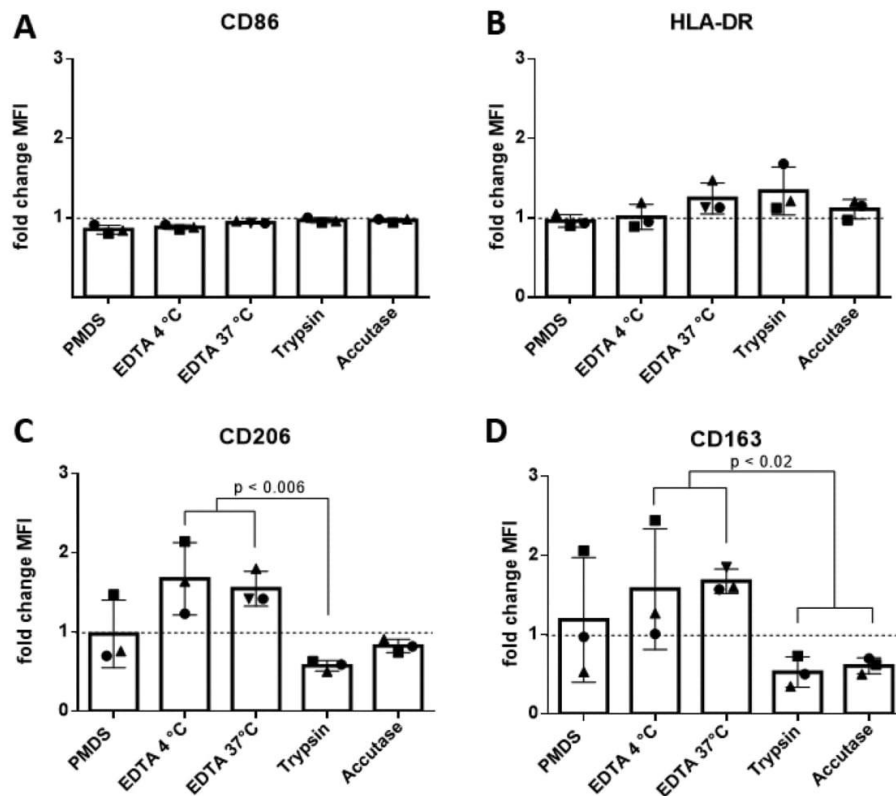


**Fig. 2.** Influence of dissociation methods on conservation of surface protein levels (MFI). Adherent monocytes were matured over a period of 8 days to MDMs and detached using different methods and temperatures. For detachment, MDMs were incubated with the respective solution for the following time intervals: PMDS (40 min), EDTA (40 min), Trypsin (10 min) and Accutase (10 min). Unless otherwise indicated, cells were detached at 37 °C. After detachment, cells were stained for the surface markers CD86 (A), HLA-DR (B), CD206 (C) and CD163 (D) and analyzed by FC. MFI of surface markers was normalized to scraping (dotted line) and is displayed as fold change. Data are presented as mean ± SD (n = 3 unique donors).

belief, we observed similar effects for both Accutase and trypsin on the loss of M2 surface markers CD206 and CD163. Although the results overall were similar, Accutase-treated samples tended to result in slightly higher levels of detected surface proteins and a more homogeneous spread of variation across donors. Therefore, after having performed the previous tests also considering viability and detachment efficiency, we concluded that Accutase provided the best balance between yield, viability and retention of surface markers on human MDMs. For this reason, we chose to examine the effect of Accutase on macrophages in greater detail.

We then investigated if time plays a role when using Accutase to retrieve adherent MDMs. At first, we tested the effect of time on cell yield by performing a time course experiment up to 10 min of Accutase treatment at 37 °C. A maximum of 10 min was employed as we had observed in previous experiments that incubation times exceeding this did not result in higher cell yields (Supplementary Figs. 2A–C). The results showed that there was no increase in the number of retrieved cells from initial treatment up to 5 min, but from this point the cell number increased steadily until peaking at 10 min incubation (Fig. 3). The cells were removed in parallel experiments using scraping, which is indicated by a dashed line on the graph.

We additionally investigated the effect of Accutase treatment over time on the detection of surface markers (Fig. 4). The results showed that, as previously observed, CD86 was the most stable of all tested markers, with only minor changes in the levels of detected protein over time for all donors. In contrast, both CD206 and CD163 showed greater variability across donors when compared to CD86, with some donors showing greater sensitivity to loss of surface antigen than others. HLA-DR was also highly variable, with some donors showing a different trend across time in the levels of protein detected (Fig. 4). Overall, we observed more variation for the detection of the M2 markers CD206 and CD163 compared to the M1 marker CD86, while HLA-DR also showed donor-dependent differences.

### 3.4. Impact of accutase treatment on macrophage phagocytic activity

MDMs are known for their phagocytic ability, especially the M2 phenotype which expresses CD206 (mannose receptor) and CD163 (hemoglobin scavenger receptor). As such these cells typically possess increased phagocytic capacity compared to M1 macrophages, since one of their main functions is the clearance of cellular debris from damaged or infected tissue. Thus, we investigated how macrophage dissociation using Accutase impacts the uptake of dextran. In these experiments, MDMs were either treated with Accutase for 3 min or 10 min and

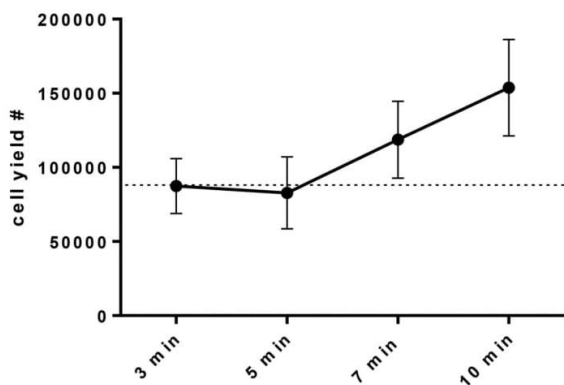


Fig. 3. Absolute numbers of macrophage yield obtained by incubation with Accutase across time. The dotted line represents the number of cells harvested by scraping. Total numbers of harvested cells per well  $\pm$  SD are shown ( $n = 3$  unique donors).

subsequently harvested and reseeded with FITC-conjugated dextran beads. As controls, macrophages were either left untreated or harvested via scraping. Uptake of FITC-dextran was examined at 30 min and 3 h in all groups and subsequently measured using FC. We observed the biggest difference in the uptake of dextran particles between the untreated control cells and treated cells. This effect was independent of the detachment procedure. There was a trend for MDMs treated with Accutase for 10 min to take up less dextran at the 30 min time point when compared with treatment for 3 min or scraping, but apart from this no major differences across experimental conditions were detected (Fig. 5).

### 3.5. Detachment efficiency of accutase from electrospun substrates

To test if Accutase treatment can effectively detach MDMs from a biomaterial, we investigated MDM removal from electrospun polymers. Electrospun materials are fibrous by nature and adherent cells are difficult to remove from the substrate as they typically infiltrate into the pores of the scaffold. However, their porous and fibrous architecture and resulting specific material characteristics make electrospun materials promising tools in regenerative medicine and tissue engineering. Two polymers widely used in regenerative medicine were chosen: PLA, a biodegradable polymer, and the non-degradable PU. Both were electrospun and prepared for cell culture according to protocols that have been established previously in our laboratory.<sup>29,35</sup> Monocytes from three donors, each with three technical replicates, were seeded on each electrospun scaffold and on standard tissue culture polystyrene plates. The cells were then cultured and matured to MDMs before being treated for removal. The results showed that after a 10 min incubation with Accutase, the highest number of cells was detached from the polystyrene control (Fig. 6A, D). Results from the PLA scaffold (Fig. 6B, E) show that a similar percentage of cells were detached from this material as the control well plate. Detachment from electrospun PU, however, was less efficient since up to 90% of the cells remained on the scaffold after Accutase treatment (Fig. 6C, F). It should be pointed out that on this material very inconsistent results were obtained across replicates.

## 4. Discussion

Investigating macrophage polarization states has gained substantial attention in the field of biomaterials over the last decade. In regenerative medicine and biomaterial research, macrophages have become promising targets for the modulation of wound healing, tissue regeneration and ECM remodeling.<sup>13,36–38</sup> In the field of medical implants, macrophages are said to be key players in maintaining implant integrity, but they may also be involved in chronic inflammation and implant failure.<sup>39,40</sup> However, the exact mechanisms of macrophage-material interactions remain elusive, as there are many unsolved challenges that prevent the comprehensive analysis of macrophage responses.<sup>31</sup> One major challenge that has been addressed in this work is the analysis of macrophages by FC.

Adhesion molecules rely on the presence of calcium and magnesium ions to facilitate cell-material interactions. EDTA chelates bivalent cations, depleting the cellular environment of these ions in free form. While this procedure works well with highly proliferative cells such as fibroblasts, human MDMs show almost no proliferating activity.<sup>41</sup> Low cell yields obtained in this study using EDTA indicate that the mere depletion of bivalent cations is not sufficient to reverse the adhesion process, but rather that active interference by enzymatic digestion is necessary to detach these cells. In the case of the commercial PMDS, while we do not know the exact composition, it is speculated that it employs a similar mechanism to EDTA to remove cells. Taken together, we hypothesize that cell biology is more relevant to the detachment process than any potential differences due to different substrates when it comes to the effectiveness of the detachment solutions used in this study. Thus we expect that the detachment solutions tested here would perform

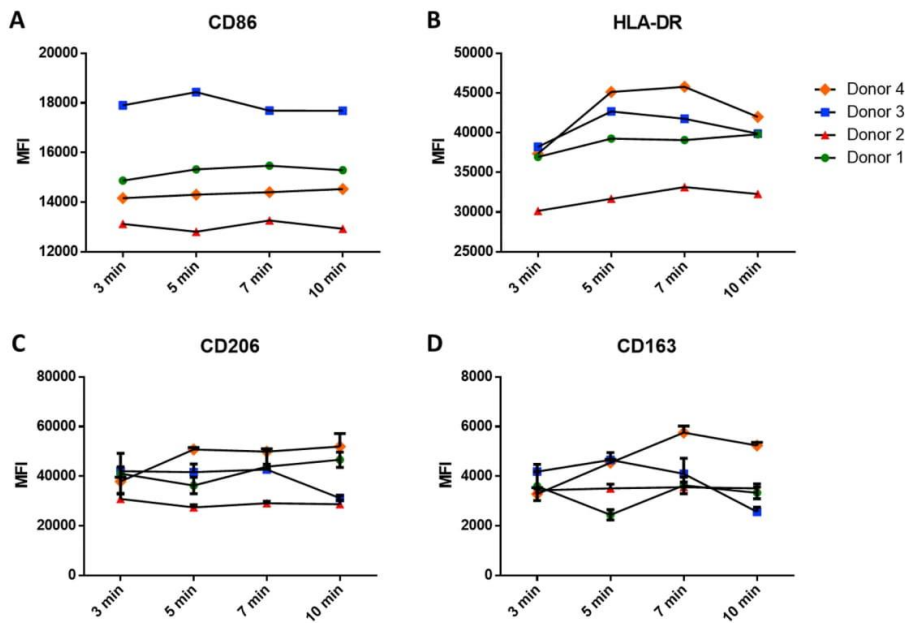


Fig. 4. Protein levels (MFI) of common macrophage surface markers across time with Accutase treatment: CD86 (A), HLA-DR (B), CD206 (C) and CD163 (D) of four donors. Mature MDMs were treated with Accutase for 3, 5, 7 and 10 min at 37 °C and analyzed by FC. Each color represents a different donor. Data are represented as mean ± SD (n = 4 unique donors).

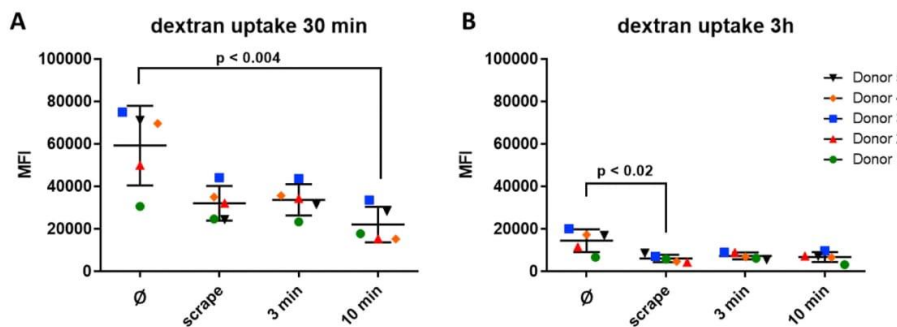


Fig. 5. MDMs were either scraped or treated with Accutase for 3 and 10 min, then reseeded and incubated with 0.5 mg/mL FITC-dextran for either (A) 30 min or (B) 3 h. Control cells (∅) were not detached and reseeded. Each color represents a different donor. Data are shown as mean ± SD (n = 5 unique donors).

similarly as we have shown when used to remove MDMs on other substrates that may show a different profile of adherent proteins or other differences in material properties.

In terms of enzymatic detachment, Chen et al.<sup>31</sup> previously showed, that both trypsin and Accutase selectively cleave the M2 surface proteins CD206 and CD163. Our study confirms these findings and further adds an additional layer of understanding by revealing substantial differences across donors that have not previously been reported. Changes in MFI of almost up to 50% were observed in some donors for CD206, while other donors appeared to be entirely unaffected to the effects of Accutase. Similar results were observed for the other M2 marker examined, CD163. While it has been claimed by Shiratori et al.<sup>42</sup> that the influence of Accutase on the detection of surface markers is negligible, we argue here that the observed changes in the levels of detected protein can significantly alter the interpretation of results, potentially to the point of altering the classification of macrophages into the M1 or M2

polarization states. In addition, the responses to Accutase seen in our study for each donor was highly variable and no general statement can be made regarding the effect of Accutase on the levels of detected proteins used for M2 characterization. This may have important consequences for the interpretation of results and for subsequent statistical analysis of experimental data, especially regarding the pooling of data from multiple donors. Though it should be acknowledged that in standard polarization experiments where cells are treated with strong stimuli such as with IFN $\gamma$  or LPS, the influence of biomaterials on macrophage response is expected to be much more subtle and less dramatic with regard to changes in surface marker expression.<sup>34,43</sup> Additional studies are necessary to provide clearer insight into the potential consequence for the use of enzymatic dissociation methods on altering the interpretation of experimental results when studying human MDMs in the context of biomaterials.

In addition to the expression of cell surface proteins, another

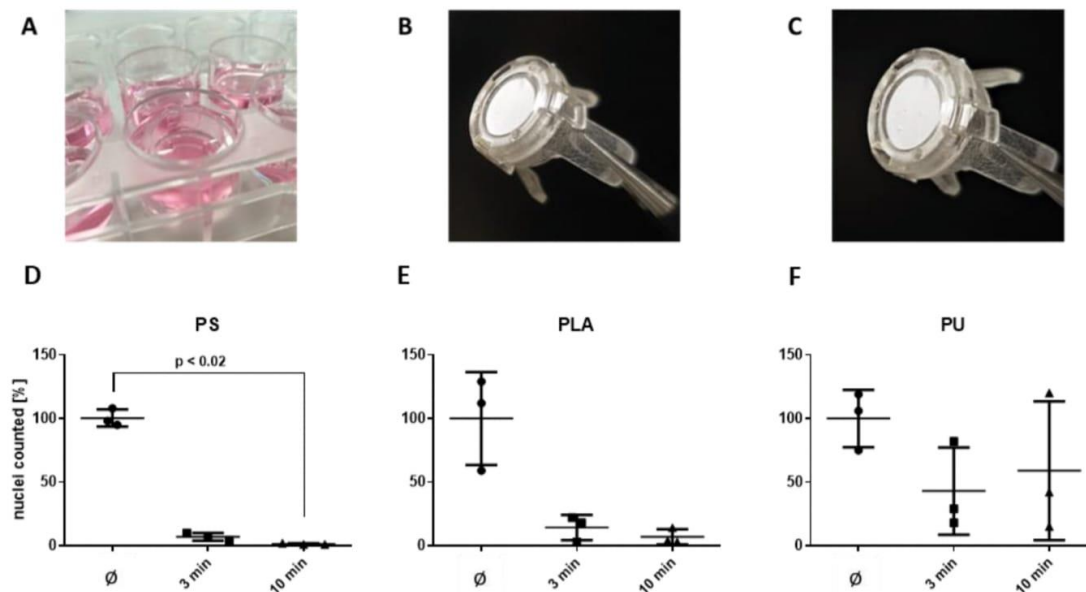


Fig. 6. Monocytes of three donors were seeded on either (A) polystyrene well plates (B) electrospun PLA or (C) electrospun PU mounted to cell crowns. Scaffolds and wells were subsequently treated with either 3 or 10 min Accutase. Controls ( $\emptyset$ ) were left untreated. Remaining cells were counted using DAPI staining and ImageJ. Untreated specimens were set at 100% nuclei counted and treated specimens were normalized against 100%. Data are represented as mean  $\pm$  SD ( $n = 3$  unique donors).

indicator of macrophage response is their ability to clear cellular debris via endocytosis. Previously, it has been shown that a correlation exists between enzymatic treatment and reduced uptake of dextran beads,<sup>31</sup> and that polarized macrophages differ in their ability to take up and process antigens.<sup>44</sup> Here, we demonstrated that despite the loss of CD206, which is responsible for the uptake of bacterial glycoproteins, uptake of dextran was not significantly decreased in cells that were treated with Accutase when compared with cells that had been detached mechanically. In fact, our results have revealed that the detachment process per se, independent of the method being mechanical or enzymatic, is responsible for a significantly reduced ability to take up dextran particles. This indicates that disruption and/or lack of cell adhesion by macrophages to a surface impacts functionality to a greater extent than enzymatic treatment. This is in accordance with studies of other cell types that depend on cell adhesion for certain endocytic pathways.<sup>45</sup> This has to be considered when designing studies that come with the need for detaching MDMs from their substrate. Further investigation is required to establish if post detachment resting is able to restore this loss in phagocytic ability. Such follow-up studies are necessary to avoid unwanted experimental artifacts caused by experimental design.

One of the main objectives of this study was to determine the efficiency of cell detachment protocols on surfaces other than polystyrene well plates. Mechanical detachment of adherent cells is a valid alternative to enzymatic digestion but can only be employed on planar substrates such as polystyrene cell culture plates. In the field of regenerative medicine, fibrous, ECM-like structures are preferably used to direct the immune response to support wound healing and regeneration.<sup>46-48</sup> In our experiments we used therefore electrospun scaffolds of two different polymers, PLA and PU, both commonly used in regenerative medicine.<sup>49-52</sup> Electrospinning of polymers allows the manufacturing of fibrous scaffolds that facilitate cell adhesion and survival by providing a natural, ECM-like environment.<sup>53</sup> Here we showed that protocols which work well on planar cell culture surfaces should not be transferred to 3D substrates without prior examination of their effectiveness. While 10 min Accutase incubation detached  $\geq 99\%$  of

MDMs from polystyrene cell culture plates and  $\geq 93\%$  from electrospun PLA, cell yields harvested from PU varied significantly between 10 and 50%. It is well established that polymer chemistry can have profound effects on cell adhesion,<sup>54,55</sup> however, in 3D biomaterials the impact on cell adhesion is multifactorial: surface energy, polarity, wettability but also fiber and pore size have the potential to affect the adherent cell.<sup>56</sup> Both electrospun materials used in this study had water contact angles in the hydrophobic range (PLA:  $137 \pm 7^\circ$ , PU:  $117 \pm 4^\circ$ ), making it less likely that this was a crucial factor in the difference in cell detachment observed. However, fiber size differed several-fold (PLA:  $156 \pm 6$  nm; PU:  $775 \pm 163$  nm) when comparing both materials. Small fiber sizes usually come with smaller pores and less potential for the cells to infiltrate, making it easier for enzymatic solutions to detach cells. This could be an explanation for the observed differences in detachment efficacy. Further studies are necessary to explore the impact of material architecture on detachment processes, in particular, to test the effectiveness of dissociation methods other than Accutase on 3D substrates.

In summary, this work highlights that detaching MDMs from substrate, regardless of method, inherently impacts cellular functionality. However, the removal of cells from substrate is required for many analysis techniques, and we show that the choice of method has important consequences for experimental results. In particular, we highlight that care should be taken when detaching MDMs by enzymatic digestion, as both trypsin and accutase selectively cleave the M2 markers CD206 and CD163 in a donor-dependent manner. However, Accutase treatment has only minor effects compared to cell scraping with regard to the alteration of surface proteins. In cases where the substrate architecture does not allow the scraping of cells, existing protocols for cell detachment have to be adjusted, because we show that the effectiveness is determined by the particular substrate in question. Overall, this work emphasises the need for any detachment protocol to balance cell yield, cell viability, impact on function and surface marker conservation, as well as in examining potential differences across donors to the chosen method.

### Declaration of competing interest

The authors declare that they have no known competing financial interests or personal relationships that could have appeared to influence the work reported in this paper.

### Acknowledgements

The authors thank Prof. Martina Seifert and Maria Schneider (both Berlin-Brandenburg Center for Regenerative Therapies, Berlin, Germany) for providing their expertise and support on macrophage culture and polarization protocols. We also would like to thank Prof. Günter Lorenz and Larysa Kutuzova (University of Reutlingen, Applied Chemistry) for providing the polyurethane used in this study. We are grateful to Simone Liebscher (Department of Women's Health, University of Tübingen) for her excellent technical assistance.

### Appendix A. Supplementary data

Supplementary data to this article can be found online at <https://doi.org/10.1016/j.regen.2020.100035>.

### Funding

This research received funding from the “Ministerium für Wirtschaft, Arbeit und Wohnungsbau” of the German state of Baden-Württemberg (Grant number: 3/4332.62-NMI/64). This work was also supported by the EU-EFRE and the German state of Baden-Württemberg (712,889).

### Author credit statement

**Nora Feuerer:** Conceptualization, Investigation, Validation, Formal Analysis, Writing – Original Draft, **Johannes Morschl:** Investigation, Formal Analysis, Writing Review & Editing, **Ruben Daum:** Resources, Writing Review & Editing, **Martin Weiss:** Resources, Writing Review & Editing, **Svenja Hinderer:** Conceptualization, Project Administration, Writing Review & Editing, **Katja Schenke-Layland:** Supervision, Funding Acquisition, Writing Review & Editing, **Christopher Shipp:** Project Administration, Conceptualization, Data Curation, Writing – Original Draft.

### References

- Leitner L, et al. Trends and economic impact of hip and knee arthroplasty in central Europe: findings from the Austrian national database. *Sci Rep.* 2018;8(1):4707.
- Burke NG, et al. Total hip replacement—the cause of failure in patients under 50 years old? *Ir J Med Sci.* 1971;188(3):879–883, 2019.
- Hallab NJ. Biologic responses to orthopedic implants: innate and adaptive immune responses to implant debris. *Spine.* 2016;41:S30–S31.
- Anderson JM, Jiang S. Implications of the acute and chronic inflammatory response and the foreign body reaction to the immune response of implanted biomaterials. *The Immune Response to Implanted Materials and Devices.* Springer; 2017:15–36.
- Barbarash L, et al. T cell response in patients with implanted biological and mechanical prosthetic heart valves. *Mediat Inflamm.* 2016;2016.
- Anderson JM, Miller KM. Biomaterial biocompatibility and the macrophage. *Biomaterials.* 1984;5(1):5–10.
- Graney PL, et al. In vitro response of macrophages to ceramic scaffolds used for bone regeneration. *J R Soc Interface.* 2016;13(120):20160346.
- Wynn TA, Vannella KM. Macrophages in tissue repair, regeneration, and fibrosis. *Immunity.* 2016;44(3):450–462.
- Chung L, et al. Key players in the immune response to biomaterial scaffolds for regenerative medicine. *Adv Drug Deliv Rev.* 2017;114:184–192.
- Bota PC, et al. Biomaterial topography alters healing in vivo and monocyte/macrophage activation in vitro. *J Biomed Mater Res.* 2010;95(2):649–657.
- Corradetti B, et al. Immune tuning scaffold for the local induction of a pro-regenerative environment. *Sci Rep.* 2017;7.
- Schneider M, et al. The choice of cryopreservation method affects immune compatibility of human cardiovascular matrices. *Sci Rep.* 2017;7(1).
- Godwin JW, Rosenthal N. Scar-free wound healing and regeneration in amphibians: immunological influences on regenerative success. *Differentiation.* 2014;87(1):66–75.
- Godwin JW, Pinto AR, Rosenthal NA. Macrophages are required for adult salamander limb regeneration. *Proc Natl Acad Sci Unit States Am.* 2013;110(23):9415–9420.

- Ferrante CJ, Leibovich SJ. Regulation of macrophage polarization and wound healing. *Adv Wound Care.* 2012;1(1):10–16.
- Eming SA, Wynn TA, Martin P. Inflammation and metabolism in tissue repair and regeneration. *Science.* 2017;356(6342):1026–1030.
- Lucas T, et al. Differential roles of macrophages in diverse phases of skin repair. *J Immunol.* 2010;184(7):3964–3977.
- Mantovani A, et al. The chemokine system in diverse forms of macrophage activation and polarization. *Trends Immunol.* 2004;25(12):677–686.
- Mosser DM, Edwards JP. Exploring the full spectrum of macrophage activation. *Nat Rev Immunol.* 2008;8(12):958–969.
- Araujo-Gomes N, et al. Complement proteins regulating macrophage polarisation on biomaterials. *Colloids Surf B Biointerfaces.* 2019;181:125–133.
- Graney PL, et al. In vitro response of macrophages to ceramic scaffolds used for bone regeneration. *J R Soc Interface.* 2016;13(120).
- Lin J, et al. Cell-material interactions in tendon tissue engineering. *Acta Biomater.* 2018;70:1–11.
- Schaub NJ, et al. The effect of engineered nanotopography of electrospun microfibers on fiber rigidity and macrophage cytokine production. *J Biomater Sci Polym Ed.* 2017; 28(13):1303–1323.
- Wang Z, et al. The effect of thick fibers and large pores of electrospun poly(epsilon-caprolactone) vascular grafts on macrophage polarization and arterial regeneration. *Biomaterials.* 2014;35(22):5700–5710.
- Quan Y, et al. Impact of cell dissociation on identification of breast cancer stem cells. *Canc Biomarkers.* 2013;12(3):125–133.
- Merten OW. Cell detachment. *Encycl. Ind. Biotechnol.: Bioprocess Bioseparat. Cell Technol.* 2009:1–22.
- Tsuji K, et al. Effects of different cell-detaching methods on the viability and cell surface antigen expression of synovial mesenchymal stem cells. *Cell Transplant.* 2017; 26(6):1089–1102.
- Piccirillo G, et al. Controlled and tuneable drug release from electrospun fibers and a non-invasive approach for cytotoxicity testing. *Sci Rep.* 2019;9(1).
- Daum R, et al. Fibronectin adsorption on electrospun synthetic vascular grafts attracts endothelial progenitor cells and promotes endothelialization in dynamic in vitro culture. *Cells.* 2020;9(3).
- Delirez N, et al. Comparison the effects of two monocyte isolation methods, plastic adherence and magnetic activated cell sorting methods, on phagocytic activity of generated dendritic cells. *Cell J.* 2013;15(3):218–223.
- Chen S, et al. Impact of detachment methods on M2 macrophage phenotype and function. *J Immunol Methods.* 2015;426:56–61.
- Schindelin J, et al. Fiji: an open-source platform for biological-image analysis. *Nat Methods.* 2012;9(7):676–682.
- Spiller KL, et al. The role of macrophage phenotype in vascularization of tissue engineering scaffolds. *Biomaterials.* 2014;35(15):4477–4488.
- Hinderer S, et al. Surface functionalization of electrospun scaffolds using recombinant human decorin attracts circulating endothelial progenitor cells. *Sci Rep.* 2018;8(1):110.
- Piccirillo G, et al. Non-invasive characterization of hybrid gelatin: poly-l-lactide electrospun scaffolds using second harmonic generation and multiphoton imaging. *J Mater Chem B.* 2018;6(40):6399–6412.
- Barthes JGD, et al. Immune assisted tissue engineering via incorporation of macrophages in cell-laden hydrogels under cytokine stimulation. *Front. Bioeng. Biotechnol.* 2019;7:29.
- Debels H, et al. Macrophages play a key role in angiogenesis and adipogenesis in a mouse tissue engineering model. *Tissue Eng.* 2013;19(23-24):2615–2625.
- Freytes DO, et al. Macrophages modulate the viability and growth of human mesenchymal stem cells. *J Cell Biochem.* 2013;114(1):220–229.
- Fehervari Z. Implant response. *Nat Immunol.* 2019;20(3):245.
- Pettersson M, Thorén MM, Johansson A. Titanium activates the NLRP-3 inflammasome in macrophages. *Clin Oral Implants Res.* 2019;30, 102–102.
- Tushinski RJ, et al. Survival of mononuclear phagocytes depends on a lineage-specific growth factor that the differentiated cells selectively destroy. *Cell.* 1982;28(1):71–81.
- Shiratori H, et al. THP-1 and human peripheral blood mononuclear cell-derived macrophages differ in their capacity to polarize in vitro. *Mol Immunol.* 2017;88: 58–68.
- Jaguin M, et al. Polarization profiles of human M-CSF-generated macrophages and comparison of M1-markers in classically activated macrophages from GM-CSF and M-CSF origin. *Cell Immunol.* 2013;281(1):51–61.
- Canton J. Phagosome maturation in polarized macrophages. *J Leukoc Biol.* 2014;96(5):729–738.
- Kawauchi T. Cell adhesion and its endocytic regulation in cell migration during neural development and cancer metastasis. *Int J Mol Sci.* 2012;13(4):4564–4590.
- Underwood RA, et al. Quantifying the effect of pore size and surface treatment on epidermal incorporation into percutaneously implanted sphere-templated porous biomaterials in mice. *J Biomed Mater Res.* 2011;98A(4):499–508.
- Madden LR, et al. Proangiogenic scaffolds as functional templates for cardiac tissue engineering. *Proc Natl Acad Sci Unit States Am.* 2010;107(34):15211–15216.
- Dawson ER, et al. Increased internal porosity and surface area of hydroxyapatite accelerates healing and compensates for low bone marrow mesenchymal stem cell concentrations in critically-sized bone defects. *Appl Sci.* 2018;8(8):1366.
- Noga S, et al. Polyurethane composites as a potential 3D scaffold for Mesenchymal Stem Cells in cartilage regeneration. *Eng. Biomater.* 2019;22.
- Chiono V, et al. Synthetic biodegradable medical polyurethanes. *Science and Principles of Biodegradable and Bioresorbable Medical Polymers.* Elsevier; 2017:189–216.
- Santoro M, et al. Poly (lactic acid) nanofibrous scaffolds for tissue engineering. *Adv Drug Deliv Rev.* 2016;107:206–212.



N. Feuerer et al.

*Journal of Immunology and Regenerative Medicine* 11 (2021) 100035

- 52 Hinderer S, et al. Engineering of a bio-functionalized hybrid off-the-shelf heart valve. *Biomaterials*. 2014;35(7):2130–2139.
- 53 Hinderer S, Layland SL, Schenke-Layland K. ECM and ECM-like materials - biomaterials for applications in regenerative medicine and cancer therapy. *Adv Drug Deliv Rev*. 2016;97:260–269.
- 54 Tamada Y, Ikada Y. Cell adhesion to plasma-treated polymer surfaces. *Polymer*. 1993; 34(10):2208–2212.
- 55 Dewez JL, et al. Adhesion of mammalian cells to polymer surfaces: from physical chemistry of surfaces to selective adhesion on defined patterns. *Biomaterials*. 1998;19 (16):1441–1445.
- 56 Di Cio S, Gautrot JE. Cell sensing of physical properties at the nanoscale: mechanisms and control of cell adhesion and phenotype. *Acta Biomater*. 2016;30:26–48.

Appendix II Feuerer N, Marzi J, Brauchle E, Carvajal Berrio D, Weiss M, Billing F, Jakobi M, Schneiderhan-Marra N, Shipp C, Schenke Layland K. Lipidome profiling with Raman Spectroscopy identifies macrophage response to surface topography of biomaterials. PNAS, 2021, 118 (52) e2113694118.



# Lipidome profiling with Raman microspectroscopy identifies macrophage response to surface topographies of implant materials

Nora Feuerer<sup>a,b</sup>, Julia Marzi<sup>a,b,c</sup>, Eva M. Brauchle<sup>a,b,c</sup>, Daniel A. Carvajal Berrio<sup>b,c</sup>, Florian Billing<sup>a</sup>, Martin Weiss<sup>a,d</sup>, Meike Jakobi<sup>a</sup>, Nicole Schneiderhan-Marra<sup>a</sup>, Christopher Shipp<sup>a</sup>, and Katja Schenke-Layland<sup>a,b,c,e,1</sup>

<sup>a</sup>NMI Natural and Medical Sciences Institute at the University of Tübingen, 72770 Reutlingen, Germany; <sup>b</sup>Institute of Biomedical Engineering, Department for Medical Technologies and Regenerative Medicine, Eberhard Karls University Tübingen, 72076 Tübingen, Germany; <sup>c</sup>Cluster of Excellence "Image-Guided and Functionally Instructed Tumor Therapies", Eberhard Karls University Tübingen, 72076 Tübingen, Germany; <sup>d</sup>Department of Women's Health, Research Institute for Women's Health, Eberhard Karls University Tübingen, 72076 Tübingen, Germany; and <sup>e</sup>Department of Medicine, Division of Cardiovascular Medicine, University of California, Los Angeles, CA 90095

Edited by Cato Laurencin, UConn Health, Farmington, CT; received July 25, 2021; accepted November 16, 2021

**Biomaterial characteristics such as surface topographies have been shown to modulate macrophage phenotypes. The standard methodologies to measure macrophage response to biomaterials are marker-based and invasive. Raman microspectroscopy (RM) is a marker-independent, noninvasive technology that allows the analysis of living cells without the need for staining or processing. In the present study, we analyzed human monocyte-derived macrophages (MDMs) using RM, revealing that macrophage activation by lipopolysaccharides (LPS), interferons (IFN), or cytokines can be identified by lipid composition, which significantly differs in M0 (resting), M1 (IFN- $\gamma$ /LPS), M2a (IL-4/IL-13), and M2c (IL-10) MDMs. To identify the impact of a biomaterial on MDM phenotype and polarization, we cultured macrophages on titanium disks with varying surface topographies and analyzed the adherent MDMs with RM. We detected surface topography-induced changes in MDM biochemistry and lipid composition that were not shown by less sensitive standard methods such as cytokine expression or surface antigen analysis. Our data suggest that RM may enable a more precise classification of macrophage activation and biomaterial-macrophage interaction.**

macrophage polarization | Raman imaging | innate immunity | biomaterials | Raman spectroscopy

**M**acrophages play an essential role in our innate immune system. They patrol tissues, detect pathogens, and respond to tissue damage (1–3). Macrophages remove pathogens and cellular debris through phagocytosis and encapsulation, and they control downstream processes such as wound healing and tissue regeneration (4, 5). To accommodate the multitude of tasks, macrophages exhibit a high degree of plasticity, which allows them to reversibly adopt different phenotypes within a short period of time (6–8). Macrophage activation is dependent on a variety of bioactive molecules and is usually controlled by complex signaling pathways in vivo. Macrophages are typically classified into the following categories: M0 (resting), M1 (proinflammatory), and M2 (anti-inflammatory). M2 macrophages are further divided into fibrotic (M2a) and regenerative (M2c) subtypes (9). This classification is not definite, as many other activation states exist (10).

Adverse immune reactions toward implant materials are known to cause chronic inflammation, tissue loss, aseptic loosening, and fibrotic encapsulation (11, 12). This process is typically associated with significant pain for the patient, the need for repeated surgeries, and implant replacement (13, 14). Recently, materials designed to modulate the immune response have seen intense interest, as they may improve implant durability and integration (15). Macrophages are key cells in this process and are highly sensitive to material surface characteristics such as topography, stiffness, or wettability (16–21). However, how these properties impact macrophage behavior is not fully understood.

Macrophage classification is typically performed using techniques such as flow cytometry (FC), analyzing RNA expression, or enzyme-linked immunosorbent assays. These end-point analytical techniques require complex processing and invasive reagents such as antibodies and primers. Cells are not analyzed in their native state, and the focus is on the expression of only predefined marker genes or proteins. As macrophage polarization is in flux, their classification into discrete categories based on a priori defined markers can be problematic (22).

Raman microspectroscopy (RM) has emerged as a powerful tool for the investigation of living cells, assessing their physiology and biochemical composition on a single-cell level without the need for processing or staining (23). RM can be used to identify chemical fingerprints or patterns of distinct cellular components such as nucleic acids, proteins, and lipids (24, 25). Previous research has demonstrated that RM can be used to reliably distinguish between different cell phenotypes or stages of the cell cycle based on the spectral information obtained by RM (25–29).

In this study, we present an approach for in situ macrophage characterization and monitoring their response to distinct surface

## Significance

**Macrophage plasticity and activation dynamics are under intense investigation because their full complexity cannot be captured by the few predefined markers that are commonly used. Macrophages are highly adherent and respond to surface microstructures in a sensitive manner. Here, we use Raman microspectroscopy and Raman imaging to study the macrophage response to defined activation stimuli and transfer these findings to macrophages cultured on titanium with varying surface roughness. We show that Raman-based methods can discriminate between macrophage phenotypes noninvasively and without the need to use antibody-based cell markers.**

Author contributions: N.F., J.M., E.M.B., C.S., and K.S.-L. designed research; N.F., J.M., D.A.C.B., and M.J. performed research; M.W. contributed new reagents/analytic tools; N.F., J.M., D.A.C.B., F.B., M.J., and K.S.-L. analyzed data; M.W. ensured accordance of the study with ethical guidelines; and N.F., J.M., E.M.B., F.B., N.S.-M., and K.S.-L. wrote the paper.

The authors declare no competing interest.

This article is a PNAS Direct Submission.

This open access article is distributed under Creative Commons Attribution-NonCommercial-NoDerivatives License 4.0 (CC BY-NC-ND).

<sup>1</sup>To whom correspondence may be addressed. Email: katja.schenke-layland@uni-tuebingen.de.

This article contains supporting information online at <http://www.pnas.org/lookup/suppl/doi:10.1073/pnas.2113694118/-/DCSupplemental>.

Published December 21, 2021.

features of titanium. By analyzing Raman spectral fingerprints of activated macrophages, we were able to characterize the cell response without detaching or exogenously labeling the cells. Information derived from these data provides valuable insight into macrophage physiology on a level that is not achievable by classical analytical techniques, potentially providing information for the field of macrophage activation. Furthermore, we demonstrate that RM can analyze material-adherent cells and that the resulting spectral information can be used to classify the macrophage response into the existing activation spectrum.

## Results

We characterized lipid spectra of four distinctively polarized human monocyte-derived macrophage (MDM) subtypes: M0 (resting), M1 (lipopolysaccharides [LPS]/IFN- $\gamma$ ), M2a (IL-4/IL-13), and M2c (IL-10) by RM. We provide evidence that Raman lipid fingerprint spectra can be used to assess activation states of adherent macrophages without additional treatment, providing insights into the impact of biomaterial surface characteristics like topography and roughness.

**Establishment of a Human Macrophage in vitro Model for RM.** A human macrophage in vitro polarization model was validated by thoroughly assessing the immune response of MDMs isolated from six healthy individual donors (three female and three male) toward polarization stimuli. Morphological characteristics, surface marker expression, and cytokine secretion are outlined in Fig. 1. Distinct morphological features such as the “fried egg” morphology (Fig. 1 *A* and *B*), spindle-shaped elongation (Fig. 1 *C* and *D*), or a mixture of both (Fig. 1 *A*) are observable by light microscopy (Fig. 1 *A–D*). Surface marker expression measured by FC of CD86 and human leukocyte antigen-DR isotype (HLA-DR) was significantly enhanced in M1 and M2a macrophages but not in M2c (Fig. 1 *E* and *F*). In contrast, M2a macrophages exhibited a significantly increased CD206 expression compared with M0 and M1 (Fig. 1 *G*), while the same could be observed for M2c macrophages regarding CD163 (Fig. 1 *H*). These findings were confirmed by imaging FC and microscopy images, of which we assessed mean fluorescence intensities (MFIs in Fig. 1 *I*).

Cytokine secretion was analyzed by Luminex technology to further characterize the immunological response toward polarization stimuli (Fig. 1 *J–Q*). A significant increase in proinflammatory cytokines secreted by M1 macrophages, such as IL-6, TNF- $\alpha$ , IL-8, and IL-1 $\beta$ , was observed, while MIP-1 $\beta$  and IL-1RA were increased in M2a macrophages and MCP-1 was increased in M2c macrophages.

**Raman Imaging Resolves Subcellular Structures in MDMs.** MDMs from the same donors were polarized, detached, fixed, and analyzed by RM. Raman imaging was employed to resolve subcellular structures of macrophages and to better visualize changes between polarization states. Using true component analysis (TCA), three main cellular components were identified that could be attributed to nucleic acids, proteins, and lipids based on their location within the cell (Fig. 2 *A–D*) and their Raman fingerprint spectra (Fig. 2 *E*). By comparing the average lipid spectrum to reports in the literature, triacylglycerides (TAGs) were identified as the main constituent of the lipid component (30). This was confirmed by in-house measurements of reference spectra. For comparison, a typical TAG spectrum is shown in Fig. 2 *E* (TAG and glyceryl trioleate).

**Raman Lipid Spectra Identify Spectral Differences between Polarized MDMs.** To determine if RM can differentiate between different macrophage polarization states, Raman spectra of each component were extracted and an average spectrum per cell and

component was calculated. Average spectra for each subcellular structure were analyzed by principal component analysis (PCA) identifying that the best separation of all subtypes was achieved by the lipid component as shown in *SI Appendix*, Fig. 1 *A–C*.

The lipid component of each cell was extracted, and 2% of the most intense component spectra were analyzed by PCA revealing distinct score clusters of M1 and M2a macrophages (Fig. 3 *A*). Statistical analysis of the PC score values confirmed significant separation between all four subtypes (Fig. 3 *B* and *C*). To identify Raman peaks responsible for the separation, PC loadings were plotted, and prominent peaks were identified as indicated by the black arrows (Fig. 3 *D* and *E*). Particularly pronounced were peaks in the lipid region at 1,655  $\text{cm}^{-1}$ , 2,855  $\text{cm}^{-1}$ , 2,965  $\text{cm}^{-1}$ , and 2,980  $\text{cm}^{-1}$ . All relevant peaks and their molecular assignments are listed in *SI Appendix*, Table 1.

For a more in-depth understanding of the molecular composition of the lipid component, an average spectrum for each MDM subtype was extracted (Fig. 3 *F*, M0 through M2c) and compared to typical lipid spectra from the literature, indicating linoleic and palmitoleic acid as likely constituents (30). Reoccurring prominent peaks in the loading plots as well as the average spectra were located at Raman shifts of 1,440  $\text{cm}^{-1}$ , 1,655  $\text{cm}^{-1}$ , 2,855  $\text{cm}^{-1}$ , 2,935  $\text{cm}^{-1}$ , and 3,010  $\text{cm}^{-1}$ .

To assess if the impact of substrate topography on macrophage phenotype can be analyzed in situ on a single-cell basis, we tested monocyte polarity on different surfaces. Human monocytes from three of the previous donors were seeded and cultured on glass (control) and two types of titanium disks with distinct surface topographies: 1) machine-polished titanium (Ti M) with a smooth surface pattern of parallel grooves and 2) acid-etched titanium (Ti A) with a rough surface (Fig. 4 *A–C*). Regions of interest (ROIs) of 150  $\times$  150  $\mu\text{m}$  were scanned, and Raman spectra were analyzed by TCA (Fig. 4 *D–F*). All three major cellular components were identified by TCA in MDMs cultured on glass, Ti M and Ti A. For validation purposes, MDM response toward the different substrates was also evaluated by classical antigen expression and cytokine secretion. We identified that the physiological response of MDMs cultured on biomaterial substrates was less pronounced compared to actively polarized MDMs. All surface antigens remained at resting level except CD206, which was significantly increased in MDMs cultured on Ti A (Fig. 4 *G–J*). The tested substrates did not trigger a release of proinflammatory cytokines such as TNF- $\alpha$  or IL-8 (Fig. 4 *K* and *L*). Notably, MIP-1 $\beta$  was not secreted in substrate-adherent MDMs, despite being highly expressed in both M1 and M2a macrophages (Fig. 4 *M*). Instead, a moderate increase in MCP-1 was observed in MDMs cultured on Ti A, a cytokine that was also increased in M2c macrophages (Fig. 4 *N*).

Average lipid RM spectra of substrate-activated MDMs were analyzed by PCA in order to assess if previously generated Raman lipid fingerprints could be employed to classify MDMs of an unknown activation state (Fig. 5 *A*). Loading plots showed a separation based on the same bands as observed in the targeted polarization experiment in Fig. 3. PC loadings revealed major peaks at 1,005  $\text{cm}^{-1}$ , 1,340  $\text{cm}^{-1}$ , 1,655  $\text{cm}^{-1}$ , 2,855  $\text{cm}^{-1}$ , and 2,945  $\text{cm}^{-1}$  (Fig. 5 *B*). A separate PCA showed that the same component was identified across donors, as outlined in the loading plot depicted in *SI Appendix*, Fig. 3. Statistical analysis of the scores of individual donors revealed a significant separation of substrate-adherent macrophages between all tested materials using only two PCs (Fig. 5 *C*). Scores of substrate-activated MDMs were projected onto the PCA previously calculated (Fig. 5 *D*) with polarized MDMs to determine whether the lipid spectra of substrate-activated macrophages are comparable to those of polarized macrophages (Fig. 5 *E* and *F*). PCA projection visualized a proximity of M2c MDMs and Ti A MDMs, which is in accordance with the increased expression of MCP-1 of MDMs cultured on Ti A. Notably, titanium-activated MDMs were, in

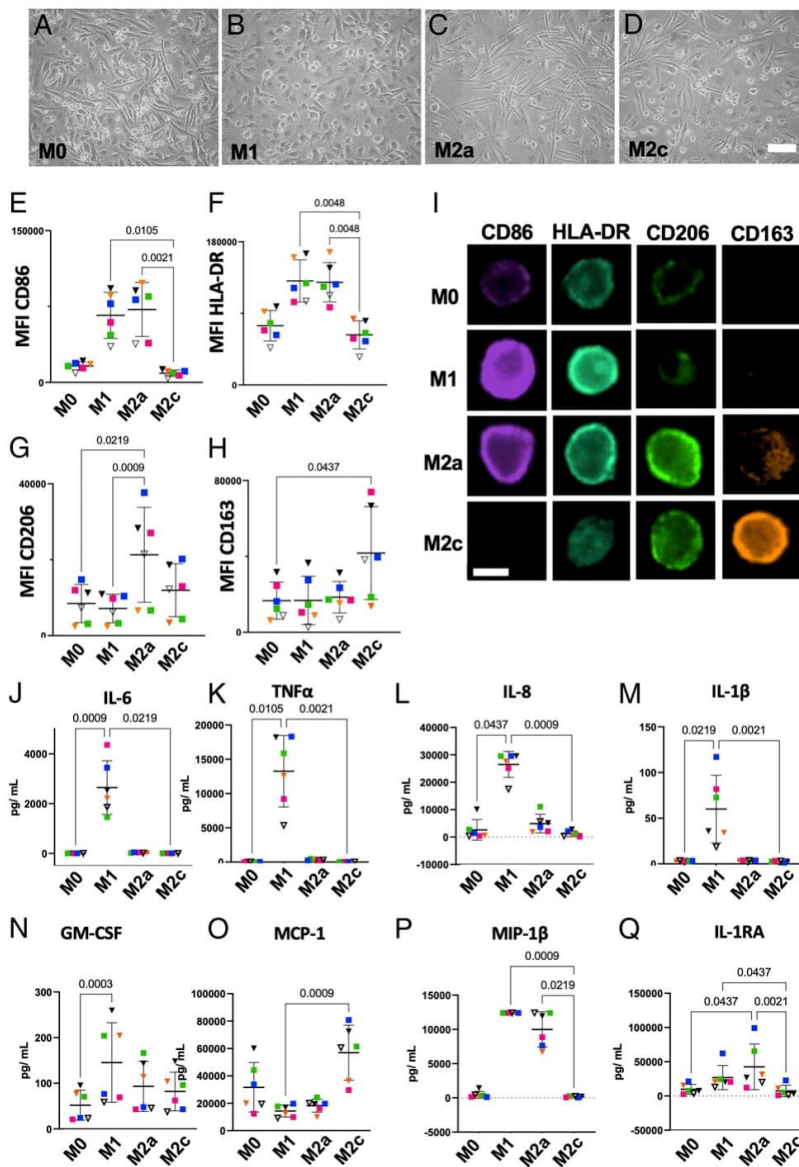


**Fig. 1.** Polarized MDMs display distinct morphological and physiological characteristics. (A–D) Brightfield images (10x magnification) show the morphology of polarized, human MDMs. (Scale bar, 50  $\mu$ m.) (E–H) MFIs of polarization-associated surface antigens as measured by FC: CD86 (M1), HLA-DR (M1), CD206 (M2a), and CD163 (M2c). Data are presented as MFI  $\pm$  SD. (I) ImageStream analyses provide representative immunofluorescence images of M0, M1, M2a, and M2c MDMs in suspension, stained for surface antigens CD86, HLA-DR, CD206, and CD163. (Scale bar, 20  $\mu$ m.) (J–Q) Expression of common immunity-mediating cytokines measured by multiplex bead sandwich assay (Luminex). Data are presented as mean  $\pm$  SD. Statistical significance was assessed using the Friedman test and Dunn’s post hoc test ( $n = 6$ ). Each donor has been assigned a unique color—male donors are indicated by squares and female donors by triangles.

general, more comparable with M2-polarized MDMs than with M1-polarized MDMs. In contrast, glass-activated macrophages were not comparable with the M1 or M2 MDMs.

**Discussion**

In this study, RM was utilized for a comprehensive characterization of stimulated MDMs to identify the MDM phenotypes M0, M1, M2a, and M2c and to determine MDM activation on titanium substrates. Our RM results suggest that the spectral information,

especially the one containing the lipid component, can be a useful tool to monitor macrophage polarization and immune–metabolic processes both in suspension and material-adherent living cells.

Because macrophages are an extremely heterogeneous cell population and many different culture systems exist to mature monocytes to macrophages, we placed special emphasis on a thorough characterization of the MDMs used in this work. Selection of culture plates, origin of supplemented serum (human, bovine, or other), and added stimulants such as LPS, interferons,

ENGINEERING

BIOPHYSICS AND COMPUTATIONAL BIOLOGY

Downloaded by guest on February 3, 2022

Feuerer et al.  
Lipidome profiling with Raman microspectroscopy identifies macrophage response to surface topographies of implant materials

PNAS | 3 of 9  
<https://doi.org/10.1073/pnas.2113694118>

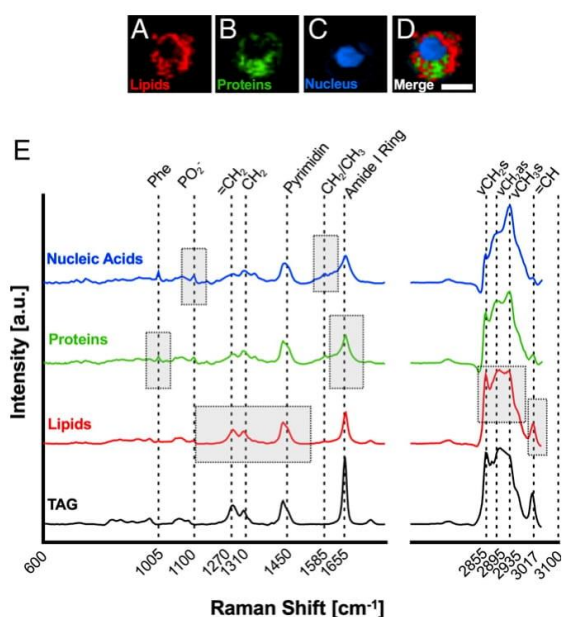


**Fig. 2.** Raman imaging resolves subcellular structures in MDMs. Identification of major cell component Raman signatures present in MDMs. (A–D) False color heat maps of (A) lipids (red), (B) proteins (green), (C) nucleic acids (blue), and (D) merged as identified by TCA. (Scale bar, 10 μm.) (E) Spectral fingerprints of MDM components. Boxes represent spectral areas typically associated with the biochemical fingerprint of the respective cell component. Phe = Phenylalanine,  $\nu$  = stretching,  $s$  = symmetric,  $a$  = asymmetric. A typical, in house-measured TAG spectrum is shown for comparison.

or cytokines can significantly impact macrophage responses. In the cell-culture system for macrophage maturation, no significant up-regulation of proinflammatory cytokines such as TNF- $\alpha$ , IL-8, IL-6, or IL-1 $\beta$  was observed, indicating a robust resting level of M0 MDMs.

There are multiple studies using Raman spectra to distinguish between cell phenotypes or different stages of the cell cycle (25, 28, 29, 31); however, only few studies have investigated if RM can be employed to distinguish macrophage polarization. In 2018, Pavillon et al. described a machine-learning model for classification of binary macrophage activation based on morphological and biochemical information retrieved by quantitative phase imaging and analysis of Raman spectra (32). A study by Bertani et al. investigated binary macrophage activation, combining hyperspectral imaging, a method comparable to RM, and multivariate data analysis (33). Although these findings are in accordance with our results, as the most prominent separation also occurred between M0 and M1 MDMs, the Raman spectra in the previous studies were obtained from the complete cell as the ROI, but individual cellular substructures such as proteins, nucleic acids, or lipids were not resolved. In addition, the studies mentioned were limited to a binary classification of cell activation, separating resting and LPS-activated MDMs (32, 33). Here, we provide evidence that resolving cellular components can provide in-depth information regarding cell metabolism and immunity, enabling MDM classification into four distinct phenotypes. The most prominent differences appeared within the lipidome, separating groups of MDMs in the PCA scatter plot.

Macrophage activation, metabolism, and fatty acid composition are strongly related (34), which is reflected in the Raman

spectra of lipids investigated in this study. In particular, Raman peaks that contributed to the separation of the different polarized groups were identified at 1,440 cm<sup>-1</sup>, 1,655 cm<sup>-1</sup>, 2,885 cm<sup>-1</sup>, and 3,010 cm<sup>-1</sup>—all peaks that are assigned to the C=C double bond of unsaturated fatty acids. Particularly of note is the olefinic stretch of C=C double bonds that are expressed at 1,655 cm<sup>-1</sup> (24). A linear dependence of the C=C stretch at 1,655 cm<sup>-1</sup> and the intensity of the CH<sub>2</sub> bending at 1,440 cm<sup>-1</sup> has been previously reported and provides information about the overall content of unsaturated compared to saturated fatty acids in the cell (35). By comparing Raman spectra obtained in this study to spectra reported in the literature, we confirmed linoleic (36) and palmitoleic (37) acid as the main constituents of the macrophage lipids detected by RM (30). In addition, the peak at 1,744 cm<sup>-1</sup> indicates the ester compound in TAGs (38). Lipids are known to regulate many cellular and immune functions such as energy storage or cell signaling. Polyunsaturated fatty acids like linoleic acid have profound effects on inflammatory processes by regulating expression of proinflammatory cytokines such as IL-1 $\beta$  or IL-6 (36). In this study, loading plots indicate that the degree of saturation in fatty acids substantially contributes to the separation of macrophage subtypes calculated by PCA. The capability of RM to trace lipids and lipid composition in macrophages has been previously shown (39–41), and lipids have been repeatedly reported to play important roles in inflammation and MDM polarization (34, 42, 43). In 2016, Montenegro-Burke et al. provided evidence that macrophage phenotypes significantly differ in their fatty acid composition (42). This is in accordance with other findings suggesting major metabolic shifts up to the Warburg effect in polarized macrophages (44), which extends (but is not limited to) protein function, cell signaling, or membrane composition. The metabolic shift that macrophages experience during the polarization process is intimately linked to changes in fatty acid composition and turnover, making lipid composition an ideal target to track macrophage polarization (34, 45, 46).

In this study, we aimed to assess if RM analysis can be utilized to monitor the lipidome of MDMs *in vitro* that have not been activated by classical stimuli like LPS or cytokines but by exposure to materials used for implants. PCA confirmed a significant separation within individual donors of glass and titanium but also between Ti M and Ti A, specimens that only differed in their surface topology. Based on the loading plots, this separation was again predominantly based on saturated versus unsaturated fatty acids and TAGs. Projection of substrate MDM data into the model of previously polarized MDMs further revealed that the means of M2c macrophages and Ti A macrophages were similar. This is in accordance with cytokine expression of MCP-1 and other studies that reported an anti-inflammatory, M2c-like phenotype on more textured topographies compared to smoother, oriented ones (18, 47, 48). Clinical research shows that implant roughness can lead to inflammation or fibrosis and therefore to poor clinical outcomes for patients that received dental and breast implants, linked to a prevalence of M2-like MDMs (49–51). As it had been previously shown, minor changes in cell physiology (e.g., due to exposure to surface roughness) are rarely comparable to activation of MDMs by LPS or IFN- $\gamma$  (52). Our findings confirm this by showing that only few MDM polarization markers were increased on substrate-adherent MDMs when compared to M0 MDMs. However, macrophages are known to be sensitive to changes in stiffness, topography, or structure in their environment, and thus, these environmental factors play key roles in foreign body response and fibrosis, in which the environment is pathologically altered. Notably, the only significant increase of polarization indicators on titanium was detected in CD206, an M2a-associated scavenger receptor responsible for the uptake of bacterial sugars that is associated with fibrosis (53). In combination with an increase of MCP-1 on titanium substrates, these data hint at an M2a–M2c MDM phenotype on titanium

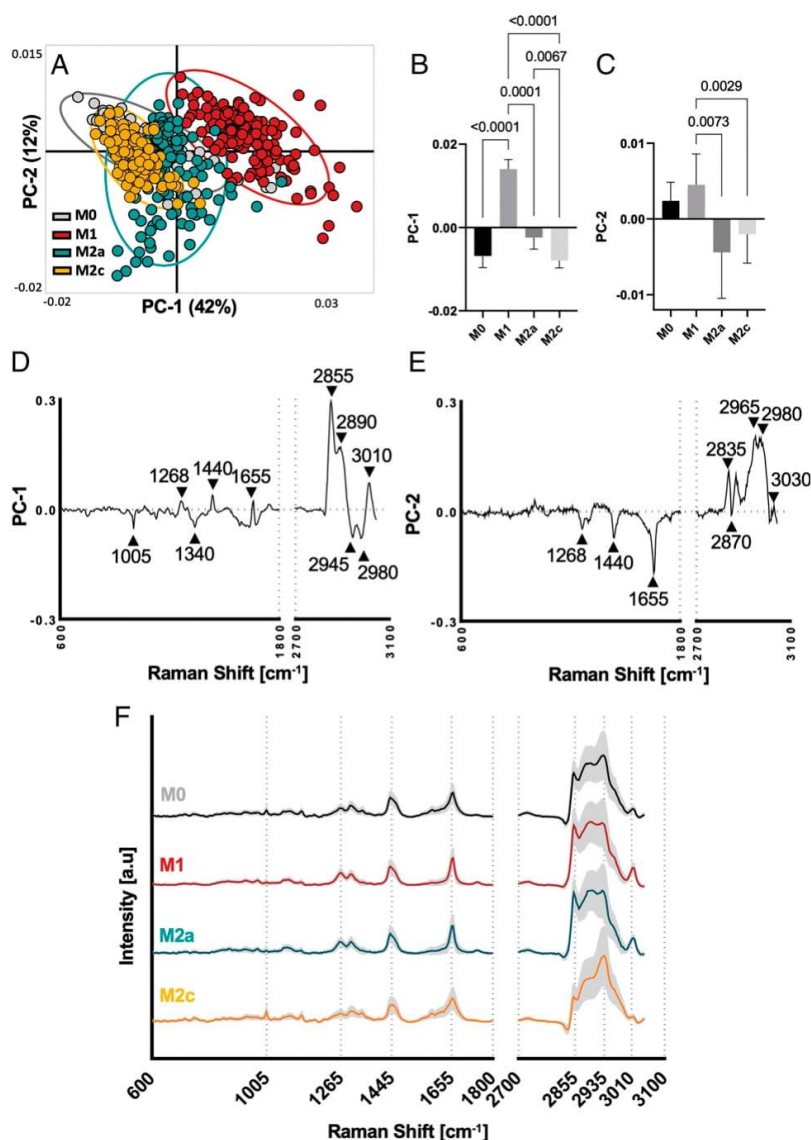


**Fig. 3.** PCA of Raman lipid spectra identifies significant differences between polarized MDMs. (A) Scatter plot of PC-1 (42%) and PC-2 (12%) visualizes spatial clustering of MDM polarization (confidence ellipse = 95%; each dot represents a single cell). (B and C) Statistical analyses of scores from PC-1 and PC-2 reveal significant differences between all four subtypes; one way ANOVA and Tukey's post hoc test,  $n = 6$ . (D and E) Loading plots describing major Raman peaks contribute to PCA separation. Peak assignments are listed in *SI Appendix, Table 1*. (F) Average lipid component Raman spectra of polarized MDMs with subtypes shown in black (M0), red (M1), blue (M2a), and yellow (M2c).

with a shift toward the M2c phenotype on the rougher titanium surface, which is confirmed by our RM data. This also corresponds to the results of previous studies, which reported an increase in anti-inflammatory phenotypes of MDMs cultured on rough surfaces in vitro (47, 48).

In summary, in this study, we demonstrated that Raman-based analytical methods combined with statistical analysis can non-invasively and marker-independently distinguish between different macrophage subtypes in situ. The lipidome of the cells was identified as a potent indicator for macrophage phenotype discrimination and for the analysis of adherent cells, which is especially helpful for the field of biomedical materials research.

**Materials and Methods**

All experiments using human samples in this study were approved by the ethics committee of the University Hospital of Tübingen (Institutional Review Board No. 495/2018BO2). Informed consent was obtained from all donors.

**Material Preparation.** Sterile Ti 15-mm disks with Ti M and Ti A surfaces were provided by the Institut Straumann AG. Disks were prepared and characterized as previously described (48, 54). Briefly, Ti M had a roughness of 0.1  $\mu\text{m}$  and Ti A 0.3  $\mu\text{m}$ . Contact angles of both materials were in the moderate hydrophilic range of about 62° to 77°. Glass coverslips were baked for 4 h at 200 °C for endotoxin removal and sterilization, then used immediately for cell-culture experiments.

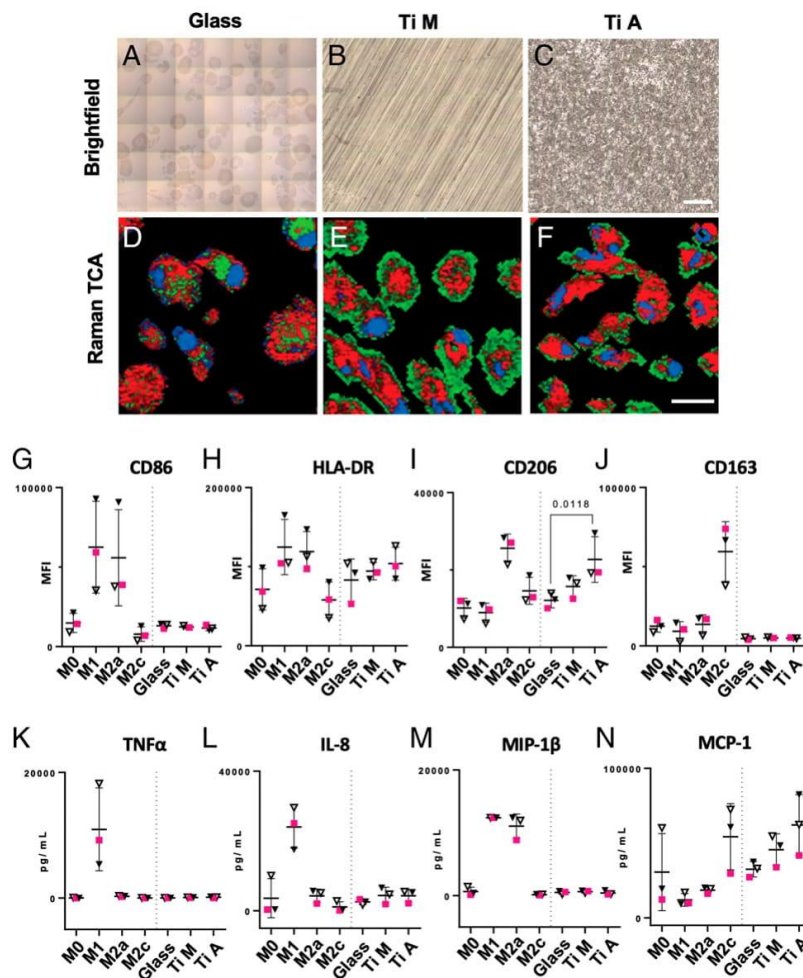


**Fig. 4.** RM allows real-time in situ analysis of MDMs on biomaterial surfaces. Raman analysis of MDMs cultured on biomaterial surfaces: (A–C) stitched brightfield images of glass, Ti M, and Ti A with MDMs adherent to the respective surface. (Scale bar, 100  $\mu\text{m}$ .) (D–F) Spectral components of RM measurements identified by TCA with lipids color coded in red, proteins in green, and nuclei in blue. (Scale bar, 20  $\mu\text{m}$ .) Images were acquired at 63 $\times$  magnification. (G–J) MFIs of MDM surface markers analyzed by FC. MFIs of surface markers from MDMs cultured on biomaterials were plotted in the same graph as data obtained by polarization experiments (M0 through M2c). (K–N) Expression levels of four representative cytokines expressed by MDMs. The results were plotted in the same graph as data obtained by polarization experiments (M0 through M2c). Statistical analysis in graphs G–N was performed by Friedman’s test and Dunn’s post hoc test, and only results for substrate-adherent MDMs are shown. Data are shown as mean  $\pm$  SD. Male donors are indicated by squares and female donors by triangles.

**Monocyte Isolation and Culture.** Whole blood was collected from healthy volunteers, and isolation procedures were performed immediately after collection. To separate peripheral blood mononuclear cells (PBMCs) from erythrocytes and granulocytes, density gradient centrifugation using SepMate tubes and Lymphoprep (both from Stemcell) was performed according to the manufacturer’s instructions. In brief, fresh whole blood containing ethylenediaminetetraacetate (EDTA) was diluted 1:1 with phosphate-buffered saline (PBS), layered over Lymphoprep in SepMate tubes, and separated by density gradient centrifugation. Supernatants containing PBMCs were decanted into fresh 50-mL falcon tubes and washed twice with PBS. PBMCs were then resuspended in cryopreservation medium (10% dimethyl sulfoxide, 20% fetal bovine serum [FBS], and 70% RPMI 1640 growth medium). For long-term storage, PBMCs were frozen at a concentration of  $1 \times 10^7$  cells/mL at  $-150^\circ\text{C}$ . Before seeding, cells were counted using a hemocytometer. Cell viability was assessed using trypan blue. Monocytes were isolated by plastic adherence from frozen PBMCs as described by Delirezh et al. (55). PBMCs were seeded at a concentration of  $5 \times 10^6$  cells/cm $^2$

and allowed to adhere for 2 h at  $37^\circ\text{C}$  and 5%  $\text{CO}_2$  in culture medium. Nonadherent cells were then aspirated and removed. The remaining adherent monocytes were washed with PBS and continually cultured to mature into macrophages.

**Macrophage Maturation and Polarization.** Monocytes were cultured in RPMI 1640 containing Glutamax supplemented with 100  $\mu\text{g}/\text{mL}$  streptomycin, 100 U/mL penicillin, and 10% heat-inactivated FBS (all from Thermo Fisher Scientific) at  $37^\circ\text{C}$  and under a 5%  $\text{CO}_2$  atmosphere in polystyrene 24-well cell-culture plates. Adherent monocytes were matured to macrophages over a period of 8 d in culture medium supplemented with 50 ng/mL macrophage colony-stimulating factor (Biolegend) at  $37^\circ\text{C}$  and 5%  $\text{CO}_2$ . Medium was changed at day 3. On day 5 of culture, medium was changed again, and stimulants were added to induce macrophage polarization: M1 (100 ng/mL LPS + 100 ng/mL IFN- $\gamma$ ), M2a (40 ng/mL IL-4 + 20 ng/mL IL-13), and M2c (20 ng/mL IL-10). LPS (*Escherichia coli*, O111:B4) was purchased from Merck Millipore. Protocols for macrophage polarization were adapted after Spiller et al. (56). IFN- $\gamma$  and



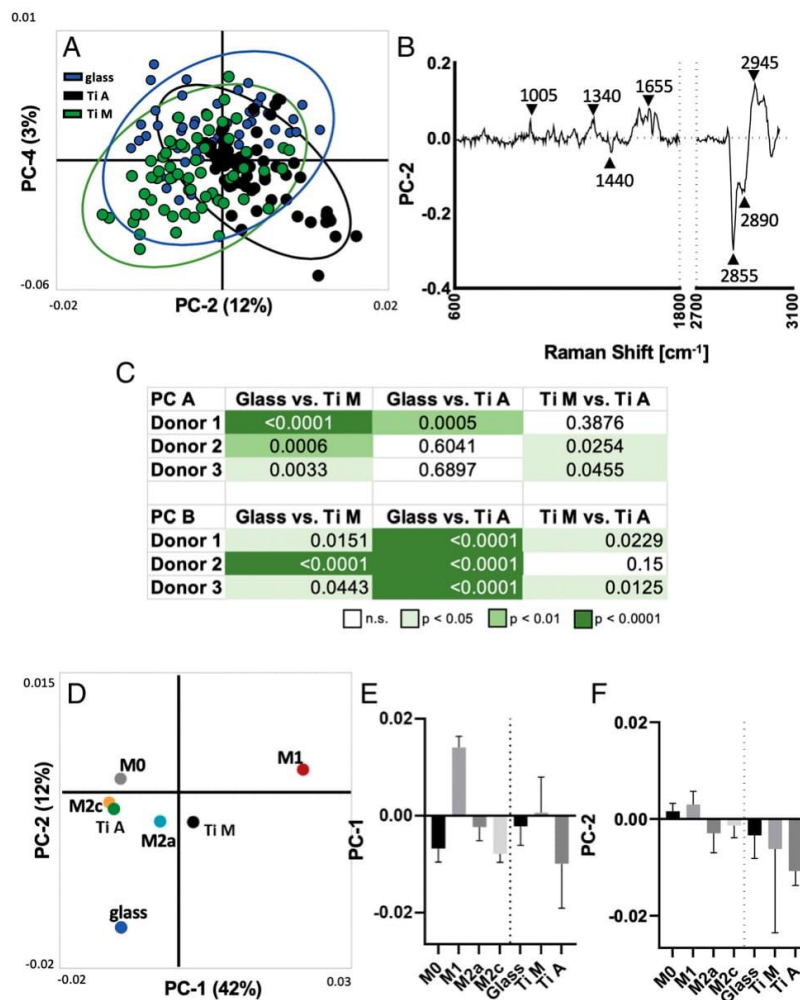


**Fig. 5.** RM lipid spectra can be used to distinguish substrate-adherent MDMs, and projected scores indicate proximity to polarization status. (A) Scatter plot of PC-2 (12%) and PC-4 (3%) visualizes spatial clustering of substrate-adherent MDMs (confidence ellipse = 95%; each dot represents a single cell). (B) Loading plot of PC-2 describes major Raman peaks contributing to PCA separation, comparable to those observed in polarized MDMs. (C) Statistical analysis of relevant components (PC A and PC B) reveal significant differences within single donors between substrates. (D) Projection of average substrate-adherent MDM scores into the PCA scores plot of the polarized MDMs. (E and F) Statistical comparison of mean score values  $\pm$  SD. Only the projected scores were analyzed for significance using the Kruskal–Wallis and Dunn’s post hoc tests.

cytokines were all purchased from Biolegend. M0 (resting) macrophages were not stimulated, but medium was changed on days 3 and 5. Likewise, monocytes cultured on biomaterials were not stimulated and were treated as M0.

**FC.** Before dissociation, cells were washed three times with fluorescence-activated cell sorting (FACS) buffer (PBS + 2% FBS + 0.05 Mm Na<sub>3</sub> + 0.1 Mm EDTA) to deplete cells of bivalent cations. Adherent macrophages were then detached by incubation with Accutase (Biolegend) for 10 min at 37 °C and 5% CO<sub>2</sub>. For FC analysis, harvested cells were blocked with 10% sterile-filtered, human, male AB serum (H2B) in FACS buffer for 20 min at 4 °C to prevent non-specific binding of antibodies. For cell-surface marker staining, the following antibodies were used: CD86-Pacific Blue (clone IT2.2), HLA-DR-Brilliant Violet 510 (clone L243), CD206-FITC (fluorescein isothiocyanate) (clone 15-2), and CD163-PE/Cy7 (clone RM3/1) (Biolegend). For staining, all antibodies were diluted 1:50 with FACS buffer, and cells were stained for 30 min at 4 °C in the dark and washed with FACS buffer subsequently. Data were acquired using a BD Biosciences LSRFortessa Cytometer and analyzed using FlowJo 10.4.2 (Tree Star). Cells were gated using forward scatter versus sideward scatter properties to exclude debris, doublets, and dead cells (7-AAD staining, Biolegend). MFIs

of the whole macrophage population were analyzed. Compensation controls were run for each experiment using software-based automatic compensation to consider potential fluorescence spillover. In addition, fluorescence minus one controls were run to determine performance of the antibody panel and the fluorescence-staining pattern of each individual antibody.

**Imaging FC.** Macrophages were detached, processed, and stained as described for regular FC analysis. Dead cells were excluded using the Zombie NIR fixable viability kit (Biolegend). At least  $1 \times 10^4$  cells per sample were acquired by the ImageStreamX mkII (Luminex Corporation) with the INSPIRE instrument controller software with 40x magnification. Data were analyzed with IDEAS image analysis software. All samples were gated on single cells in focus that were Zombie NIR negative. An unstained control sample was used to determine background fluorescence.

**Cytokine Analysis by Multiplexed Bead-Based Sandwich Immunoassay.** Cell-culture supernatants were collected on day 8, centrifuged at 5,000 rpm for 3 min, and stored at  $-80$  °C until analysis. Levels of IL-6, IL-8, TNF- $\alpha$ , IL-1 $\beta$ , IL-1RA, MCP-1, MIP-1 $\beta$ , and granulocyte-macrophage colony-stimulating

Feuerer et al.  
Lipidome profiling with Raman microspectroscopy identifies macrophage response to surface topographies of implant materials

PNAS | 7 of 9  
<https://doi.org/10.1073/pnas.2113694118>

factor (GM-CSF) were determined using a set of “in house–developed” Luminex-based sandwich immunoassays each consisting of commercially available capture and detection antibodies and calibrator proteins. All assays were thoroughly validated ahead of the study with respect to accuracy, precision, parallelism, robustness, specificity, and sensitivity (57). Samples were diluted at least 1:2 or higher. After incubation of the prediluted samples or calibrator protein with the capture-coated microspheres, beads were washed and incubated with biotinylated detection antibodies. Streptavidin–phycoerythrin was added after an additional washing step for visualization. For control purposes, calibrators and quality control samples were included on each microtiter plate. All measurements were performed on a Luminex FlexMap 3D analyzer system, using Luminex xPONENT 4.2 software (Luminex). For data analysis, MasterPlex QT version 5.0 was employed. Standard curve and quality control samples were evaluated according to internal criteria adapted to the Westgard Rules [3] to ensure proper assay performance.

**RM.** RM analysis of macrophages was performed on a customized WiTec Raman system (WiTec GmbH) equipped with a green laser (532 nm) and a charge-coupled device spectrograph with a grating of 600 g/mm. Images were acquired using a 63× apochromat water-immersion objective, an integration time of 0.5 s, a pixel resolution of  $1 \times 1 \mu\text{m}$ , and a laser power of 50 mW for cells in suspension or 25 mW for adherent cells. Macrophages adherent to glass or titanium disks were stained with FITC–phalloidin before analysis to locate cells and ROIs. All cells were fixed with 4% paraformaldehyde for 10 min at room temperature before Raman analysis. For each donor and subtype, 30 cells were measured.

**Data Processing.** Raman data were processed using the Project FIVE 5.2 software (WiTec GmbH). Cosmic rays were removed, and a baseline correction was employed on all spectra. All preprocessing steps were published previously in detail (58). Spectra were cropped from the range of  $300 \text{ cm}^{-1}$  to  $3,045 \text{ cm}^{-1}$ . TCA was employed to identify nucleic acids, proteins, and lipids. In brief, TCA is a nonnegative matrix factorization-based multivariate analysis tool that identifies dominant spectral components in a dataset. These components can then be visualized by false color intensity distribution heat maps. To extract single spectra for each of the three cellular components, masks were

generated based on TCA heat maps. A total of 2% of the most intense spectra were extracted, and a total average spectrum per cell was calculated. To reduce dimensionality of the spectral data, PCA was performed using the Unscrambler X 14.0 software (Camo Software). PCA is an exploratory, linear transformation technique used to increase interpretability of the data while minimizing information loss. It accomplishes dimensionality reduction by calculating eigenvectors of the data’s covariance matrix (58, 59). Here, spectral ranges of  $400$  to  $1,800 \text{ cm}^{-1}$  and  $2,700$  to  $3,045 \text{ cm}^{-1}$  were investigated by PCA analysis. PCA results are presented as score plots and loading plots. The 95% confidence ellipses were calculated using Origin Pro-9.1 software (Origin-Lab). Loadings show the original variables’ contribution to the component and were used to identify relevant and comparable PCs for further analysis.

**Statistical Analysis.** All relevant statistical parameters such as sample size, replicate types, and *P* values are described in the corresponding figures. Donors are represented by *n*. For polarized macrophages, six donors were analyzed, and for substrate macrophages, three donors were analyzed. Gaussian distributions of data were tested using the Kolmogorov–Smirnov test. Unless otherwise indicated, data were analyzed for significance using the Kruskal–Wallis test with Dunn’s post hoc test with Graph Pad Prism 8.0.0 (Graph Pad Software, Inc.). *P* values  $<0.05$  were considered significant.

**Data Availability.** All study data are included in the article and/or *SI Appendix*.

**ACKNOWLEDGMENTS.** We thank Simone Pöschel (ImageStream Core Facility, University Hospital Tübingen) for her assistance with the ImageStream measurements. We also express our gratitude to Svenja Hinderer, Elena Rapp, and Bernadette Walter (Natural and Medical Sciences Institute Reutlingen), as well as Simone Liebscher (University of Tübingen), for their excellent technical support and scientific discussions. We thank Shannon Lee Layland (University of Tübingen) for his helpful comments on the manuscript. This work was financially supported by the Ministry of Baden-Württemberg for Economic Affairs, Labor, and Tourism; the Ministry of Science, Research, and the Arts of Baden-Württemberg (Grant SI-BW 01222-91 to K.S.-L.); and the Deutsche Forschungsgemeinschaft (Grants INST 2388/33-1, INST 2388/64-1, GRK 2543/1, and Germany’s Excellence Strategy EXC 2180-390900677 all to K.S.-L.).

- S. A. Eming, T. A. Wynn, P. Martin, Inflammation and metabolism in tissue repair and regeneration. *Science* **356**, 1026–1030 (2017).
- C. J. Ferrante, S. J. Leibovich, Regulation of macrophage polarization and wound healing. *Adv. Wound Care (New Rochelle)* **1**, 10–16 (2012).
- M. Lech, H.-J. Anders, Macrophages and fibrosis: How resident and infiltrating mononuclear phagocytes orchestrate all phases of tissue injury and repair. *Biochim. Biophys. Acta* **1832**, 989–997 (2013).
- J. W. Godwin, N. Rosenthal, Scar-free wound healing and regeneration in amphibians: Immunological influences on regenerative success. *Differentiation* **87**, 66–75 (2014).
- J. W. Godwin, A. R. Pinto, N. A. Rosenthal, Macrophages are required for adult salamander limb regeneration. *Proc. Natl. Acad. Sci. U.S.A.* **110**, 9415–9420 (2013).
- K. Y. Gerrick *et al.*, Transcriptional profiling identifies novel regulators of macrophage polarization. *PLoS One* **13**, e0208602 (2018).
- Y. Okabe, R. Medzhitov, Tissue-specific signals control reversible program of localization and functional polarization of macrophages. *Cell* **157**, 832–844 (2014).
- Y.-C. Liu, X.-B. Zou, Y.-F. Chai, Y.-M. Yao, Macrophage polarization in inflammatory diseases. *Int. J. Biol. Sci.* **10**, 520–529 (2014).
- P. J. Murray *et al.*, Macrophage activation and polarization: Nomenclature and experimental guidelines. *Immunity* **41**, 14–20 (2014).
- D. M. Mosser, J. P. Edwards, Exploring the full spectrum of macrophage activation. *Nat. Rev. Immunol.* **8**, 958–969 (2008).
- L. Chung, D. R. Maestas Jr., F. Housseau, J. H. Elisseeff, Key players in the immune response to biomaterial scaffolds for regenerative medicine. *Adv. Drug Deliv. Rev.* **114**, 184–192 (2017).
- J. M. Anderson, K. M. Miller, Biomaterial biocompatibility and the macrophage. *Biomaterials* **5**, 5–10 (1984).
- N. J. Hallab, Biologic responses to orthopedic implants: Innate and adaptive immune responses to implant debris. *Spine* **41**, S30–S31 (2016).
- J. M. Anderson, S. Jiang, “Implications of the acute and chronic inflammatory response and the foreign body reaction to the immune response of implanted biomaterials” in *The Immune Response to Implanted Materials and Devices*, B. Corradetti, Ed. (Springer, 2017), pp. 15–36.
- J. L. Dziki *et al.*, Solubilized extracellular matrix bioscaffolds derived from diverse source tissues differentially influence macrophage phenotype. *J. Biomed. Mater. Res. A* **105**, 138–147 (2017).
- D. Abeyayehu *et al.*, Galectin-1 promotes an M2 macrophage response to polydioxanone scaffolds. *J. Biomed. Mater. Res. A* **105**, 2562–2571 (2017).
- N. Araújo-Gomes *et al.*, Complement proteins regulating macrophage polarisation on biomaterials. *Colloids Surf. B Biointerfaces* **181**, 125–133 (2019).
- K. A. Barth, J. D. Waterfield, D. M. Brunette, The effect of surface roughness on RAW 264.7 macrophage phenotype. *J. Biomed. Mater. Res. A* **101**, 2679–2688 (2013).
- M. Bartneck *et al.*, Inducing healing-like human primary macrophage phenotypes by 3D hydrogel coated nanofibres. *Biomaterials* **33**, 4136–4146 (2012).
- V. Bonito *et al.*, Modulation of macrophage phenotype and protein secretion via heparin-IL-4 functionalized supramolecular elastomers. *Acta Biomater.* **71**, 247–260 (2018).
- M. Waters, P. VandeVord, M. Van Dyke, Keratin biomaterials augment anti-inflammatory macrophage phenotype in vitro. *Acta Biomater.* **66**, 213–223 (2018).
- Z. Ye, C. A. Sarkar, Towards a quantitative understanding of cell identity. *Trends Cell Biol.* **28**, 1030–1048 (2018).
- R. Smith, K. L. Wright, L. Ashton, Raman spectroscopy: An evolving technique for live cell studies. *Analyst (Lond.)* **141**, 3590–3600 (2016).
- J. R. Beattie, S. E. J. Bell, B. W. Moss, A critical evaluation of Raman spectroscopy for the analysis of lipids: Fatty acid methyl esters. *Lipids* **39**, 407–419 (2004).
- R. Daum, E. M. Brauchle, D. A. C. Berrio, T. P. Jurkowski, K. Schenke-Layland, Non-invasive detection of DNA methylation states in carcinoma and pluripotent stem cells using Raman microspectroscopy and imaging. *Sci. Rep.* **9**, 7014 (2019).
- N. Stone, C. Kendall, J. Smith, P. Crow, H. Barr, Raman spectroscopy for identification of epithelial cancers. *Faraday Discuss.* **126**, 141–157 (2004).
- J. M. Surmacki, B. J. Woodhams, A. Haslehurst, B. A. J. Ponder, S. E. Bohniek, Raman micro-spectroscopy for accurate identification of primary human bronchial epithelial cells. *Sci. Rep.* **8**, 12604 (2018).
- E. Brauchle, S. Thude, S. Y. Brucker, K. Schenke-Layland, Cell death stages in single apoptotic and necrotic cells monitored by Raman microspectroscopy. *Sci. Rep.* **4**, 4698 (2014).
- J. Marzi, E. M. Brauchle, K. Schenke-Layland, M. W. Rolle, Non-invasive functional molecular phenotyping of human smooth muscle cells utilized in cardiovascular tissue engineering. *Acta Biomater.* **89**, 193–205 (2019).
- K. Czamara *et al.*, Raman spectroscopy of lipids: A review. *J. Raman Spectrosc.* **46**, 4–20 (2015).
- M. Pudlas, E. Brauchle, T. J. Klein, D. W. Hutmacher, K. Schenke-Layland, Non-invasive identification of proteoglycans and chondrocyte differentiation state by Raman microspectroscopy. *J. Biophotonics* **6**, 205–211 (2013).
- N. Pavillon, A. J. Hobro, S. Akira, N. I. Smith, Noninvasive detection of macrophage activation with single-cell resolution through machine learning. *Proc. Natl. Acad. Sci. U.S.A.* **115**, E2676–E2685 (2018).
- F. R. Bertani *et al.*, Classification of M1/M2-polarized human macrophages by label-free hyperspectral reflectance confocal microscopy and multivariate analysis. *Sci. Rep.* **7**, 8965 (2017).

34. A. Batista-Gonzalez, R. Vidal, A. Criollo, L. J. Carreño, New insights on the role of lipid metabolism in the metabolic reprogramming of macrophages. *Front. Immunol.* **10**, 2993 (2020).
35. H. Wu *et al.*, In vivo lipidomics using single-cell Raman spectroscopy. *Proc. Natl. Acad. Sci. U.S.A.* **108**, 3809–3814 (2011).
36. S. D. Pauls *et al.*, Anti-inflammatory effects of  $\alpha$ -linolenic acid in M1-like macrophages are associated with enhanced production of oxylipins from  $\alpha$ -linolenic and linoleic acid. *J. Nutr. Biochem.* **57**, 121–129 (2018).
37. S. Wang *et al.*, In vitro fatty acid enrichment of macrophages alters inflammatory response and net cholesterol accumulation. *Br. J. Nutr.* **102**, 497–501 (2009).
38. H. Takahashi, A. Yanamisawa, S. Kajimoto, T. Nakabayashi, Observation of the changes in the chemical composition of lipid droplets using Raman microscopy. *Phys. Chem. Chem. Phys.* **22**, 21646–21650 (2020).
39. C. Matthäus *et al.*, “Monitoring intra-cellular lipid metabolism in macrophages by Raman-and CARS-microscopy” in *Biophotonics: Photonic Solutions for Better Health Care II*, J. Popp, W. Drexler, V. V. Tuchin, D. L. Matthews, Eds. (SPIE, 2010), pp. 771511.
40. C. Matthäus *et al.*, Noninvasive imaging of intracellular lipid metabolism in macrophages by Raman microscopy in combination with stable isotopic labeling. *Anal. Chem.* **84**, 8549–8556 (2012).
41. C. Stiebing *et al.*, Raman imaging of macrophages incubated with triglyceride-enriched oxLDL visualizes translocation of lipids between endocytic vesicles and lipid droplets. *J. Lipid Res.* **58**, 876–883 (2017).
42. J. R. Montenegro-Burke *et al.*, Lipid profiling of polarized human monocyte-derived macrophages. *Prostaglandins Other Lipid Mediat.* **127**, 1–8 (2016).
43. V. Bhaskar *et al.*, Monoclonal antibodies targeting IL-1 beta reduce biomarkers of atherosclerosis in vitro and inhibit atherosclerotic plaque formation in apolipoprotein E-deficient mice. *Atherosclerosis* **216**, 313–320 (2011).
44. E. M. Palsson-McDermott *et al.*, Pyruvate kinase M2 regulates Hif-1 $\alpha$  activity and IL-1 $\beta$  induction and is a critical determinant of the Warburg effect in LPS-activated macrophages. *Cell Metab.* **21**, 65–80 (2015).
45. J. Korbecki, K. Bajdak-Rusinek, The effect of palmitic acid on inflammatory response in macrophages: An overview of molecular mechanisms. *Inflamm. Res.* **68**, 915–932 (2019).
46. S.-S. Im *et al.*, Linking lipid metabolism to the innate immune response in macrophages through sterol regulatory element binding protein-1a. *Cell Metab.* **13**, 540–549 (2011).
47. Y. Zhang, X. Cheng, J. A. Jansen, F. Yang, J. J. P. van den Beucken, Titanium surface characteristics modulate macrophage polarization. *Mater. Sci. Eng. C* **95**, 143–151 (2019).
48. K. M. Hotchkiss *et al.*, Titanium surface characteristics, including topography and wettability, alter macrophage activation. *Acta Biomater.* **31**, 425–434 (2016).
49. F. Jordana, L. Susbielles, J. Colat-Parros, Periimplantitis and implant body roughness: A systematic review of literature. *Implant Dent.* **27**, 672–681 (2018).
50. D. J. Cohen *et al.*, Performance of laser sintered Ti-6Al-4V implants with bone-inspired porosity and micro/nanoscale surface roughness in the rabbit femur. *Biomed. Mater.* **12**, 025021 (2017).
51. M. Atlan, G. Nuti, H. Wang, S. Decker, T. Perry, Breast implant surface texture impacts host tissue response. *J. Mech. Behav. Biomed. Mater.* **88**, 377–385 (2018).
52. N. Bloise *et al.*, Engineering immunomodulatory biomaterials for regenerating the infarcted myocardium. *Front. Bioeng. Biotechnol.* **8**, 292 (2020).
53. J. Wang *et al.*, Microcystin-LR ameliorates pulmonary fibrosis via modulating CD206<sup>+</sup> M2-like macrophage polarization. *Cell Death Dis.* **11**, 136 (2020).
54. G. Zhao *et al.*, High surface energy enhances cell response to titanium substrate microstructure. *J. Biomed. Mater. Res. A* **74**, 49–58 (2005).
55. N. Delirez, E. Shojaeefar, P. Parvin, B. Asadi, Comparison the effects of two monocyte isolation methods, plastic adherence and magnetic activated cell sorting methods, on phagocytic activity of generated dendritic cells. *Cell J.* **15**, 218–223 (2013).
56. K. L. Spiller *et al.*, The role of macrophage phenotype in vascularization of tissue engineering scaffolds. *Biomaterials* **35**, 4477–4488 (2014).
57. J. O. Westgard, P. L. Barry, M. R. Hunt, T. Groth, A multi-rule Shewhart chart for quality control in clinical chemistry. *Clin. Chem.* **27**, 493–501 (1981).
58. A. Zbinden *et al.*, Non-invasive marker-independent high content analysis of a microphysiological human pancreas-on-a-chip model. *Matrix Biol.* **85-86**, 205–220 (2020).
59. I. T. Jolliffe, J. Cadima, Principal component analysis: A review and recent developments. *Philos. Trans.- Royal Soc., Math. Phys. Eng. Sci.* **374**, 20150202 (2016).

ENGINEERING

BIOPHYSICS AND  
COMPUTATIONAL BIOLOGY



## Supporting Information

Lipidome profiling with Raman microspectroscopy identifies macrophage response to surface topographies of implant materials

Nora Feuerer<sup>a,b</sup>, Julia Marzi<sup>a,b,c</sup>, Eva M. Brauchle<sup>a,b,c</sup>, Daniel A. Carvajal Berrio<sup>b,c</sup>, Florian Billing<sup>a</sup>, Martin Weiss<sup>a,d</sup>, Meike Jakobi<sup>a</sup>, Nicole Schneiderhan-Marra<sup>a</sup>, Christopher Shipp<sup>a</sup>, Katja Schenke-Layland<sup>a,b,c,e</sup>

<sup>a</sup> *NMI Natural and Medical Sciences Institute at the University of Tübingen, Reutlingen, Germany*

<sup>b</sup> *Institute of Biomedical Engineering, Department for Medical Technologies and Regenerative Medicine, Eberhard Karls University Tübingen, Germany*

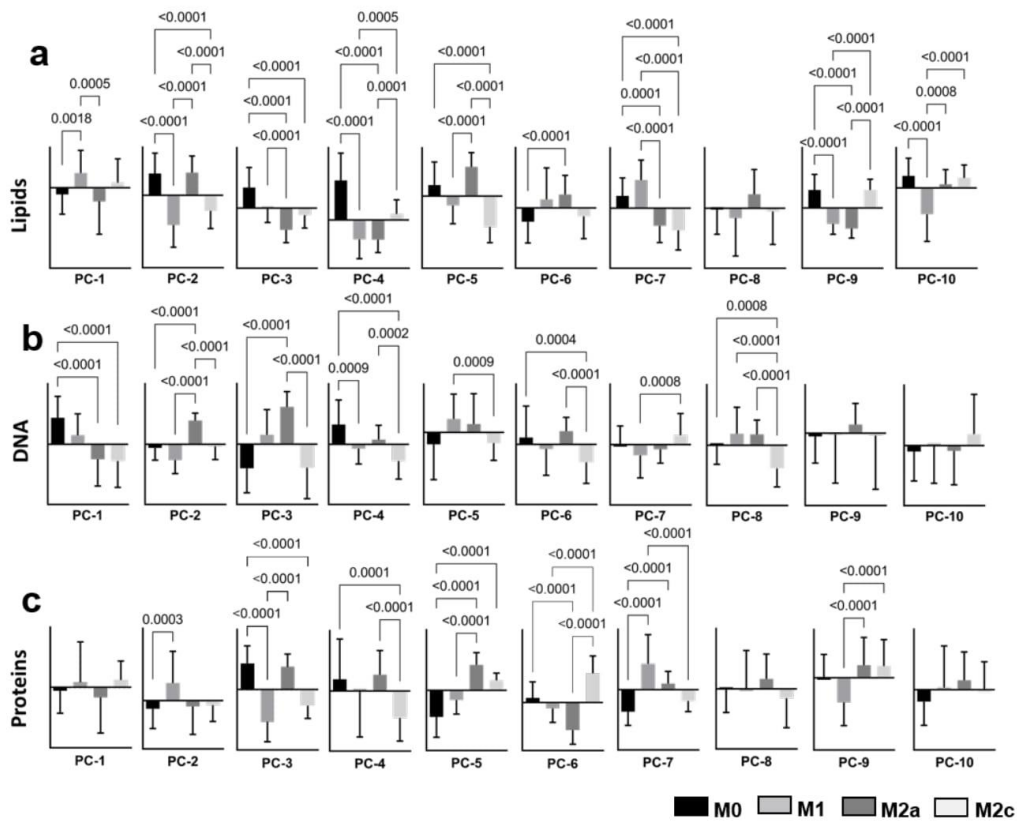
<sup>c</sup> *Cluster of Excellence iFIT (EXC 2180) "Image-Guided and Functionally Instructed Tumor Therapies", Eberhard Karls University Tübingen, Germany*

<sup>d</sup> *Department of Women's Health, Research Institute for Women's Health, Eberhard Karls University Tübingen, Germany*

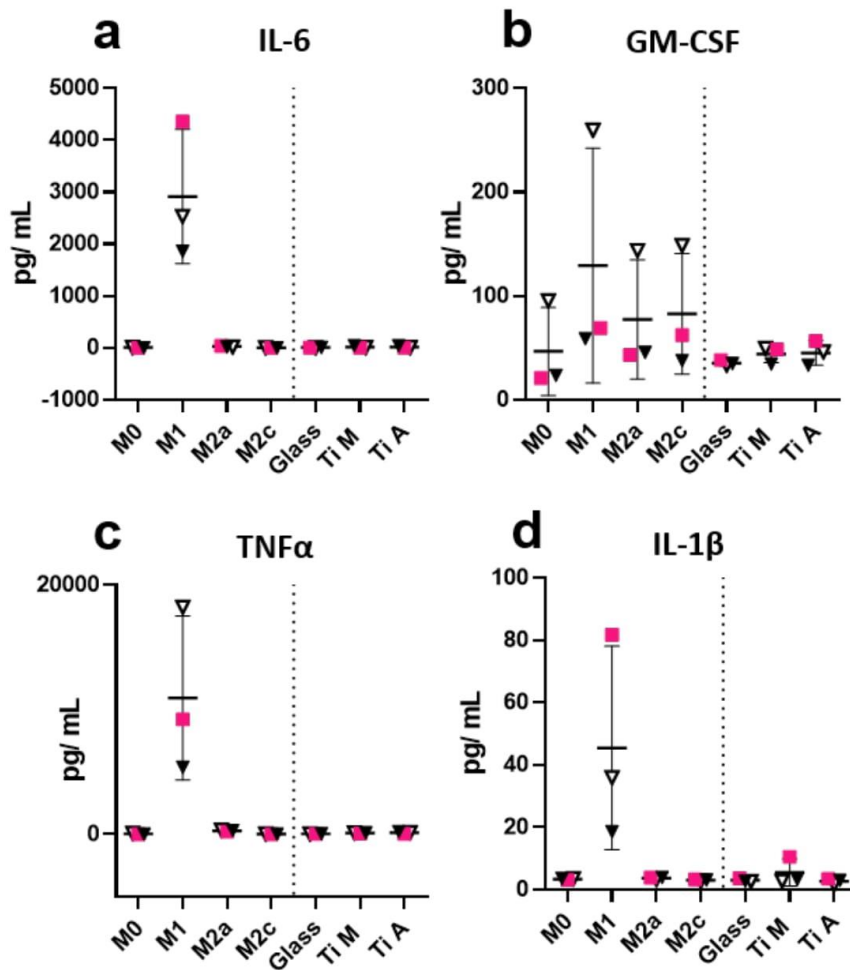
<sup>e</sup> *Department of Medicine/Cardiology, University of California Los Angeles, Los Angeles/CA, USA*

Corresponding Author: Katja Schenke-Layland

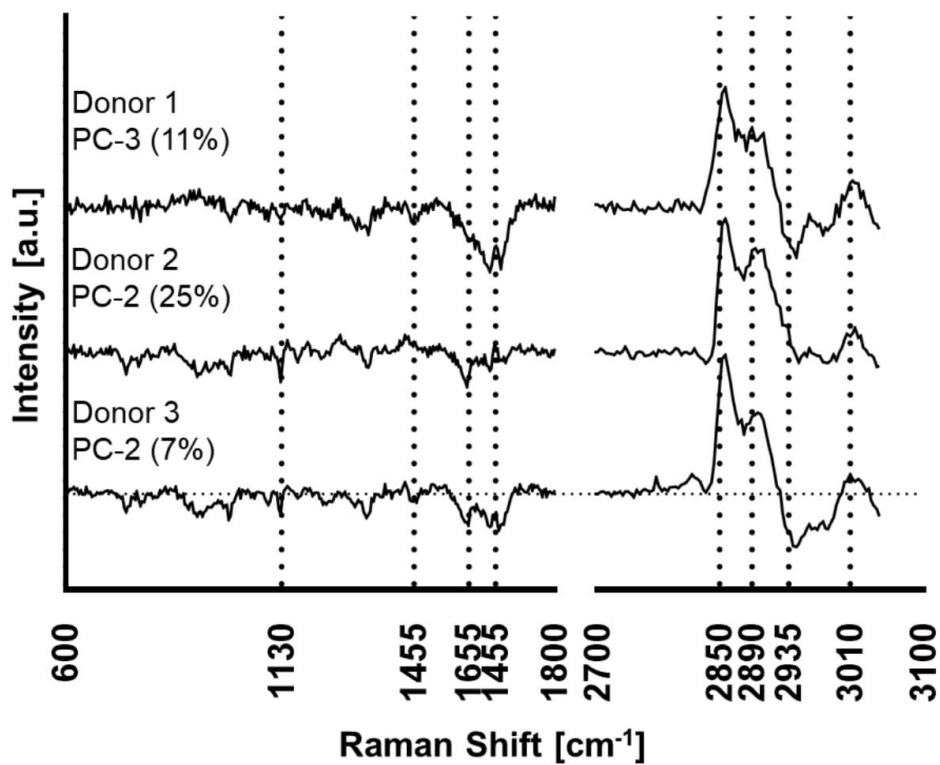
Email: [katja.schenke-layland@uni-tuebingen.de](mailto:katja.schenke-layland@uni-tuebingen.de)



**Supporting Figure 1. Analysis of PCA scores of major cell components helps identifying optimal separation of MDM subtypes.** First 10 principal components of (a) lipids, (b) nucleic acids, and (c) proteins were analyzed for significance using Kruskal-Wallis + Dunn's post hoc test. Scores are plotted as mean  $\pm$  SD. Each subtype contains data of 30 cells from each donor (total of 180 cells).



**Supporting Figure 2. Expression of inflammation-associated cytokines is not increased on glass and titanium.** To assess activation status of MDMs cultured on biomaterial surfaces, inflammation-associated cytokines were analyzed by multiplex bead immuno-sandwich assay. IL-6 (a), GM-CSF (b), TNFα (c), and IL-1β (d) did not show increased expression compared to M0 MDMs.



**Supporting Figure 3. Loadings plots indicate comparable biochemical changes occurring in all donors in MDMs adherent to biomaterials.** To assess if Raman spectral information can be used to identify MDM polarization in individual donors, direction vectors that define the multivariate model need to be compared. Here, the original variables have comparable loadings, indicating that separation is based on similar biochemical changes within the cell.

**Supporting Table 1. Raman peaks of MDM components and their associated molecular assignments.**



<b>Peak [<math>\text{cm}^{-1}</math>]</b>	<b>Molecular Assignment</b>	<b>Component</b>	<b>Reference</b>
748	Ring breathing vibrations of nucleic acids and tryptophan	DNA	[7, 8]
923	C-H stretch of proline	Proteins	[9]
935	A-helix	Protein	[4, 8]
1005	Symmetric ring breathing of Phenylalanin (Phe)	Protein	[4, 8]
1100	$\text{PO}_2^-$	DNA	[2, 8]
1127	C-N stretching	Proteins	
1235	extended Amide III, peptide backbone	Proteins	[4]
1270	$=\text{CH}_2$ , C=C in USFA	Lipids	[9]
1310	$\text{CH}_3\text{CH}_2$ twisting mode	Lipids	[8]
1340	Adenin	DNA	[4]
1350	Thymine, Adenine, Guanine	DNA	[4]
1440	$\text{CH}_3/\text{CH}_2$ scissoring, $\text{CH}_2$ deformation	Lipids	[8, 9]
1450	$\text{CH}_2$ bending	Proteins	[9]
1585	C=C olefinic stretch	Proteins	[9]
1655	C=C lipid stretch	Lipids	[4, 8]
2850 - 2855	$=\text{CH}_2$ , symmetric stretching	Lipids	[9]
2886 - 2895	$=\text{CH}_2$ , asymmetric stretching	Lipids	[9]
2920 - 2935	$=\text{CH}_3$ , symmetric stretching	Lipids	[9]
2950	$=\text{CH}_3$ , asymmetric stretching	Lipids	[9]
2980	CH stretching	Lipids	[9]
3005 - 3020	$=\text{CH}$ stretching of USFA	Lipids	[9]



Appendix III Feuerer N, Carvajal Berrio D, Marzi J, Brauchle E, Weiss M, Billing F, Segan S, Rothbauer U, Shipp C, Schenke Layland K Raman microspectroscopy identifies biochemical activation fingerprints in THP-1 and PBMC derived monocytes, 2021 in prep.

Article

# Raman Microspectroscopy Identifies Biochemical Activation Fingerprints in THP-1- and PBMC-Derived Macrophages

Nora Feuerer <sup>1,2,†</sup>, Daniel A. Carvajal Berrio <sup>1,3,†</sup>, Florian Billing <sup>2</sup>, Sören Segan <sup>2</sup>, Martin Weiss <sup>2,4</sup> , Ulrich Rothbauer <sup>2,5</sup>, Julia Marzi <sup>1,2,3,\*</sup>  and Katja Schenke-Layland <sup>1,2,3,6</sup>

- <sup>1</sup> Institute of Biomedical Engineering, Department for Medical Technologies and Regenerative Medicine, Eberhard Karls University Tübingen, 72076 Tübingen, Germany; nora.feuerer@nmi.de (N.F.); daniel.carvajal-berrio@uni-tuebingen.de (D.A.C.B.); katja.schenke-layland@uni-tuebingen.de (K.S.-L.)
- <sup>2</sup> NMI Natural and Medical Sciences Institute at the University of Tübingen, 72770 Reutlingen, Germany; florian.billing@nmi.de (F.B.); soerensegan@gmail.com (S.S.); martin.weiss@med.uni-tuebingen.de (M.W.); ulrich.rothbauer@nmi.de (U.R.)
- <sup>3</sup> Cluster of Excellence iFIT (EXC 2180) “Image-Guided and Functionally Instructed Tumor Therapies”, Eberhard Karls University Tübingen, 72076 Tübingen, Germany
- <sup>4</sup> Department of Women’s Health, Research Institute of Women’s Health, Eberhard Karls University Tübingen, 72076 Tübingen, Germany
- <sup>5</sup> Pharmaceutical Biotechnology, Eberhard Karls University Tübingen, 72076 Tübingen, Germany
- <sup>6</sup> Department of Medicine/Cardiology, University of California Los Angeles (UCLA), Los Angeles, CA 90095, USA
- \* Correspondence: julia.marzi@uni-tuebingen.de; Tel.: +49-707-1298-5204
- † These authors contributed equally to this work.



**Citation:** Feuerer, N.; Carvajal Berrio, D.A.; Billing, F.; Segan, S.; Weiss, M.; Rothbauer, U.; Marzi, J.; Schenke-Layland, K. Raman Microspectroscopy Identifies Biochemical Activation Fingerprints in THP-1- and PBMC-Derived Macrophages. *Biomedicines* **2022**, *10*, 989. <https://doi.org/10.3390/biomedicines10050989>

Academic Editors: Alexander N. Orekhov, Evgeny E. Bezsonov and Alexei Gratchev

Received: 11 March 2022

Accepted: 23 April 2022

Published: 25 April 2022

**Publisher’s Note:** MDPI stays neutral with regard to jurisdictional claims in published maps and institutional affiliations.



**Copyright:** © 2022 by the authors. Licensee MDPI, Basel, Switzerland. This article is an open access article distributed under the terms and conditions of the Creative Commons Attribution (CC BY) license (<https://creativecommons.org/licenses/by/4.0/>).

**Abstract:** (1) The monocytic leukemia cell line THP-1 and primary monocyte-derived macrophages (MDMs) are popular in vitro model systems to study human innate immunity, wound healing, and tissue regeneration. However, both cell types differ significantly in their origin and response to activation stimuli. (2) Resting THP-1 and MDMs were stimulated with lipopolysaccharide (LPS) and interferon  $\gamma$  (IFN $\gamma$ ) and analyzed by Raman microspectroscopy (RM) before and 48 h after activation. Raman data were subsequently analyzed using principal component analysis. (3) We were able to resolve and analyze the spatial distribution and molecular composition of proteins, nucleic acids, and lipids in resting and activated THP-1 and MDMs. Our findings reveal that proinflammatory activation-induced significant spectral alterations at protein and phospholipid levels in THP-1. In MDMs, we identified that nucleic acid and non-membrane-associated intracellular lipid composition were also affected. (4) Our results show that it is crucial to carefully choose the right cell type for an in vitro model as the nature of the cells itself may impact immune cell polarization or activation results. Moreover, we demonstrated that RM is a sensitive tool for investigating cell-specific responses to activation stimuli and monitoring molecular changes in subcellular structures.

**Keywords:** macrophage polarization; Raman imaging; molecular phenotyping; immune in vitro test system

## 1. Introduction

Macrophages were thought to be merely phagocytic cells that clear tissues of pathogens and cellular debris [1]. However, macrophages are highly heterogeneous and versatile cells, which can adapt to a vast range of different phenotypes, often termed polarization, and take over distinct tasks in human immunity. For example, macrophages act as antigen-presenting cells that activate the adaptive immune system and trigger inflammation, secrete and remodel components of the extracellular matrix, and they interact with non-immune cells such as fibroblast and endothelial cells. Therefore, macrophages play a profound role in fibrosis and wound healing [2–4]. Macrophage plasticity is primarily manifested in comprehensive transcriptional and metabolic alterations that are precisely regulated by a

variety of signaling pathways, leading to extensive changes in the biochemical composition of the cells [5,6].

RM and Raman imaging have become important methods in materials and biological sciences to analyze the biochemical composition of inorganic and organic samples [7,8]. In biomedicine, Raman-based methods are increasingly used for live-cell studies. They do not require sample pre-processing such as fixation or antibody staining, allowing the study of living specimens [9,10]. Because the chemical composition of a cell is complex and highly heterogeneous, the evaluation of the Raman spectrum of a cell requires intense data processing and careful interpretation. However, modern algorithms already allow the identification and visualization of subcellular structures such as DNA, lipids, or proteins based on their Raman fingerprint [9,11]. Moreover, identification of minute changes in the spectral signatures can be assigned to changes in the molecular composition of a cell or a cellular structure and therefore allow for marker-independent cellular phenotyping [12,13] or monitoring of (patho-)physiological changes or drug-induced effects [14,15].

The THP-1 monocytic cell line and MDMs circulating in the peripheral blood are both popular models for studying macrophage biology [16]. Both cell models come with the typical advantages and disadvantages of cell lines in contrast to primary cells: easy access, safety concerns, and reproducibility must be carefully balanced when choosing one over the other. In addition, there is ample evidence that the malignant origin of the THP-1 cell line causes severe alterations in cell biology and activation [17]. The capability of THP-1 cells to adequately mimic macrophage biology has therefore been questioned on numerous accounts [18].

This study is designed to implement Raman imaging and multivariate data analysis to holistically analyze and compare cellular phenotypes of THP-1 cells and MDMs on a subcellular resolution. On a single cell level, insights into the biochemical remodeling of nucleic acids, lipids, and cytoplasmic structures through cell activation processes and differences in activation patterns will be elaborated.

## 2. Materials and Methods

### 2.1. Peripheral Blood Mononuclear Cell-Derived Monocyte Isolation and Culture

Human blood samples were retrieved in accordance with the Declaration of Helsinki, which was approved by the Ethics Committee of the Medical Faculty at the University of Tübingen (IRB# 495/2018BO2). Peripheral blood mononuclear cells (PBMCs) were isolated using density gradient centrifugation of freshly collected whole blood from one healthy volunteer after obtaining informed consent [19]. Monocytes were isolated by plastic adherence as described before [20]. After isolation, PBMCs were seeded at a concentration of  $5 \times 10^6$  cells/cm<sup>2</sup> at 37 °C and 5% CO<sub>2</sub> in a culture medium. After 2 h, all non-adherent cells were aspirated and removed. The remaining adherent monocytes were washed with PBS and continually cultured to mature into macrophages.

### 2.2. Macrophage Maturation and Polarization

RPMI 1640 with Glutamax™ supplemented with 100 µg/mL streptomycin, 100 U/mL penicillin, and 10% heat-inactivated fetal bovine serum (FBS) (all from Thermo Fisher, Waltham, MA, USA) was used to culture monocytes in polystyrene 24-well cell culture plates (ibidi, Planegg, Germany) at 37 °C and under a 5% CO<sub>2</sub> humidified atmosphere. The culture medium was supplemented with 50 ng/mL macrophage colony-stimulating factor (M-CSF; Biolegend, Amsterdam, The Netherlands) to mature monocytes into macrophages over 8 days. Medium changes were performed on days 3 and 5. On day 5, 100 ng/mL Lipopolysaccharide (LPS) (*E. Coli*, O111:B4; Merck Millipore, Darmstadt, Germany) and 100 ng/mL IFN $\gamma$  (Biolegend) were added to induce macrophage activation. Control M0 (resting) macrophages were not stimulated, but the medium was changed on days 3 and 5. Four hours prior to analysis, MDMs were treated with GolgiPlug™ (BD Bioscience, NJ, USA) to block the intracellular protein transport and enhance the detectability of cytokine production.

### 2.3. THP-1 Culture

The human monocytic leukemia cell line THP-1 (ATCC, Manassas, VA, USA) was cultured in T75 flasks (Greiner Bio-One, Kremsmünster, Austria) in RPMI 1640 with Gluta-max™ supplemented with 100 µg/mL streptomycin, 100 U/mL penicillin and 10% FBS at 37 °C, under a 5% CO<sub>2</sub> humidified atmosphere. Cells were split upon a concentration confluency between  $8 \times 10^5$  and  $1 \times 10^6$  cells/ml. For all experiments, cells from passages 10 to 15 were used. THP-1 cells were treated with 50 ng/mL phorbol-12-myristate-13-acetate (PMA) (Sigma-Aldrich, St. Louis, MO, USA) for 48 h to induce macrophage differentiation. The differentiation process was performed in 6-well plates (Corning, Wiesbaden, Germany) at a density of  $2 \times 10^6$  cells/well. Subsequently, after differentiation, the PMA-containing medium was removed, and cells were cultured for an additional 48 h without PMA. PMA-treated cells were detached using 0.05% trypsin/EDTA (Gibco) and reseeded in a polystyrene 24-well cell culture plate (ibidi GmbH) for 48 h. For activation, cells were stimulated 2 h after seeding with 100 ng/mL LPS and 100 ng/mL IFN $\gamma$  for 48 h.

### 2.4. Flow Cytometry

For flow cytometry (FC) analysis, cells were dissociated with Accutase (Biolegend) and processed as described before [20]. For extracellular antigen staining, the following antibodies were used: CD86-Pacific Blue™, human leukocyte antigen DR (HLA-DR)-Brilliant Violet (BV) 510, CD206-FITC, and CD163-PE/Cy7 (all from Biolegend). For intracellular cytokine staining, cells were resuspended in Cytotfix/ Cytoperm solution for 20 min at 4 °C and washed with Permashield (both BD Bioscience, East Rutherford, NJ, USA). The following intracellular antibodies were then diluted in Permashield at a concentration of 1:50, and cells were stained for 30 min at 4 °C in the dark: tumor necrosis factor  $\alpha$  (TNF $\alpha$ )-BV711 (#502939, Interleukin 6 (IL-6)-PE/Cy5 (#501117), Interleukin 10 (IL-10)-PE/Dazzle (#501425), Monocyte chemoattractant protein 1 (MCP-1)-PE/Cy7 (502613) (all Biolegend) and Interleukin 1 Receptor Antagonist (IL1RA)-PE (#340525, BD Bioscience). Mean fluorescence intensities (MFI) were analyzed using a BD Biosciences LSRFortessa Cytometer (East Rutherford, NJ, USA). Data were interpreted using FlowJo™ 10.4.2 (Tree Star, Ashland, OR, USA). A forward scatter versus sideward scatter gating strategy was employed to exclude debris, doublets, and dead cells (7-AAD staining, Biolegend). Each experiment was compensated using UltraComp eBeads (Thermo Fisher, Waltham, MA, USA) and software-based automatic compensation to correct fluorescence spillover. Fluorescence minus one controls were performed to determine the background fluorescence of the antibody panel.

### 2.5. Raman Microspectroscopy

RM was performed using a customized WiTec alpha 300R Raman system (WiTec GmbH, Ulm, Germany) equipped with a green laser (532 nm) and a charged-coupled device spectrograph with a grating of 600 g/mm. Raman images comprising the whole cell area were acquired.  $30 \times 30$  µm scans of single macrophages were acquired using a 63 $\times$  apochromat water dipping objective (Carl Zeiss AG, Jena, Germany), an integration time of 0.5 s, a pixel resolution of  $1 \times 1$  µm, and a laser power of 50 mW. A total of 30 cells were measured for each M0 and M1 replicate.

### 2.6. Data Processing

Raman data were processed using the Project FIVE 5.2 software (WiTec GmbH, Ulm, Germany). Cosmic rays were removed, and a baseline correction was employed on all spectra. Spectra were cropped to the range from 300 cm<sup>-1</sup> to 3045 cm<sup>-1</sup>. True Component Analysis (TCA) was employed to identify major spectral components in the images. To extract single spectra, masks were generated based on TCA heat maps. To reduce the dimensionality of the spectral data, principal component analysis (PCA) was performed using the Unscrambler  $\times$  14.0 software (Camo Software, Oslo, Norway) [21]. For PCA analysis, the spectral fingerprint region between 400–1800 cm<sup>-1</sup> was investigated. PCA results are presented as score plots and loading plots. In brief, PCA is an unsupervised

algorithm elaborating spectral differences and similarities on a vector-based approach. The identified vectors are also called principal components (PCs), where PC-1 explains the most relevant difference in the data set, PC-2 the second most relevant difference, etc. PC-1 often only describes differences based on spectral intensities or background signals. PCs were selected based on a clustering of the data sets of interest and the biological relevance of the most influencing peaks in the assigned loadings plot.

### 2.7. Statistical Analysis

All statistical analyses were performed by a two-tailed student's *t*-test with a *p*-value of 0.05 with Graph Pad Prism 9.2.0 (Graph Pad Software Inc. San Diego, CA, USA). Graphs are box and whiskers plots where the whiskers have been calculated using the Tukey method. All experiments were performed as triplicates. MDMs originate from 3 different isolations from one donor. A total of 90 cells per condition were measured.

## 3. Results

### 3.1. Definition of Activation Patterns of THP-1 Macrophages and MDMs by Flow Cytometry

State-of-the-art characterization of immune cells and their subpopulations includes investigating their expression of specific surface markers and cytokines. To define macrophage activation by LPS and IFN $\gamma$ , routine FC was performed (Figure 1). Upon LPS-IFN $\gamma$  activation, THP-1 and MDMs responded with a significantly increased expression of the surface antigen HLA-DR and elevated expression patterns of cytokines IL-6, TNF, and IL-1RA, which indicate an activated cellular phenotype. Similarly, no significant changes in CD206 and IL-10 were observed for both cell types. Expression baselines and activation levels differed between THP-1 and MDMs for several of these markers. Differences between THP-1 and MDMs were also reflected in increased CD86 levels as well as decreased CD163 levels in activated macrophages, solely shown in MDMs, but not in THP-1. For MCP-1, inverse effects were observed between the two groups.

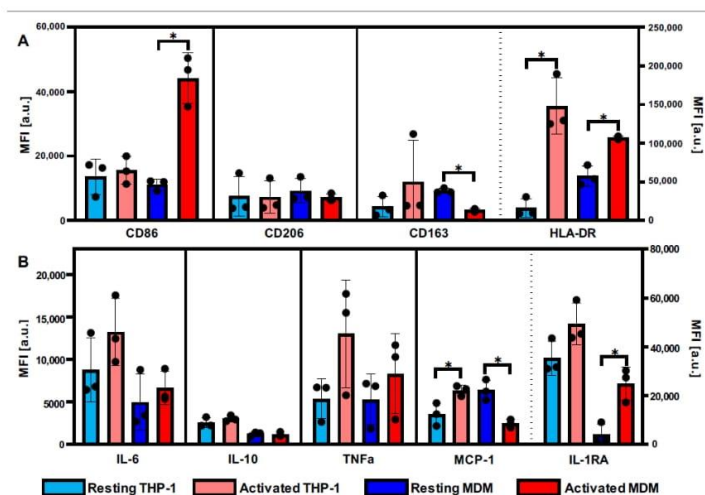


**Figure 1.** THP-1-derived macrophages and MDMs differ in their molecular activation patterns. Expression of (A) surface antigens and (B) cytokines of THP-1 (light colors) and MDMs (intense colors) before (blue) and after (red) LPS-IFN $\gamma$  activation. Data represent mean fluorescence intensity (MFI) values  $\pm$  SD; *n* = 3; pairwise comparison via student's *t*-test, \* *p*  $\leq$  0.05. Boxplots after the dotted line are assigned to the right y-axis. HLA-DR: human leukocyte antigen DR isotypes; IL: interleukin; TNF: tumor necrosis factor; MCP: monocyte chemoattractant protein; IL-1RA: interleukin 1 receptor antagonist.

### 3.2. Raman Imaging Provides Spatial Resolution of Subcellular Structures in Macrophages

THP-1 and PBMC-derived monocytes were matured into M0 and M1 macrophages and characterized by RM and Raman imaging. Raman scans were segmented by TCA into false color-coded intensity distribution heat maps (Figure 2A,B). Four major spectral components were identified, localizing nucleic acids (blue), cytoplasm (green), and two lipid-related components—referred to as *lipids A* (red) and *lipids B* (pink) (Figure 2C).

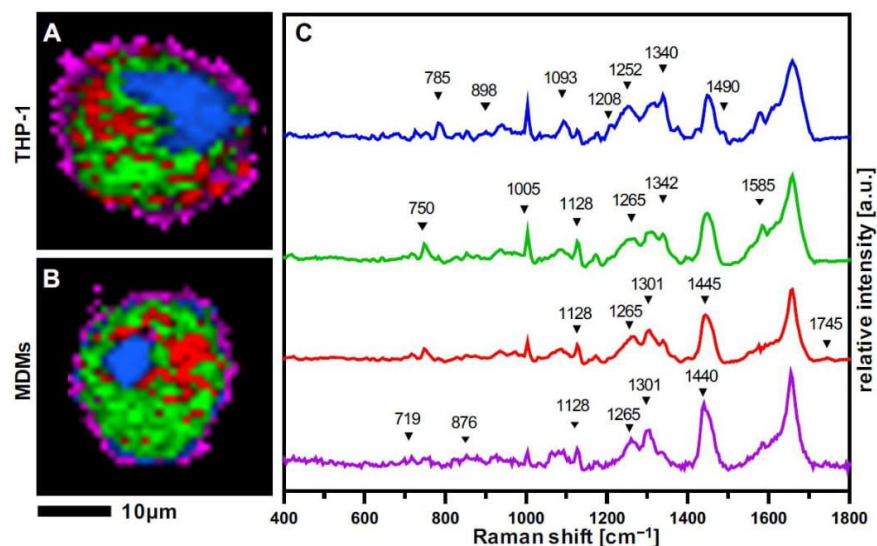


**Figure 2.** Raman imaging of resting macrophages. True component analysis (TCA) segmentation of subcellular structures allowed to generate intensity distribution heatmaps of (A) THP-1 macrophages and (B) MDMs. Characteristic spectral signatures (C) identified and localized nucleic acids (blue), cytoplasm (green), lipids A (red), and lipids B (purple). Scale bar equals 10  $\mu\text{m}$ .

Nucleic acids were identified based on characteristic bands at  $785\text{ cm}^{-1}$ ,  $1093\text{ cm}^{-1}$ ,  $1340\text{ cm}^{-1}$ , and  $1576\text{ cm}^{-1}$ , assigned to DNA. The spectral component describing cytoplasmic molecules displays bands at  $750\text{ cm}^{-1}$ ,  $1005\text{ cm}^{-1}$ ,  $1585\text{ cm}^{-1}$ , and  $1660\text{ cm}^{-1}$  associated with molecular vibrations from proteins and mitochondrial activity. The lipid feature was further distinguished into *lipids A*, rather located inside the cells with representative Raman bands at  $1128\text{ cm}^{-1}$ ,  $1265\text{ cm}^{-1}$ ,  $1301\text{ cm}^{-1}$ , and  $1445\text{ cm}^{-1}$ , as well as *lipids B*, which showed additional bands at  $719\text{ cm}^{-1}$  and  $876\text{ cm}^{-1}$  located at the outer surrounding of the cell. The same major spectral components and similar distribution patterns were retrieved from resting THP-1 and MDMs. A comprehensive overview of all relevant peaks and their molecular assignments is provided in Table 1.

**Table 1.** Major Raman peaks and their molecular assignments.

Wavenumber [ $\text{cm}^{-1}$ ]	Vibration Mode	Assignment
695	DNA bases (G & T)	DNA [22,23]
719	Symmetric stretch vibration of choline group	Phospholipids [24]
750	Pyrrole ring breathing	Cytochrome C [25,26]
776–780	Symmetric breathing of tryptophan	Proteins [27,28]

Table 1. Cont.

Wavenumber [cm <sup>-1</sup> ]	Vibration Mode	Assignment
785–790	Ring breathing modes (DNA/RNA bases)	DNA [22,23]
868	C-O-O skeletal vibration	Lipids [24]
876	Asymmetric vibration choline N(CH <sub>3</sub> ) <sub>3</sub>	Phospholipids [24]
898	Adenine	DNA [22,23]
940	C-C skeletal vibration (backbone)	Proteins [27,28]
1005	Symmetric ring breathing of phenylalanine	Proteins [27,28]
1093	Symmetric PO <sub>2</sub> <sup>-</sup> stretching vibration of the DNA backbone	DNA [22,23]
1128	C-N stretching (proteins); C-C vibration in fatty acids	Proteins; Lipids [24,27,28]
1173	C-C vibrations fatty acids	Lipids [24]
1208	Adenine, Thymine (ring breathing modes)	DNA [22,23]
1252	Guanine, cytosine (NH <sub>2</sub> )	DNA [22,23]
1265	Amide III; =CH <sub>2</sub> vibration in lipids	Proteins; Lipids [24,27,28]
1301	C-H vibration	(Phospho-) Lipids [24]
1340	Adenine, guanine & CH deformation in proteins	DNA [22,23], Proteins [29]
1435–1445	CH <sub>3</sub> /CH <sub>2</sub> scissoring	Lipids [24]
1450	CH <sub>2</sub> deformation	Proteins [27,28]
1585	C=C olefinic stretch	Proteins [27,28]
1630	DNA bases (C, G, T)	DNA [30]
1640	C=C vibrations (fatty acids)	Lipids [24]
1655–1670	Amide I, C=C vibrations	Lipids; Proteins [24,27,28]
1745	C=O vibrations triacylglycerids	Lipids [24]

### 3.3. THP-1 Macrophages and MDMs Differ in Their Molecular Composition

In addition to defining the spatial distribution of subcellular structures, in-depth analyses were performed to investigate the molecular composition in both cell types. Multivariate data analysis allowed us to identify minor spectral differences, as the average spectra exhibited very similar signatures (Figure 3B). For each single-cell Raman scan, spectra were extracted for each of the four cellular components, further used for PCA. First, THP-1 and MDMs were compared in their resting state (M0). PCA comparison of the cytoplasm signatures of non-activated THP-1 and MDMs is demonstrated in Figure 3; PCA results of the other components—nuclei, Lipids A, and Lipids B—are shown in Supplementary Figure S1. The PC-2/PC-3 scores plot exhibits a cluster formation separating THP-1 and MDMs according to the underlying spectral signatures of the cells (Figure 3A). The explained variance represented by PC-2 was significantly different between the two analyzed cell populations (Figure 3C). The corresponding vector highlighting the most influencing spectral features is shown in the loadings plot (Figure 3D). Peaks in the positive PC-2 loadings dominated the spectral information originating from the data clustering in the positive PC-2 scores range—in this case the THP-1 data. Negative peaks in the loadings were more prominent in the spectra from MDMs. The spectral differences between THP-1 and MDMs were assigned to an increased cytochrome c signal at 750, 1128, and 1585 cm<sup>-1</sup>

in THP-1, and a stronger contribution of protein signals at 1003, 1335, 1450, and 1665  $\text{cm}^{-1}$  in MDMs.

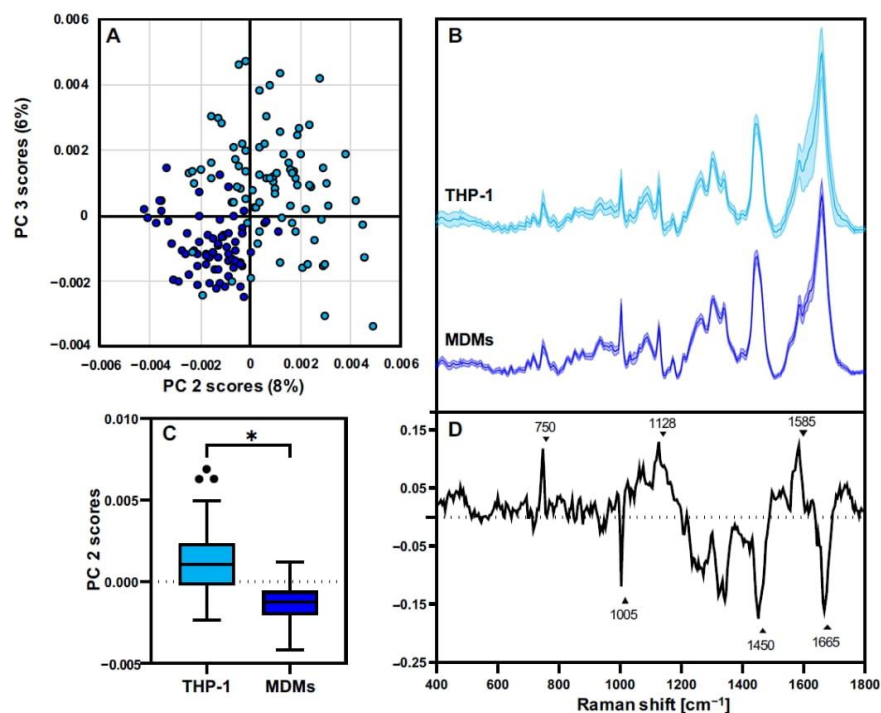


**Figure 3.** PCA comparison of cytoplasm features identifies differences in the molecular composition between resting THP-1 and MDMs. (A) PC 2/PC 3 scores plot of single-cell cytoplasm spectra extracted from THP-1 (light blue) and MDMs (blue) demonstrates a separation of both groups. (B) Mean cytoplasm spectra from THP-1 (light blue) and MDMs (blue). (C) Statistical analysis of the PC 2 score values reveals significant differences within the cytoplasm from both cell sources. Boxplots show mean single cell PC 2 score values  $\pm$  SD,  $n = 90$ , student's  $t$ -test, \*  $p \leq 0.05$ . (D) The corresponding PC 2 loadings plot exhibits the molecular vibrations differentiating the cytoplasmic composition between both cell types.

### 3.4. THP-1 and MDMs Have a Different Response to Proinflammatory Activation

The effect of macrophage activation was determined and compared between THP-1 and MDMs. The LPS-IFN $\gamma$ -induced proinflammatory response was evaluated by PCAs, including spectra from THP-1 and MDMs in both resting and activated states (Figure 4, for PCA scores plots see Supplementary Figure S2). Separate analyses were conducted for each of the four cellular structures—nucleic acids, proteins, *lipids A*, and *lipids B*. For all PCAs, the most relevant PCs for separating M0 and M1 macrophages were identified, and single-cell PC score values were statistically compared (Figure 4A–D). Activation-induced changes were especially prominent in nuclei-derived information and *lipids B*, which demonstrated a clustering between resting and activated phenotypes at high explained variance values in PC-1. Differences in cytoplasmic proteins and *lipids A* did only appear at lower PCs. Moreover, MDMs showed significant differences between M0 and M1 states within all analyzed cellular components, whereas proinflammatory changes in THP-1 were mainly linked to alterations in only two of the four components—proteins and *lipids B*. The most influencing Raman bands for each analysis are highlighted in the assigned loadings plots (Figure 4E).



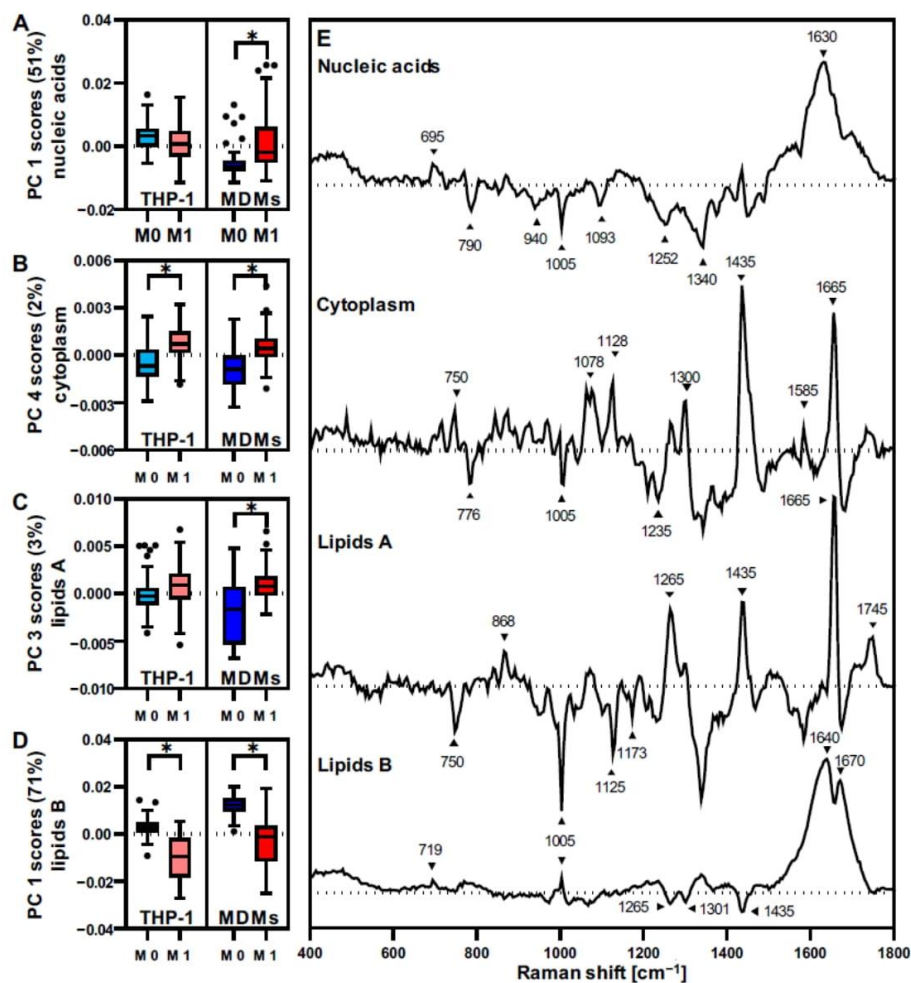


**Figure 4.** Raman spectra and PCA reflect proinflammatory activation in macrophages. Individual PCAs for (A) nucleic acids, (B) cytoplasm, (C) lipids A, and (D) lipids B were performed for data generated for THP-1 and MDMs before and after LPS-IFN $\gamma$  activation. Statistical analyses of the most relevant PC score values demonstrate significant differences in resting and activated MDMs for each of the components, but for THP-1 only within cytoplasmic proteins and lipids B. Boxplots indicate mean single cell PC score values  $\pm$  SD,  $n = 90$ , pairwise comparison by student's  $t$ -test,  $* p \leq 0.05$ . (E) Corresponding loadings of the selected PCs describe the molecular changes specific to the separation upon activation.

To have a deeper insight into the molecular protein modifications driven by the LPS-IFN $\gamma$  proinflammatory response, independent PCAs including only the data from one cell type were performed. MDMs or THP-1 were separately analyzed with a PCA from extracted spectra from cytoplasm before and after LPS-IFN $\gamma$  activation (Figure 5). PCA score graphs for THP-1 (Figure 5A) and MDMs (Figure 5B) demonstrated the strongest separation between M0 and M1 macrophages. THP-1 clustering was described by PC 4 with an explained variance of 2%, and MDMs showed a separation in PC 2 with 4% of the total variance. Statistical analysis from the selected PCs scores confirmed that the separation seen on the score graphs was significant (Figure 5C,D). The respective loadings plots for both PCAs (Figure 5E) showed differences in the cytoplasmic molecular composition induced

by LPS-IFN $\gamma$  activation for THP-1 and MDMs. However, the separation and assigned molecular changes were driven by different spectral patterns for the two groups.

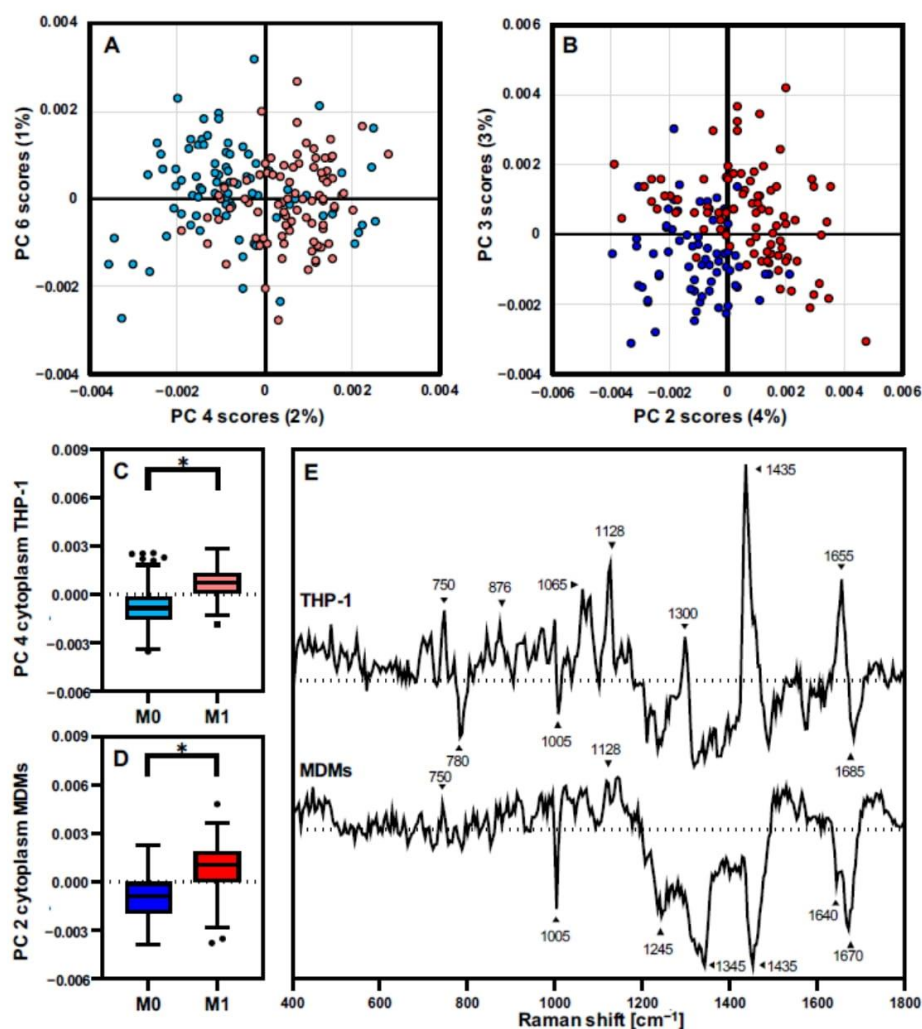


**Figure 5.** In-depth analysis of cell type-specific changes in cytoplasmic composition upon proinflammatory response. Individual PCAs for the cytoplasmic spectra from THP-1 (A,C) and MDMs (B,D) identified the most prominent molecular modifications after LPS-IFN $\gamma$  treatment for each cell source. Boxplots indicate mean single cell PC score values  $\pm$  SD,  $n = 90$ , pairwise comparison by student's  $t$ -test, \*  $p \leq 0.05$ . (E) The underlying molecular changes exhibit different signatures and patterns, as indicated by the loadings plots.

#### 4. Discussion

The impact of LPS-IFN $\gamma$  activation on macrophages derived from the THP-1 cell line and primary-isolated PBMCs were compared by assessing their phenotype using RM and Raman imaging, which allowed a holistic view of the cellular composition.

The biological differences between THP-1 macrophages and MDMs have been addressed and discussed by many studies. For example, NF $\kappa$ B activation and gene transcription profiles of THP-1-derived macrophages were similar to that of human MDMs [31,32], whereas opposing results were observed for cytokine expression profiles. Recently, Shi-

ratori et al. showed that polarization and activation profiles differ between MDMs and THP-1 derived macrophages in vitro [33].

In addition, several studies have investigated if macrophage activation can be detected using Raman spectroscopy [34,35]. However, no available study directly compares molecular Raman fingerprints of different macrophage model systems before and after activation.

We were able to show that the information obtained by RM and Raman imaging can be utilized to track molecular changes during the activation process of macrophages and provide insight into diverging molecular mechanisms between different model systems.

To further highlight the benefits of RM, we additionally performed routine FC measurements of common immune surface antigens indicative of immune cell activation.

Although comparable relative responses were observed investigating THP-1 and MDM by FC, differences in baseline expression and relative change in expression after activation were identified, especially for the markers MCP-1 and the costimulatory surface antigen CD86—also known as B7.2, which is essential for successful T cell activation. While a significant increase occurred in MDMs, no increase above resting level was observed in THP-1 macrophages for CD86. As THP-1 is a monocytic leukemia-derived cell line, it can be speculated that the failure to upregulate CD86 for further T cell activation could be an immune evasion mechanism typical for some types of cancer [36]. Similarly, a significant drop of CD163, a scavenger receptor often used as an anti-inflammatory marker as it indicates the clearance of cellular debris and onset of the healing process, was observed in activated MDMs but not in THP-1 macrophages. For MCP-1, opposing effects between the two cultures were identified after activation, with an upregulation in THP-1 macrophages and a downregulation in MDMs. Similar to what was seen for HLA-DR and IL-10, THP-1 cells responded with higher MCP-1 expression when compared with PBMC-derived macrophages [33]. Besides the variation in cell sensitivity, other effects such as the higher genetic variability of MDMs could also contribute to the reported results. In addition, the kinetics of cellular mechanisms can be altered between cell lines and primary cells, with variances in expression profiles growing with incubation time [33]. Altogether, the FC results suggest that the THP-1 cell line lacks some important mechanisms of proinflammatory actions, such as the up- or downregulation of immune response-modulating antigens that are still present in MDMs.

While the FC analysis of surface marker antigens and intracellular cytokines provides a first assessment of activated signaling pathways, it does not capture the extended effects of cellular remodeling. Previous studies have reported a less pronounced polarization profile of THP-1 macrophages after proinflammatory activation compared to MDMs [18]. Here, we were able to show that THP-1 macrophages and MDMs both responded to the challenge with LPS/IFN $\gamma$ ; however, analysis of the Raman spectra revealed distinct remodeling patterns in individual cell components.

RM has been widely employed for the phenotypic classification of cells [13,15,37]. Nevertheless, the characterization and identification of macrophage polarization or activation via RM remains in its early stages. Pavillon [34] and Töpfer et al. [35] have used RM to characterize the monocyte cell lines Raw264 and THP-1 to recapitulate the proinflammatory response after LPS-IFN $\gamma$  treatment. In our study, we demonstrated that besides marker-independent localization of subcellular structures using Raman imaging, RM could identify subtle changes in the molecular composition of nucleic acids, proteins, and lipids that occur upon macrophage inflammatory response in the investigated cell models. Different spectral signatures were obtained from resting THP-1 and MDMs, and cytoplasm-derived PCA scores plots showed a highly heterogeneous scattering in the data. Major differences within the spectral signatures were described by increased cytochrome c bands at 750, 1128, and 1585  $\text{cm}^{-1}$  in THP-1 spectra, assigned to the activity of mitochondria, which are known to be regulatory organelles that highly contribute to the immune response [38]. Moreover, differences in cytoplasm composition could correspond to the observed tendency towards increased levels in basal cytokine expression of THP-1 macrophages demonstrated by FC data. MDM spectra showed a stronger impact of protein and amino acid features,

demonstrated by increased bands at  $935\text{ cm}^{-1}$  (C-C stretching; proline, valine) [39,40],  $1449\text{ cm}^{-1}$  (C-H vibration) [41], and  $1665\text{ cm}^{-1}$  (Amide I) [42], which are commonly associated with structural vibrations related to the 3D configuration of proteins but can also correlate to a spectral contribution of the inflammasome, a multiprotein complex involved in the initiation of an immune response [43]. Furthermore, the other analyzed cellular structures (nuclei and lipids) demonstrated differences in their molecular composition between the two cell sources (Figure S1). These findings of individual characteristics of resting cell line-derived and primary macrophages comply with previous studies reporting differences in resistance to apoptosis, number of mitochondria, and cytokine expression between THP-1-derived macrophages and MDMs, which are also in dependence on the used THP-1 differentiation protocol [16,18].

In addition to resting macrophages, the sensitivity to LPS-IFN $\gamma$ -driven proinflammatory activation was monitored and appeared to have greater effects on the phenotypic remodeling of MDM compared to THP-1. MDM activation resulted in significant modifications of nucleic acids, proteins, *lipids A*, and *lipids B*. By contrast, THP-1 activation was only significantly reflected in protein and *lipids B* composition. Based on our PCA results, proteins and *lipids B* are the cellular components that are more sensitive and robust to indicate macrophage polarization. An in-depth analysis of the loadings plots demonstrated a decrease in DNA contribution, increased lipid-related spectral features, and shifts in the protein patterns upon activation. Protein spectral changes due to macrophage activation were dominated by changes in structural bands at  $1435\text{ cm}^{-1}$  (CH $_2$  scissoring) [44] and  $1665\text{ cm}^{-1}$  (Amide I) [42]. The modifications in *lipids B* reflect a prominent amide I with a modified topography at the sub-bands center at  $1640\text{ cm}^{-1}$  and  $1670\text{ cm}^{-1}$ . Alterations within the amide I substructure upon macrophage polarization have been linked to changes in lipid composition [45,46], more specifically to the composition of phospholipids [47]. THP-1 and MDMs showed similar trends regarding these major features; however, relative changes appeared to be more significant for MDMs. Comparable results were obtained by Chaudary et al., who reported different spectral patterns and changes occurring for THP-1 and primary blood-derived cells upon monocyte-to-macrophage differentiation [48]. However, the authors applied different activation protocols among the cells—using PMA for THP-1 and LPS for MDMs. This might affect the polarization pathway and efficacy. THP-1-derived macrophages have been reported to express lower levels of CD14 when compared with MDMs [49]. This surface protein plays an important role in detecting LPS as it forms a highly sensitive complex with TLR4 and MD2 [50]. Accordingly, MDMs have been reported to be more responsive to LPS-activation than THP-1 monocytes [50], which is also reflected by our Raman data, showing relatively higher effects upon activation in MDMs compared to THP-1 cells. These results emphasize the necessity to carefully select an appropriate cell source for an in vitro model.

## 5. Conclusions

Our study shows that RM and Raman imaging allow for the marker-independent evaluation of macrophage LPS-IFN $\gamma$ -driven proinflammatory changes in both THP-1 and MDMs. Moreover, based on the Raman spectral signature of resting and activated macrophages, it was possible to show that, although both cell types were polarized by the LPS-IFN $\gamma$  activation, THP-1 cells were less responsive than MDMs. Compared to cell line-derived macrophages, proinflammatory changes in MDMs were reflected in all the identified subcellular structures, suggesting a global response across the immune cell.

**Supplementary Materials:** The following supporting information can be downloaded at: <https://www.mdpi.com/article/10.3390/biomedicines10050989/s1>, Figure S1: Principal component analysis (PCA) comparison of extracted spectra from TCA maps of resting THP-1 and MDM-derived macrophages; Figure S2: PCA scores plots corresponding to the multivariate analysis between resting and activated THP-1 and MDM-derived macrophages.

**Author Contributions:** N.F., D.A.C.B. and K.S.-L. designed the study. N.F., D.A.C.B. and S.S. performed experiments and analyzed data. N.F., D.A.C.B., F.B. and J.M. interpreted data and wrote the manuscript. J.M. and K.S.-L. revised the manuscript. K.S.-L., J.M. and U.R. supervised the study. M.W. ensured the accordance of the study with ethical guidelines and provided blood samples from healthy individuals. All authors have read and agreed to the published version of the manuscript.

**Funding:** This work was financially supported by the Ministry of Baden-Württemberg for Economic Affairs, Labor and Tourism (3-4332.62-NMI/65), and the Deutsche Forschungsgemeinschaft (INST 2388/33-1, INST 2388/64-1, GRK 2543, and Germany's Excellence Strategy—EXC 2180-390900677).

**Institutional Review Board Statement:** Human blood samples were retrieved in accordance with the Declaration of Helsinki, which was approved by the Ethics Committee of the Medical Faculty at the University of Tübingen (IRB# 495/2018BO2).

**Informed Consent Statement:** Informed consent was obtained from all subjects involved in the study.

**Data Availability Statement:** Not applicable.

**Acknowledgments:** The authors thank Eva Brauchle (University of Tübingen) and Christopher Shipp (NMI) for their scientific advice.

**Conflicts of Interest:** The authors declare no conflict of interest.

## References

1. Godwin, J.W.; Pinto, A.R.; Rosenthal, N.A. Macrophages are required for adult salamander limb regeneration. *Proc. Natl. Acad. Sci. USA* **2013**, *110*, 9415–9420. [[CrossRef](#)] [[PubMed](#)]
2. Gerrick, K.Y.; Gerrick, E.R.; Gupta, A.; Wheelan, S.J.; Yegnasubramanian, S.; Jaffee, E.M. Transcriptional profiling identifies novel regulators of macrophage polarization. *PLoS ONE* **2018**, *13*, e0208602. [[CrossRef](#)] [[PubMed](#)]
3. Liu, Y.-C.; Zou, X.-B.; Chai, Y.-F.; Yao, Y.-M. Macrophage Polarization in Inflammatory Diseases. *Int. J. Biol. Sci.* **2014**, *10*, 520–529. [[CrossRef](#)]
4. Okabe, Y.; Medzhitov, R. Tissue-Specific Signals Control Reversible Program of Localization and Functional Polarization of Macrophages. *Cell* **2014**, *157*, 832–844. [[CrossRef](#)] [[PubMed](#)]
5. Murray, P.J.; Allen, J.E.; Biswas, S.K.; Fisher, E.A.; Gilroy, D.W.; Goerdt, S.; Gordon, S.; Hamilton, J.A.; Ivashkiv, L.B.; Lawrence, T.; et al. Macrophage Activation and Polarization: Nomenclature and Experimental Guidelines. *Immunity* **2014**, *41*, 14–20. [[CrossRef](#)] [[PubMed](#)]
6. Mosser, D.M.; Edwards, J.P. Exploring the full spectrum of macrophage activation. *Nat. Rev. Immunol.* **2008**, *8*, 958–969. [[CrossRef](#)] [[PubMed](#)]
7. Smith, R.; Wright, K.L.; Ashton, L. Raman spectroscopy: An evolving technique for live cell studies. *Analyst* **2016**, *141*, 3590–3600. [[CrossRef](#)] [[PubMed](#)]
8. Butler, H.J.; Ashton, L.; Bird, B.; Cinque, G.; Curtis, K.; Dorney, J.; Esmonde-White, K.; Fullwood, N.J.; Gardner, B.; Martin-Hirsch, P.L.; et al. Using Raman spectroscopy to characterize biological materials. *Nat. Protoc.* **2016**, *11*, 664–687. [[CrossRef](#)] [[PubMed](#)]
9. Beattie, J.R.; Bell, S.E.J.; Moss, B.W. A critical evaluation of Raman spectroscopy for the analysis of lipids: Fatty acid methyl esters. *Lipids* **2004**, *39*, 407–419. [[CrossRef](#)]
10. Krafft, C. Raman spectroscopy and microscopy of cells and tissues. In *Encyclopedia of Biophysics*; Springer: Berlin/Heidelberg, Germany, 2013; p. 2178. [[CrossRef](#)]
11. Zbinden, A.; Marzi, J.; Schlünder, K.; Probst, C.; Urbanczyk, M.; Black, S.; Brauchle, E.M.; Layland, S.L.; Kraushaar, U.; Duffy, G.; et al. Non-invasive marker-independent high content analysis of a microphysiological human pancreas-on-a-chip model. *Matrix Biol.* **2020**, *85–86*, 205–220. [[CrossRef](#)] [[PubMed](#)]
12. Fore, S.; Chan, J.; Taylor, D.; Huser, T. Raman spectroscopy of individual monocytes reveals that single-beam optical trapping of mononuclear cells occurs by their nucleus. *J. Opt.* **2011**, *13*, 044021. [[CrossRef](#)] [[PubMed](#)]
13. Marzi, J.; Brauchle, E.M.; Schenke-Layland, K.; Rolle, M.W. Non-invasive functional molecular phenotyping of human smooth muscle cells utilized in cardiovascular tissue engineering. *Acta Biomater.* **2019**, *89*, 193–205. [[CrossRef](#)] [[PubMed](#)]
14. Notarstefano, V.; Sabbatini, S.; Pro, C.; Belloni, A.; Orilisi, G.; Rubini, C.; Byrne, H.J.; Vaccari, L.; Giorgini, E. Exploiting fourier transform infrared and Raman microspectroscopies on cancer stem cells from oral squamous cells carcinoma: New evidence of acquired cisplatin chemoresistance. *Analyst* **2020**, *145*, 8038–8049. [[CrossRef](#)] [[PubMed](#)]
15. Brauchle, E.; Thude, S.; Brucker, S.Y.; Schenke-Layland, K. Cell death stages in single apoptotic and necrotic cells monitored by Raman microspectroscopy. *Sci. Rep.* **2014**, *4*, 4698. [[CrossRef](#)]
16. Daigneault, M.; Preston, J.A.; Marriott, H.M.; Whyte, M.K.B.; Dockrell, D.H. The Identification of Markers of Macrophage Differentiation in PMA-Stimulated THP-1 Cells and Monocyte-Derived Macrophages. *PLoS ONE* **2010**, *5*, e8668. [[CrossRef](#)]
17. Chanput, W.; Mes, J.J.; Wichers, H.J. THP-1 cell line: An in vitro cell model for immune modulation approach. *Int. Immunopharmacol.* **2014**, *23*, 37–45. [[CrossRef](#)]

18. Tedesco, S.; De Majo, F.; Kim, J.; Trenti, A.; Trevisi, L.; Fadini, G.P.; Bolego, C.; Zandstra, P.W.; Cignarella, A.; Vitiello, L. Convenience versus biological significance: Are PMA-differentiated THP-1 cells a reliable substitute for blood-derived macrophages when studying in vitro polarization? *Front. Pharmacol.* **2018**, *9*, 71. [[CrossRef](#)]
19. Feuerer, N.; Morschl, J.; Daum, R.; Weiss, M.; Hinderer, S.; Schenke-Layland, K.; Shipp, C. Macrophage retrieval from 3D biomaterials: A detailed comparison of common dissociation methods. *J. Immunol. Regen. Med.* **2020**, *11*, 100035. [[CrossRef](#)]
20. Feuerer, N.; Marzi, J.; Brauchle, E.M.; Berrio, D.A.C.; Billing, F.; Weiss, M.; Jakobi, M.; Schneiderhan-Marra, N.; Shipp, C.; Schenke-Layland, K. Lipidome profiling with Raman microspectroscopy identifies macrophage response to surface topographies of implant materials. *Proc. Natl. Acad. Sci. USA* **2021**, *118*, e2113694118. [[CrossRef](#)]
21. Spiers, R.M.; Marzi, J.; Brauchle, E.M.; Cross, S.E.; Vaughan, R.H.; Bateman, P.A.; Hughes, S.J.; Schenke-Layland, K.; Johnson, P.R. Donor age significantly influences the Raman spectroscopic biomolecular fingerprint of human pancreatic extracellular matrix proteins following collagenase-based digestion. *Acta Biomater.* **2019**, *99*, 269–283. [[CrossRef](#)]
22. Peticolas, W.L. [17] Raman spectroscopy of DNA and proteins. *Methods Enzymol.* **1995**, *246*, 389–416. [[CrossRef](#)] [[PubMed](#)]
23. Prescott, B.; Steinmetz, W.; Thomas, G.J. Characterization of DNA structures by laser Raman spectroscopy. *Biopolymers* **1984**, *23*, 235–256. [[CrossRef](#)] [[PubMed](#)]
24. Czamara, K.; Majzner, K.; Pacia, M.Z.; Kochan, K.; Kaczor, A.; Baranska, M. Raman spectroscopy of lipids: A review. *J. Raman Spectrosc.* **2015**, *46*, 4–20. [[CrossRef](#)]
25. Spiro, T.G.; Streckas, T.C. Resonance Raman Spectra of Hemoglobin and Cytochrome c: Inverse Polarization and Vibronic Scattering. *Proc. Natl. Acad. Sci. USA* **1972**, *69*, 2622–2626. [[CrossRef](#)] [[PubMed](#)]
26. Okada, M.; Smith, N.I.; Palonpon, A.F.; Endo, H.; Kawata, S.; Sodeoka, M.; Fujita, K. Label-free Raman observation of cytochrome c dynamics during apoptosis. *Proc. Natl. Acad. Sci. USA* **2011**, *109*, 28–32. [[CrossRef](#)] [[PubMed](#)]
27. Lord, R.; Yu, N.-T. Laser-excited Raman spectroscopy of biomolecules: I. Native lysozyme and its constituent amino acids. *J. Mol. Biol.* **1970**, *50*, 509–524. [[CrossRef](#)]
28. Chen, M.C.; Lord, R.C. Laser-excited Raman spectroscopy of biomolecules. VI. Polypeptides as conformational models. *J. Am. Chem. Soc.* **1974**, *96*, 4750–4752. [[CrossRef](#)]
29. Notingher, I.; Verrier, S.; Haque, S.; Polak, J.M.; Hench, L.L. Spectroscopic study of human lung epithelial cells (A549) in culture: Living cells versus dead cells. *Biopolymers* **2003**, *72*, 230–240. [[CrossRef](#)]
30. He, Z.; Han, Z.; Kizer, M.; Linhardt, R.J.; Wang, X.; Sinyukov, A.M.; Wang, J.; Deckert, V.; Sokolov, A.V.; Hu, J.; et al. Tip-Enhanced Raman Imaging of Single-Stranded DNA with Single Base Resolution. *J. Am. Chem. Soc.* **2018**, *141*, 753–757. [[CrossRef](#)]
31. Kohro, T.; Tanaka, T.; Murakami, T.; Wada, Y.; Aburatani, H.; Hamakubo, T.; Kodama, T. A Comparison of Differences in the Gene Expression Profiles of Phorbol 12-myristate 13-acetate Differentiated THP-1 Cells and Human Monocyte-derived Macrophage. *J. Atheroscler. Thromb.* **2004**, *11*, 88–97. [[CrossRef](#)]
32. Sharif, O.; Bolshakov, V.N.; Raines, S.; Newham, P.; Perkins, N.D. Transcriptional profiling of the LPS induced NF-kappaB response in macrophages. *BMC Immunol.* **2007**, *8*, 1. [[CrossRef](#)]
33. Shiratori, H.; Feinweber, C.; Luckhardt, S.; Linke, B.; Resch, E.; Geisslinger, G.; Weigert, A.; Parnham, M.J. THP-1 and human peripheral blood mononuclear cell-derived macrophages differ in their capacity to polarize in vitro. *Mol. Immunol.* **2017**, *88*, 58–68. [[CrossRef](#)] [[PubMed](#)]
34. Pavillon, N.; Hobro, A.J.; Akira, S.; Smith, N.I. Noninvasive detection of macrophage activation with single-cell resolution through machine learning. *Proc. Natl. Acad. Sci. USA* **2018**, *115*, E2676–E2685. [[CrossRef](#)] [[PubMed](#)]
35. Töpfer, N.; Müller, M.; Dahms, M.; Ramoji, A.; Popp, J.; Slevogt, H.; Neugebauer, U. Raman spectroscopy reveals LPS-induced changes of biomolecular composition in monocytic THP-1 cells in a label-free manner. *Integr. Biol.* **2019**, *11*, 87–98. [[CrossRef](#)] [[PubMed](#)]
36. Ugurel, S.; Uhlig, D.; Pföhler, C.; Tilgen, W.; Schadendorf, D.; Reinhold, U. Down-regulation of HLA class II and costimulatory CD86/B7-2 on circulating monocytes from melanoma patients. *Cancer Immunol. Immunother.* **2004**, *53*, 551–559. [[CrossRef](#)] [[PubMed](#)]
37. Daum, R.; Brauchle, E.M.; Berrio, D.A.C.; Jurkowski, T.P.; Schenke-Layland, K. Non-invasive detection of DNA methylation states in carcinoma and pluripotent stem cells using Raman microspectroscopy and imaging. *Sci. Rep.* **2019**, *9*, 7014. [[CrossRef](#)]
38. Tur, J.; Vico, T.; Lloberas, J.; Zorzano, A.; Celada, A. Chapter One—Macrophages and Mitochondria: A Critical Interplay Between Metabolism, Signaling, and the Functional Activity. In *Advances in Immunology*; Alt, F.W., Ed.; Academic Press: Cambridge, MA, USA, 2017; pp. 1–36.
39. Huang, Z.; McWilliams, A.; Lui, H.; McLean, D.I.; Lam, S.; Zeng, H. Near-infrared Raman spectroscopy for optical diagnosis of lung cancer. *Int. J. Cancer* **2003**, *107*, 1047–1052. [[CrossRef](#)]
40. Stone, N.; Kendall, C.; Shepherd, N.; Crow, P.; Barr, H. Near-infrared Raman spectroscopy for the classification of epithelial pre-cancers and cancers. *J. Raman Spectrosc.* **2002**, *33*, 564–573. [[CrossRef](#)]
41. Liu, Z.; Davis, C.; Cai, W.; He, L.; Chen, X.; Dai, H. Circulation and long-term fate of functionalized, biocompatible single-walled carbon nanotubes in mice probed by Raman spectroscopy. *Proc. Natl. Acad. Sci. USA* **2008**, *105*, 1410–1415. [[CrossRef](#)]
42. Cheng, W.-T.; Liu, M.-T.; Liu, H.-N.; Lin, S.-Y. Micro-Raman spectroscopy used to identify and grade human skin pilomatrixoma. *Microsc. Res. Tech.* **2005**, *68*, 75–79. [[CrossRef](#)]
43. Pétrilli, V.; Dostert, C.; Muruve, A.D.; Tschopp, J. The inflammasome: A danger sensing complex triggering innate immunity. *Curr. Opin. Immunol.* **2007**, *19*, 615–622. [[CrossRef](#)]

44. Ruiz-Chica, A.J.; Medina, M.A.; Sánchez-Jiménez, F.; Ramírez, F.J. Characterization by Raman spectroscopy of conformational changes on guanine–cytosine and adenine–thymine oligonucleotides induced by aminoxy analogues of spermidine. *J. Raman Spectrosc.* **2004**, *35*, 93–100. [[CrossRef](#)]
45. Zhang, C.; Wang, Y.; Wang, F.; Wang, Z.; Lu, Y.; Xu, Y.; Wang, K.; Shen, H.; Yang, P.; Li, S.; et al. Quantitative profiling of glycerophospholipids during mouse and human macrophage differentiation using targeted mass spectrometry. *Sci. Rep.* **2017**, *7*, 412. [[CrossRef](#)] [[PubMed](#)]
46. Montenegro-Burke, J.R.; Sutton, J.A.; Rogers, L.M.; Milne, G.L.; McLean, J.A.; Aronoff, D.M. Lipid profiling of polarized human monocyte-derived macrophages. *Prostaglandins Other Lipid Mediat.* **2016**, *127*, 1–8. [[CrossRef](#)] [[PubMed](#)]
47. Shirota, K.; Yagi, K.; Inaba, T.; Li, P.-C.; Murata, M.; Sugita, Y.; Kobayashi, T. Detection of Sphingomyelin Clusters by Raman Spectroscopy. *Biophys. J.* **2016**, *111*, 999–1007. [[CrossRef](#)] [[PubMed](#)]
48. Chaudhary, N.; Nguyen, T.N.Q.; Cullen, D.; Meade, A.D.; Wynne, C. Discrimination of immune cell activation using Raman micro-spectroscopy in an in-vitro & ex-vivo model. *Spectrochim. Acta Part A Mol. Biomol. Spectrosc.* **2020**, *248*, 119118. [[CrossRef](#)]
49. Bosshart, H.; Heinzlmann, M. Lipopolysaccharide-mediated cell activation without rapid mobilization of cytosolic free calcium. *Mol. Immunol.* **2004**, *41*, 1023–1028. [[CrossRef](#)]
50. Park, B.S.; Song, D.H.; Kim, H.M.; Choi, B.-S.; Lee, H.; Lee, J.-O. The structural basis of lipopolysaccharide recognition by the TLR4–MD-2 complex. *Nature* **2009**, *458*, 1191–1195. [[CrossRef](#)]